

(1)

AD-A227 724

1990

Thesis/Dissertation

A Comparison of Diagnostic and Kinematic Vertical Motion  
Fields Associated with Curved and Straight Jet Streak  
Adjustment processes

Glenn Ernest Van Knowe

AFIT Student at: St Louis University

AFIT/CI/CIA - 90-099

AFIT/CI  
Wright-Patterson AFB OH 45433

Approved for Public Release IAW AFR 190-1  
Distribution Unlimited  
ERNEST A. HAYGOOD, 1st Lt, USAF  
Executive Officer, Civilian Institution Programs

DTIC  
ELECTED  
OCT 24 1990  
S B D  
CC

154

UNCLASSIFIED

A COMPARISON OF DIAGNOSTIC AND KINEMATIC  
VERTICAL MOTION FIELDS ASSOCIATED WITH  
CURVED AND STRAIGHT JET STREAK ADJUSTMENT PROCESSES

Glenn Ernest Van Knowe, B.S.

A Digest Presented to the Faculty of the Graduate School  
of Saint Louis University in Partial Fulfillment of  
the Requirements for the Degree of  
Master of Science

1990

80

## DIGEST

Investigative research was performed on real and simulated jet streaks to determine the relationship of the diagnostic Rossby number with kinematic, balanced and non-balanced omega fields as a function of magnitude, wind shear and curvature. Hydrodynamic instability was also examined as influencing omega values. A two-layer primitive equation model was used to produce forty five jet streak cases. Seven cases were quasi-barotropic with upper winds equal to the lower level winds. Twenty four were equivalent barotropic with the upper level winds set to equal three times the magnitude of the lower level winds. Four cases were run with a beta plane versus a constant f plane. The remaining ten cases were simulated baroclinic conditions. One cyclonic jet streak using operational data also examined.

Model results indicated a consistent weakening for both the 800 mb and 400 mb wind maximums for all jet streak cases when the upper and lower - level waves were in phase and of the same speed. When the upper level was set to equal 3 times the magnitude of the lower jet while maintaining the upper and lower level waves in phase resulted in a larger wind decrease while the 800mb level showed an increase over the 24 hours of the run in each jet streak case. For the beta and easterly jet streak cases the upper level decrease was somewhat less. The baroclinic cases showed a very slight decrease or increase over the 24 hours of the run.

Values of the calculated Rossby numbers displayed a strong correlation with the strength of both the kinematic and non-balanced vertical motions. The Rossby number - vertical motion relationships were essentially linear unless hydrodynamic instabilities were present. Inertial instability altered the Rossby number - vertical motion relationship by the largest amount. The effect of inertial instability was to greatly increase the magnitude of the vertical motion for the same Rossby number.

The removal of vertical shear reduced the values of vertical motion and Rossby numbers to very low numbers in all cases. This indicated vertical shear (thermal wind) is required to initiate significant vertical motions. The variability of curvature indicated that increasing the curvature increased both the Rossby number and vertical motion. The cyclonic cases showed the largest increase. On the other hand, the increases of vertical motion due to inertial instability was more likely with strong anticyclonic jet streaks.

The results of the numerical model simulated jet streaks were compared to observed cyclonic jet streak in the atmosphere. The comparisions indicated that actual jet streaks cause similar vertical motion patterns. The actual vertical motion magnitudes are less than the model vertical motions because of the more complicated adjustment mechanisms in the real atmosphere as compared to the model. The results indicated that the larger the Rossby number the more the vertical motion pattern varied from that of the Q-G theory vertical motions in both the model and the real atmosphere.

Accession For	
NTIS GRA&I	<input checked="" type="checkbox"/>
DTIC TAB	<input type="checkbox"/>
Unannounced	<input type="checkbox"/>
Justification	
By _____	
Distribution/ _____	
Availability Codes	
Dist	Avail and/or Special
A-1	

A COMPARISON OF DIAGNOSTIC AND KINEMATIC  
VERTICAL MOTION FIELDS ASSOCIATED WITH  
CURVED AND STRAIGHT JET STREAK ADJUSTMENT PROCESSES

Glenn Ernest Van Knowe, B.S.

A Report Presented to the Faculty of the Graduate School  
of Saint Louis University in Partial Fulfillment of  
the Requirements for the Degree of  
Master of Science

1990

*COMMITTEE IN CHARGE OF CANDIDACY:*

Associate Professor James T. Moore,  
*Chairperson and Advisor*

Professor Gandikota V. Rao

Assistant Professor Lawrence Coy

## ACKNOWLEDGEMENTS

The author wishes to express his appreciation to Dr. James T. Moore, advisor and chairman of the research committee, for his constant support and encouragement during the completion of this thesis. The author also wishes to express his appreciation to Dr. Gandikota V. Rao and Dr. Lawrence Coy, of the research committee, for their time and effort in reviewing this thesis. A special thanks is given for the computer expertise and assistance of Jim Whistler. Also, the author would like to thank Ms. Juanita Ryles for her typing help. Finally, I wish to express my most grateful thanks to my wife Sandi and son Jason for their help, patience and understanding without which this research would not have been completed.

## TABLE OF CONTENTS

Title	Page
1. Introduction .....	1
2. Background and Objectives .....	3
a. Evaluation of Dynamical Adjustment .....	3
b. Ageostrophy and Inertial Gravity Waves .....	6
c. I-G Waves and Kinematic Fields .....	8
d. Hydrodynamic Instabilities Associated with Jets ...	10
e. Problems in Measuring Winds .....	27
f. Numerical Models Useful for Jet Streaks .....	28
g. Specific Research Objectives .....	30
3. Methodology .....	32
a. Primateive Equation Model .....	32
1) Description of the Model .....	32
2) The Governing Equations .....	33
b. Computations Using Rawinsonde Data .....	41
1) Rawinsonde Data Used .....	41
2) Objective Analysis Method .....	42
3) Method of Extrapolation .....	43
4) Analytical Procedures .....	43
c. Parameterization and Model Operation.....	46
4. Results .....	53
a. Types of Jet Streak Simulations and Case Studies ..	53
b. Velocity, Kinetic Energy and Momentum Changes ....	53

TABLE OF CONTENTS (CONTINUED)

Title	Page
c. Rossby Number - Vertical Motion Relationships .....	61
d. Hydrodynamic Instabilities .....	67
e. Model Case Studies .....	72
1) Straight-Line Equivalent and Quasi Barotropic .....	72
2) Anticyclonic Equivalent and Quasi Barotropic ..	88
3) Cyclonic Equivalent and Quasi Barotropic .....	95
4) Beta Plane Cases .....	112
5) Baroclinic Cases .....	128
f. Operational Case Study .....	130
g. Role of The Inertial Gravity Wave .....	134
h. Potential Model Problems .....	140
i. Conceptual Models Consistent with Results .....	144
5. Summary and Conclusions .....	149
REFERENCES .....	152

## LIST OF TABLES

Table 1 List of PE model runs.

Table 2 Scale analysis for the forcing functions of the balanced omega equation for the synoptic scale. All terms are in units of Pa-1 s-3.

Table 3 Values of psi amplitude for various cases.

Table 4 Summary of velocity changes and vertical wind shear for all PE model runs.

Table 5 Summary of Rossby numbers and vertical motions for all PE model runs.

Table 6 Summary of cyclonic curvature variation.

Table 7 Summary of anticyclonic curvature variation.

Table 8 Rossby number comparisons for straight-line, cyclonic and anticyclonic jet streaks.

Table 9 Summary of beta plane case.

Table 10 Summary of baroclinic cases.

## LIST OF FIGURES

### Figure

Fig. 1 Fig. 1 Schematic representation of the ageostrophic motions (heavy arrows) and associated patterns of convergence (CON) and divergence (DIV) in the vicinity of (a) a straight jet streak in the absence of along-contour thermal advection and (b) a uniform jet streak within a stationary synoptic-scale wave. Both representations are assumed to apply at or near the level of maximum wind, where the horizontal wind distribution is most distinct and the flow is approximately horizontal. Solid lines indicate geopotential height of a constant pressure surface; dashed lines are isotachs (maximum wind speed shaded). Adapted from Shapiro and Kennedy (1981).

Fig. 2 Jet streak configurations and associated fields of divergence/convergence (Beebe and Bates, 1955).

Fig. 3 a) Parcel motion in a stably stratified atmosphere creating an I-G wave (After Hooke, 1982). b) Idealized cross section showing phases of the geopotential, temperature, and, velocity perturbations for an internal gravity wave. Thin arrows indicate phase of perturbation velocity field, blunt arrows indicate the phase velocity (After Wallace and Kousky, 1968).

Fig. 4 Outline of Hydrodynamic instability.

Fig. 5 Kelvin-Helmholtz instability of stratified shear flow.

Fig. 6 Subharmonic resonance.

Fig. 7 The imbalance of forces of a jet streak.

Fig. 8 a) Gravity-wave energy and phase propagation (after Hooke, 1986). b) Gravity-wave generation by penetrative convection (after Hooke, 1986). c) Areas of jet streak destabilization due to gravitational modes.

Fig. 9 Vorticity pattern for a straight-line jet streak.

Fig. 10 a) Neutral stability curve for a two-level baroclinic model with beta = 0 (Holton, 1979). Neutral stability curve for the two-level baroclinic model beta not equal to zero (Holton, 1979).

Fig. 11 Locations of U.S. and Canadian rawinsonde stations to be used in this study.

Fig. 12 Vertical structure and placement of variable in the model (Houghton et al., 1981).

Fig. 13 Example of the grid values and corresponding area of U.S.

Fig. 14 ANSIT file example for various jet streak cases.

Fig. 15 Example of ANSPE file.

Fig. 16 Plotting answer file examples.

Fig. 17 Barnes (1973) response function for observational data set.

Fig. 18 Straight-line PE vertical motion versus Rossby number.  
Fig. 19 Straight-line I-G vertical motion versus Rossby number.

Fig. 20 Equivalent barotropic PE vertical motion versus Rossby number.

Fig. 21 Equivalent barotropic I-G vertical motion versus Rossby number.

Fig. 22 Equivalent barotropic balanced vertical motions versus Rossby number.

Fig. 23 Equivalent barotropic PE vertical motion versus curvature.

Fig. 24 Equivalent barotropic vertical motion versus vertical shear.

Fig. 25 Initial 400 mb winds for Quasi and equivalent barotropic conditions.

Fig. 26 12 hour 400 mb winds for Straight-line equivalent barotropic conditions.

Fig. 27 12 hour 400 mb winds for straight-line quasi-barotropic conditions.

Fig. 28 Initial hour balanced and PE equivalent barotropic vertical motion.

Fig. 29 Initial and 12 hour balanced and PE quasi-barotropic vertical motion.

Fig. 30 12 hour vertical motion PE equivalent barotropic conditions.

Fig. 31 12 hour balanced equivalent barotropic vertical motion.

Fig. 32 12 hour vertical motion IG equivalent barotropic conditions.

Fig. 33 Initial hour equivalent barotropic absolute vorticity.

Fig. 34 12 hour equivalent barotropic absolute vorticity.

Fig. 35 Initial hour equivalent barotropic absolute vorticity variation with latitude.

Fig. 36 12 hour equivalent barotropic absolute vorticity variation with latitude.

Fig. 37 Initial hour Rossby number (Ro) for equivalent barotropic conditions.

Fig. 38 12 hour Rossby number (Ro) equivalent barotropic.

Fig. 39 12 hour inertially unstable absolute vorticity values.

Fig. 40 12 hour inertially unstable PE vertical motion.

Fig. 41 Initial hour anticyclonic 400 mb wind speed.

Fig. 42 12 hour anticyclonic 400 mb wind speed.

Fig. 43 Initial hour PE vertical motion.

Fig. 44 12 hou. PE vertical motion.

Fig. 45 Initial hour absolute vorticity.

Fig. 46 12 hour absolute vorticity.

Fig. 47 Initial hour absolute vorticity variation with latitude.

Fig. 48 12 hour absolute vorticity variation with latitude.

Fig. 49 Initial hour Rossby number (Ro) for equivalent barotropic conditions.

Fig. 50 12 hour Rossby number (Ro) for equivalent barotropic conditions.

Fig. 51 Initial hour cyclonic 400 mb wind speed.

Fig. 52 12 hour cyclonic 400 mb wind speed equivalent barotropic conditions.

Fig. 53 12 hour cyclonic wind speed quasi-barotropic conditions.

Fig. 54 Initial hour PE vertical motions for equivalent barotropic conditions.

Fig. 55 12 hour PE vertical motions for equivalent barotropic conditions.

Fig. 56 12 hour balanced vertical motion for equivalent barotropic conditions.

Fig. 57 12 hour I-G vertical motions for equivalent barotropic conditions.

Fig. 58 Initial hour absolute vorticity for equivalent barotropic conditions.

Fig. 59 12 hour absolute vorticity for equivalent barotropic conditions.

Fig. 60 Initial hour absolute vorticity variation with latitude.

Fig. 61 12 hour absolute vorticity variation with latitude.

Fig. 62 Overlay of jet axis, vorticity variation with latitude and absolute vorticity for initial hour.

Fig. 63 Initial hour Rossby number ( $\text{Ro}$ ).

Fig. 64 12 hour Rossby number ( $\text{Ro}$ ).

Fig. 65 Inertial unstable absolute vorticity values.

Fig. 66 Inertial unstable PE vertical motion.

Fig. 67 Initial hour cyclonic 400 mb  $\text{Ro} = 1.4$ .

Fig. 68 12 hour cyclonic 400 mb  $\text{Ro} = 0.85$ .

Fig. 69 12 hour PE vertical motion for straight-line  $f$  plane.

Fig. 70 12 hour PE vertical motion for straight-line beta plane.

Fig. 71 12 hour PE vertical motion for an inertially unstable anticyclonic jet streak on a  $f$  plane.

Fig. 72 12 hour PE vertical motion for an inertially unstable anticyclonic jet streak on a beta plane.

Fig. 73 Initial hour PE vertical motion easterly low level jet.

Fig. 74 12 hour PE vertical motion low level easterly jet.

Fig. 75 Comparison of straight-line (A) with cyclonic vertical motion (B).

Fig. 76 a) PE model isotachs and b) vertical motions.

Fig. 77 a) 10 Jan 1990 isotachs and b) vertical motions.

Fig. 78 a) PE model 12 hour I-G vertical motions 38 m/s straight-line jet streak. b) PE model 12 hour I-G vertical motions 38 m/s cyclonic jet streak. c) PE model 12 hour I-G vertical motions 38 m/s anticyclonic jet streak.

Fig. 79 Conceptual model of the large scale balanced kinematic vertical motions as a jet streak propagates through a short wave trough and ridge (after Molinaro, 1988).

Fig. 80 a) Example of a direct thermal circulation. b) Example of an indirect thermal circulation.

Fig. 81 Conceptual model of idealized kinematic vertical motions to include I-G wave motions. Vertical motion is on the left and chi fields are on the right. Dashed lines indicate upward motion, solid lines downward motion for vertical motion.

## 1. INTRODUCTION

The existence of a narrow band of very strong organized tropospheric winds we now call the jet stream was discovered as the result of high altitude flights between 6 to 12 km (20,000 to 40,000 feet) during World War II. The jet stream, a macro scale phenomena, was soon linked to the general circulation and tropospheric- stratospheric relationships. It also became evident that the jet stream could provide the dynamics for both frontogenesis and cyclogenesis through the adjustment processes associated with the area of maximum wind speeds. These jet stream maxima but have more recently been called jet streaks.

The entire jet stream system is a very large scale feature having a horizontal dimension scale of 1000 - 8000 km. On the other hand the jet streak is an order of magnitude smaller with a horizontal scale between 200 and 1000 km . Using Orlanski's (1975) scheme , the jet stream system is predominantly in the macro  $\beta$  horizontal scale while the jet streak is meso  $\alpha$  scale (Orlanski, 1975). The classic definition of the synoptic scale encompasses both the larger meso  $\alpha$  and smaller macro  $\beta$  phenomena ranging from 1000 - 2500 km (Huschke, 1959). Therefore, the adjustment process associated with jet streaks is a hybrid phenomena requiring both synoptic-scale essentially balanced quasi-geostrophic dynamic principles and ageostrophic unbalanced mesoscale dynamic principles (Bluestein, 1986). A good method for studying the kinematic fields accompanying jet streaks is to examine the unbalanced vertical motions and ageostrophic wind flow associated with the jet streaks' direct and indirect thermal circulations. The development of ageostrophic wind components associated with jet streaks takes place simultaneously with the development of vertical motion.

The typical vertical motion and divergence - convergence pattern for well defined straight jet streaks at their maturity have been investigated and described by many

authors (e.g. Beebe and Bates, 1955). A few qualitative analysis have been done on the effects of adding curvature to jet streaks and the resulting vertical motions (e.g. Bluestein and Thomas, 1984). However, little quantitative analysis of curved jet streaks and jet streaks in the process of forming and weakening has been done. The result has been the overemphasis of the classic four cell vertical motion - divergence pattern. This has resulted in the general assumption by the operational meteorological community that the vertical motion and divergence pattern of straight jet streaks is present throughout the life cycle of all jet streaks. Such assumptions may result in the misdiagnosis of the synoptic scale vertical motions. This is critical both to the understanding of the dynamics of synoptic and subsynoptic scale systems as well as to making accurate operational meteorological forecasts.

In order to understand the true vertical motion patterns that result from the adjustment processes of a jet streak the production of unbalanced vertical motions must be examined. The most likely cause of vertical motions associated with jet streaks are fundamentally unbalanced inertial-gravity (I-G) waves produced by the jet streak (Houghton, et al 1981). Van Tuyl and Young (1982) showed that the production of I-G waves for straight jet streaks is a function of maximum winds speed, vertical wind shear and horizontal wind shear along with the strength of the vertical motions. They developed a relationship between the large synoptic scale Rossby number and both the production of I-G waves and strength of vertical motions. Molinaro (1988) developed a separate relationship for curved jet streaks. The purpose of this paper is to examine the concept of the Rossby number in order to develop a more general diagnostic relationship between the production of I-G waves, vertical motion strength and Rossby number. In addition, the possibility of the existence of hydrodynamic instabilities that may impact the jet streak adjustment process will be examined.

## 2. Background and Objectives

### a. Evaluation of Dynamical Adjustment

There are several methods that may be used to investigate the dynamical adjustment processes that occur in the jet streak. Various methods employ the use of the ageostrophic winds. All methods using the ageostrophic wind are based on the basic ageostrophic relationship:

$$\vec{V}_{ag} = \vec{V} - \vec{V}_g \quad (1)$$

where  $\vec{V}$  is the observed wind  $\vec{V}_g$  is the geostrophic wind and  $\vec{V}_{ag}$  is the ageostrophic wind. The most common form as described by Haltiner and Martin (1957), separates the ageostrophic wind into three components, the local wind tendency, inertial - advective and convective - inertial winds.  $\vec{V}_{ag}$  can be written as:

$$\vec{V}_{ag} = \frac{\hat{k}}{f} \times \frac{d\vec{V}}{dt} \quad (2)$$

and rewritten in pressure coordinates as:

$$\vec{V}_{ag} = \frac{\hat{k}}{f} \times \left( \begin{matrix} A & B & C \end{matrix} \right) \vec{V} \quad (3)$$

where A is the local wind tendency B is the inertial - advection and C the convective - inertial terms. Term A evaluates the effect of changes in the observed winds on the geostrophic wind over time, term B evaluates the effect of changes in wind speed and direction downstream on the ageostrophic wind and term C evaluates the creation of ageostrophic wind components due to the vertical movement of an air parcel into varying pressure gradients. A second method discussed by Shapiro and Kennedy (1981) and used by Molinaro (1988) separates the ageostrophic wind into along-contour and cross-contour components with respect to the geostrophic wind. The

equation for this relationship is given as:

$$\vec{V}_{ag} = \vec{V}_{ac} + \vec{V}_{cc} \quad (4)$$

where  $V_{ac}$  and  $V_{cc}$  are the along- and cross- contour ageostrophic wind components, respectively. The advantage of splitting the ageostrophic wind into these two components is the ability to isolate the particular component which are associated with a specific kinematic properties of the jet streak.

Equation (3) can be simplified by making several restrictive assumptions that make the equation easier to calculate and understand. However, the assumptions restrict the meteorological conditions for which they are valid. The assumptions made by Hoskins (1975) were adiabatic conditions, frictionless flow, hydrostatic equilibrium and the validity of the geostrophic momentum approximation given by:

$$\left| \frac{d\vec{V}_{ag}}{dt} \right| \ll \left| \frac{d\vec{V}_g}{dt} \right| \quad (5)$$

Thus (3) can be redefined as:

$$\vec{V}_{ag} \approx \frac{\hat{k}}{f} \times \begin{matrix} A & B \\ \left( \frac{\partial}{\partial t} + \vec{V} \cdot \nabla \right) \vec{V}_g \end{matrix} \quad (6)$$

In this case term A is called the isallobaric term which evaluates the impact of pressure or height field changes on the ageostrophic wind. Term B is called the inertial-geostrophic-advection term which is used to describe the effect of downstream change of the geostrophic wind on the ageostrophic wind.

The along-contour wind component is associated with the curvature of the shortwave while the cross-contour component is associated with the along-stream wind shear of the jet streak. These two ageostrophic components have been linked by Keyser and Shapiro (1986) to both the vertical circulation and divergence fields within baroclinic flows. Molinaro (1988) showed the relative importance of curvature in developing an along-contour wind component for several types of jet streaks.

Another method utilizing ageostrophic winds, to be employed in this report is to use the relationship of the Rossby number to the vertical motions associated with the jet streaks. The non-dimensional Rossby number is defined as the ratio of the inertial advective force to the Coriolis force. The Rossby number is a good method to quantitatively evaluate the validity of the geostrophic approximation for a given set of meteorological conditions. Houghton et al. (1981), Van Tuyl and Young (1982) and Molinaro (1988) evaluated the production of I-G waves and resulting vertical motions based on the large scale Rossby number ( $\tilde{Ro}$ ), which is given as:

$$\tilde{Ro} = \frac{U}{fL} \quad (7)$$

where  $U$  is the maximum core speed at 400 mb,  $f$  is the Coriolis parameter and  $L$  is the characteristic wavelength.  $L$  is taken to be 1000 km for synoptic scale systems. Holton (1979) gives:

$$\tilde{Ro} = \frac{U}{fR} \quad (8)$$

for curved flow where  $R$  is the radius of curvature. For most synoptic scale jet streaks  $R = L$  and is not very useful in distinguishing for the curvature effect on the synoptic scale. However, Van Tuyl and Young (1982) give a form of the Rossby number based on the defining equation:

$$Ro = \frac{\left| \frac{\partial \vec{V}}{\partial t} \right|}{f \left| \vec{V} \right|} \quad (9)$$

which can be shown to equal:

$$Ro = \frac{\left| \vec{V}_{ag} \right|}{\left| \vec{V} \right|} \quad (10)$$

for frictionless flow. The Rossby number in this form is a good method to quantita-

tively measure the degree of ageostrophy. Van Tuyl and Young (1982) felt that (10) was a more dynamically oriented Rossby number equivalent and could be used to make a more detailed evaluation of the adjustment process and resulting vertical motion I-G wave patterns.

Van Tuyl and Young (1982) as well as other studies have shown the importance of ageostrophic winds in the vicinity of straight-line I-G wave patterns.

b. Ageostrophy and Inertial-Gravity waves

Van Tuyl and Young (1982) as well as other studies have shown the importance of ageostrophic winds in the vicinity of straight-line upper-level jet streaks to the formation of associated kinematic fields. Molinaro (1988) demonstrated the significant role that curvature also plays in creating ageostrophic winds. If the actual wind was always in true geostrophic balance the flow could be completely defined by geopotential height fields. However, it is the ageostrophic component of the actual wind that causes the adjustments in the mass-momentum fields.

Thus the mesoscale meteorological environment is altered by the ageostrophic wind resulting in many of the more significant observed weather changes and phenomena such as organized convection. It is imperative that operational meteorologists understand the impact of ageostrophy on both the synoptic scale and immediate mesoscale environment.

When looking at the two components of the ageostrophic winds it becomes evident that the cross-contour component is related to the magnitude of the horizontal wind shear. Shapiro and Kennedy (1981) described the convergence-divergence caused by the cross-contour ageostrophic wind component in Fig. 1a. The convergence-divergence pattern caused by the along-contour ageostrophic wind component is described in Fig. 1b. The description of the cross-contour convergence-divergence areas is essentially identical to the straight jet streak convergence-divergence areas

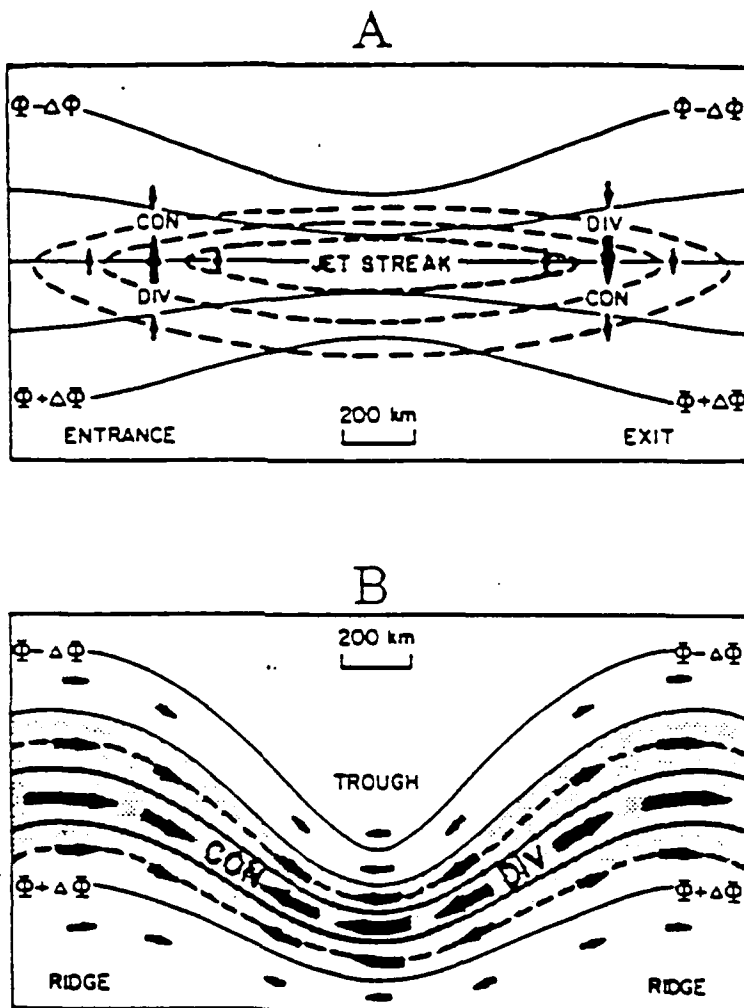


Fig. 1 Schematic representation of the ageostrophic motions (heavy arrows) and associated patterns of convergence (CON) and divergence (DIV) in the vicinity of (a) a straight jet streak in the absence of along-contour thermal advection and (b) a uniform jet streak within a stationary synoptic-scale wave. Both representations are assumed to apply at or near the level of maximum wind, where the horizontal wind distribution is most distinct and the flow is approximately horizontal. Solid lines indicate geopotential height of a constant pressure surface; dashed lines are isotachs (maximum wind speed shaded). Adapted from Shapiro and Kennedy (1981).

(Fig. 2a) of Beebe and Bates (1955). The along-contour component is related to curvature and is described by Shapiro and Kennedy (1981) in Fig. 1b. In the real atmosphere curvature as caused by a baroclinic shortwave would often be superimposed on a jet streak. Beebe and Bates 1955 (Fig. 2b and 2c) demonstrated qualitatively the readjustment of the convergent- divergent pattern of a jet streak due to the superposition of either a shortwave trough or ridge on the jet streak.

Molinaro (1988) separated the ageostrophic wind into along and cross contour components when analyzing for both speed and curvature. His results showed that curvature can very often dominate the vertical motion and divergence field. These results help to quantify the qualitative studies on the effects of curvature on the vertical motion field done by Bluestein and Thomas (1984). The result should serve the operational meteorological community by providing guidance as to the relative importance of curvature and speed to the production of vertical motion by a jet streak.

#### c. I-G Waves and Kinematic Fields

Houghton et al (1981) describes how vertical motions can be broken into two parts. One is a balanced component which is similar to the quasi-geostrophic approximation. The other is a fundamentally quasi-geostrophic approximation. The major component of the unbalanced motions is derived from the production of unbalanced I-G waves produced by the adjustment process of a jet streak.

The production of I-G waves have been linked to significant weather events by previous studies especially convective storms (e.g. Uccellini, 1975). The most significant I-G waves for the production of severe convection are large amplitude I-G waves with periods on the order of three hours. Van Tuyl and Young (1982) demonstrated that straight jet streaks can produce I-G waves of this type. Molinaro (1988) described how adding curvature as the result of superimposing a baroclinic wave can enhance the I-G wave development.

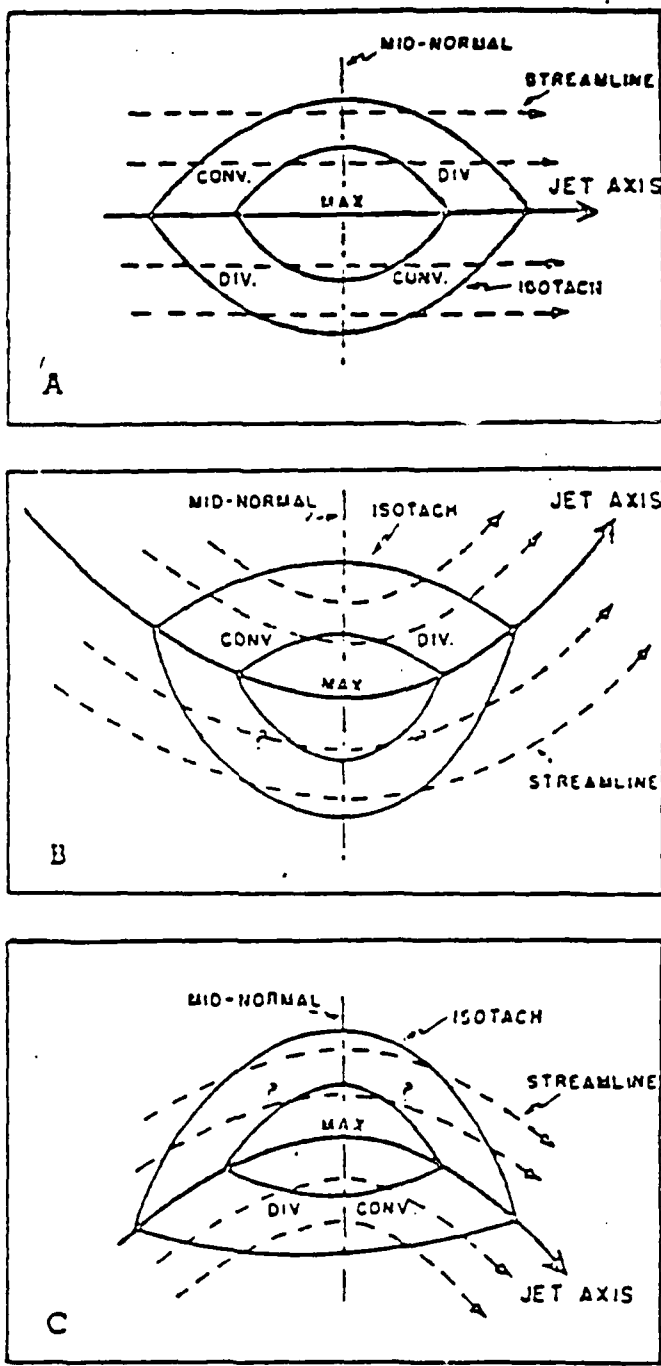


Fig. 2 Jet streak configurations and associated fields of divergence/convergence (Beebe and Bates, 1955).

The kinematic fields needed to study the production of I-G waves are mid-level vertical motion and upper-level divergence. To calculate mid-level vertical motion the kinematic omega relationship is used:

$$\omega_P = \omega_{P+\Delta P} + \overline{(\nabla \cdot \vec{V}_2)} \Delta P \quad (11)$$

The development of vertical motion and divergence are diagnostic evidence for the development of an ageostrophic circulation in the upper level-jet streak. In order to compute the role that the unbalanced I-G waves play in the total vertical motion, a knowledge of the balanced vertical motions is required. In the past the quasi-geostrophic approximation has been used to identify balanced motion. However, the quasi-geostrophic approximation still retains some unbalanced modes in its solution to vertical motion. Krishnamurti (1968) provided a solution for obtaining the truly balanced motions by developing a balanced model. The unbalanced vertical motions can be obtained by finding the difference between the kinematic vertical motions and the balanced vertical motions. The unbalanced vertical motions were related to the production of I-G waves by both Houghton et al (1981) and Van Tuyl and Young (1982) for straight jet streaks. Fig. 3a shows how parcel motion in a stable atmosphere will create I-G waves, Fig. 3b shows the thermal structure and phase velocity of an I-G wave. Molinaro (1988) showed how curvature, especially cyclonic, enhanced the unbalanced vertical motion and thus increased the production of gravity waves, by analyzing the effects of the along- and cross-contour ageostrophic wind components. A list of the cases investigated in this research is provided in Table 1.

#### d. Hydrodynamic Instabilities Associated with Jet Streaks

Past jet streak studies have alluded to the potential of hydrodynamic instabilities occurring in conjunction with jet streaks (e.g. Van Tuyl and Young, 1982), which would greatly alter the divergence and vertical motion pattern. The major difficulty in analyzing for the presence of a particular hydrodynamic instability is to find a

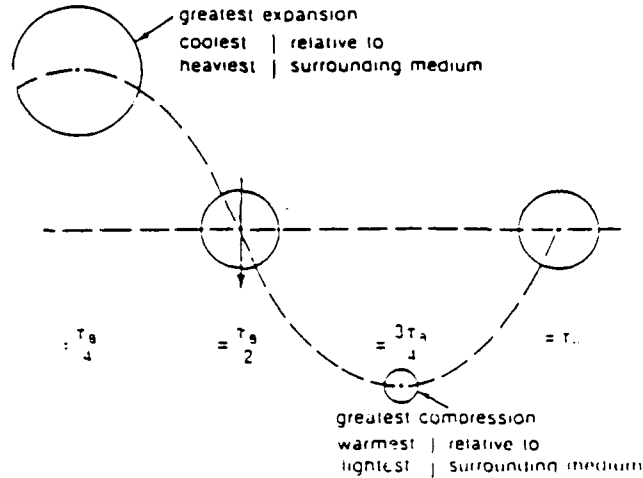


Fig. 3a Parcel motion in a stably stratified atmosphere creating an I-G wave  
(After Hooke, 1966.)

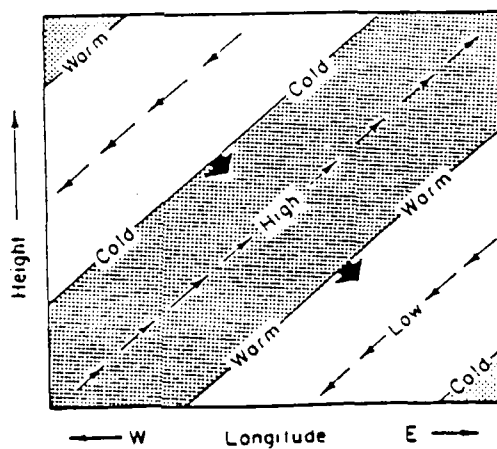


Fig. 3b Idealized cross section showing phases of the geopotential, temperature, and velocity perturbations for an internal gravity wave. Thin arrows indicate phase of perturbation velocity field, blunt arrows indicate the phase velocity. (After Wallace and Kousky, 1968.)

LIST OF PE MODEL RUNS TABLE 1

QB = quasi-barotropic                    EJ = low-level easterly jet  
EB = equivalent barotropic              ST = straight  
BC = baroclinic                         CY = cyclonic  
BETA = beta plane                        AC = anticyclonic

NUMBER	DESCRIPTION	INITIAL VELOCITY (100 m)
**QBAR0**		
1	ST QB	11.9
2	ST QB	25.5
3	ST QB	35.6
4	ST QB	38.2
5	ST QB	50.8
6	CY QB	34.7
7	AC QB	34.5
**EQBAR**		
8	ST EB	28.0
9	ST EB	38.6
10	ST EB	52.0
11	CY EB	26.0
12	CY EB	34.2
13	CY EB	37.0
14	CY EB	52.0
15	CY EB	68.9
16	AC EB	28.0
17	AC EB	35.6
18	AC EB	52.0
19	AC EB	74.0
20	BETA EB ST	38.6
21	BETA EB CY	35.6
22	BETA EB AC	35.6
23	BETA AC UNST	73.4

\*\*BAROC\*\* (SEPERATION IN KM)

24	ST BC (8)	38.6
25	ST BC (14)	38.5
26	ST BC (20)	38.5
27	CY BC (8)	35.0
28	CY BC (14)	35.0
29	CY BC (20)	35.1
30	AC BC (8)	35.7
31	AC BC (14)	35.8
32	AC BC (20)	36.0
33	EJ BC	34.5

\*\*CURVATURE\*\* (RADIUS OF CURVE.)

34	CY (+0.75)	38.0
35	CY (+1.00)	38.0
36	CY (+1.25)	38.0
37	CY (+1.50)	38.0
38	CY (+1.75)	38.0
39	CY (+2.00)	38.0
40	AC (-0.75)	38.0
41	AC (-1.00)	38.0
42	AC (-1.25)	38.0
43	AC (-1.50)	38.0
44	AC (-1.75)	38.0
45	AC (-2.00)	38.0

method that isolates both necessary and sufficient condition for the particular instability.

Instability in general terms is experienced for a fluid in steady state flow for which certain disturbances grow with time and may or may not reach a new steady state. An alternate view of instability can be described as starting with nearly identical situations and letting initial conditions vary only a little. The fluid is unstable if the solutions diverge with time to create very different conditions from one another. This means that instability infers a certain amount of unpredictability. The atmosphere is a fluid that is believed to be fundamentally unstable in the sense described above. This fact is demonstrated by the various numerical simulation models along with atmospheric observations. Jet streaks are subject to various specific forms of instability that can greatly impact the secondary circulations and vertical motion patterns associated with the jet streak.

There are often terminology differences to describe identical instabilities. To avoid confusion, the approach outlined in Fig. 4 will be used.

Computational instability is introduced into the wave solutions through the finite difference approximations equations of the actual differential wave equation. That is, computational instability is the spurious growth of a wave due solely to the method of computation and not to any physical cause. There are two fundamental results of computational instability. First, small waves, real or noise, which violate specified computational stability criterion (i.e., CFL) will amplify spuriously and eventually destroy a numerical solution. Also, increased sensitivity to initial conditions will cause slightly different initial conditions to eventually produce very different wave solutions. Computational instability is of particular concern because of the high speed gravity waves produced during the adjustment process. The model used in this study eliminates linear computational instabilities and non-linear instabilities are not present for realistic meteorological conditions through 24 hours.

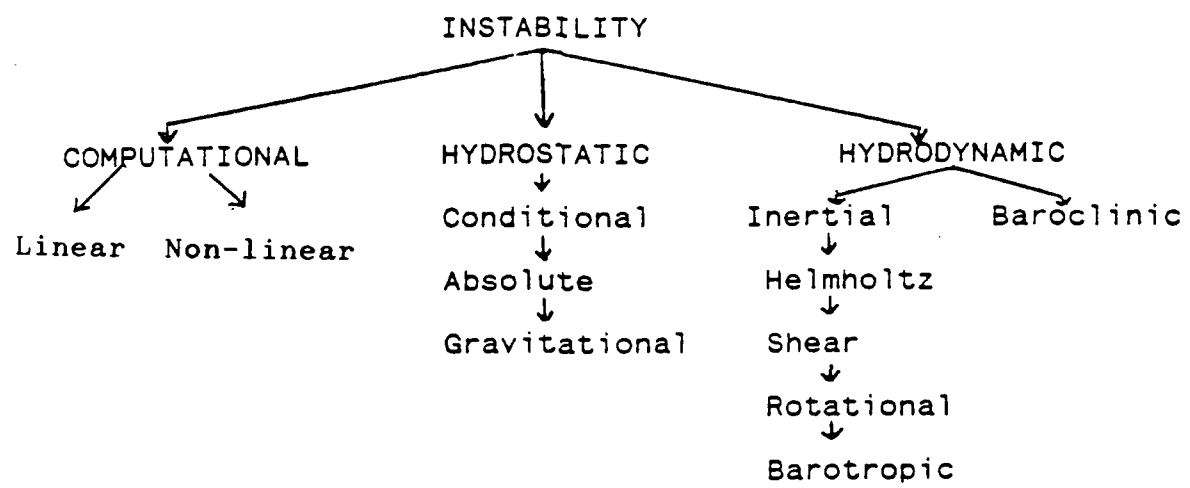


Fig.4 Outline of Hydrodynamic instability.

Hydrostatic instability deals with vertical parcel displacement in an atmosphere that is under hydrostatic equilibrium. Essentially static instability involves an environmental lapse rate that is greater than the dry or moist adiabatic lapse rate depending on saturation conditions. Hydrostatic equilibrium will also affect jet streak adjustment as statically stable conditions are required to produce gravity waves. Essentially, in a statically unstable atmosphere, any gravity waves produced would have an infinitely large amplitude growing without bounds. In addition, static stability will modify vertical wave speed.

Hydrodynamic instability deals with the instability of parcel displacement or waves in a moving fluid system in which the hydrostatic approximation may or may not be valid. There are two basic forms of hydrodynamic instability. Inertial instability occurs when the only form of energy transferred from the steady state to the disturbance is kinetic. Baroclinic instability involves the transfer of potential energy of the mean flow to the potential and kinetic energy of the disturbance. First the several forms of inertial instability will be looked at in greater detail.

Helmholtz (or Kelvin-Helmholtz) shear instability is an inertial instability form that arises from a shear discontinuity in the current speeds at the interface of two fluids with density differences in two dimensional flow. The normal vertical shear in the atmosphere is Helmholtz unstable but generally not strong enough to overcome static stability. Miles and Howard (1961) demonstrated that a necessary but not sufficient condition to ensure instability is  $Ri < \frac{1}{4}$ . Figure 5 shows Helmholtz instability for a fresh water-brine layered shear flow. In the atmosphere the unstable Helmholtz waves will tend to grow in wavelength and interact with stable gravity waves as depicted in Fig. 6. The most intense Helmholtz waves are found near the upper tropospheric jet stream or with strong mountain waves (Lilly, 1986). Helmholtz instability is below the resolution of our model and will not be considered as playing a role.



Figure 5 Kelvin-Helmholtz instability of stratified shear flow. A horizontal rectangular tube is filled with water above colored brine. The fluids are allowed to diffuse for about an hour, after which the tube is quickly tilted  $6^\circ$ . The brine accelerates down the slope, and the water accelerates up the slope. Sinusoidal instability of the interface occurs after a few seconds and has here grown nonlinearly into overturning waves. (From Thorpe, 1971.)

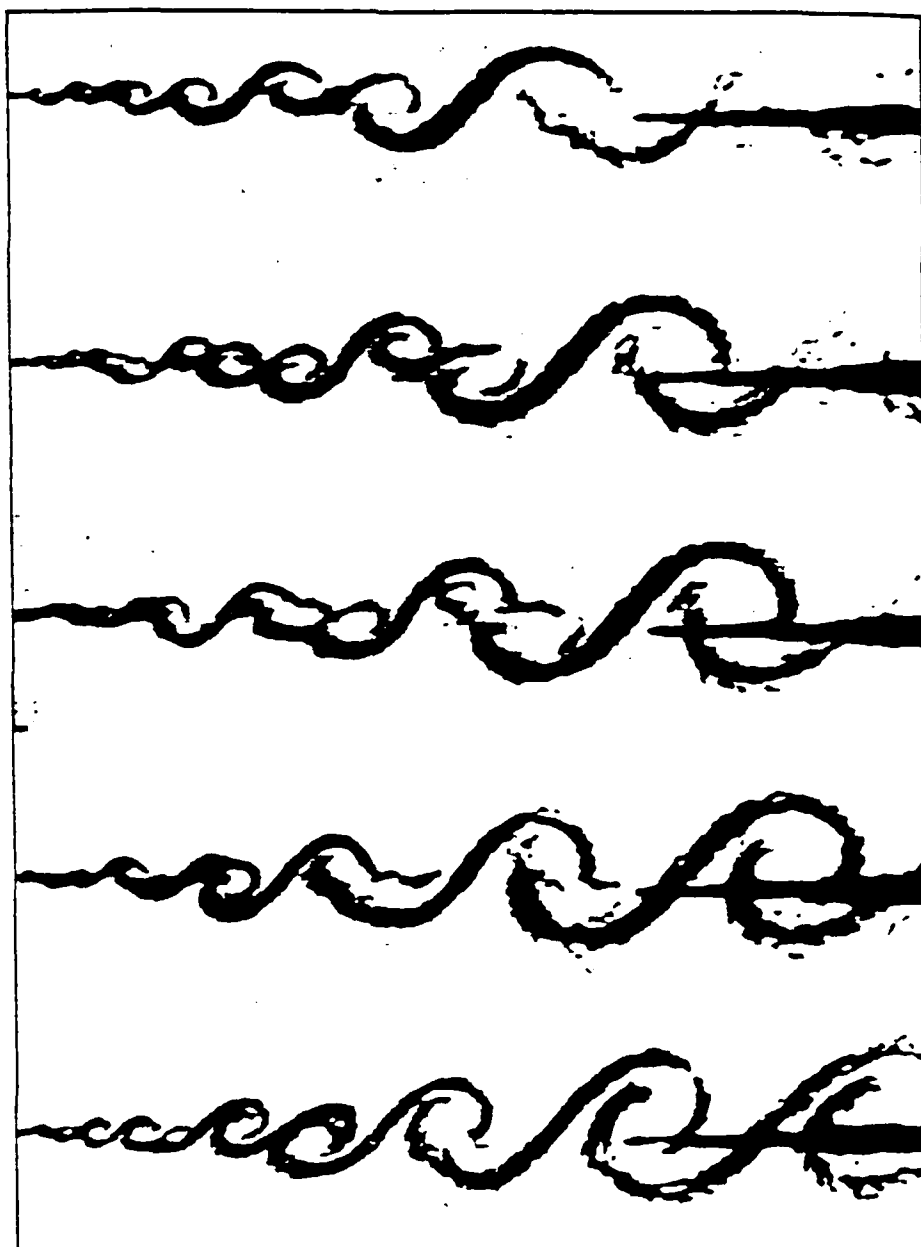


Figure 6 Subharmonic resonance. The small vortex rolls in the left part of the top frame are seen to combine into larger rolls in the later frames. (LILLY, 1986)

Shear instability is a term used to describe a complex inertial instability observed for wavelengths of  $\simeq 1000$  km in a two fluid system possessing static stability. Shear instability is associated along with baroclinic instability with the growth of cyclonic waves on the polar front (Huschke, 1959).

Rotational inertial instability, which is often just referred to as inertial instability, is the instability of a rotating fluid where the kinetic energy of the disturbance grows at the expense of the kinetic energy of rotation. The rotating fluid will be unstable if the angular momentum decreases outward meeting the following criteria:

$$R \frac{\partial \omega_a}{\partial R} + 2\omega_a < 0 \quad (12)$$

where  $R$  = distance from the center of rotation

$\omega_a$  = absolute angular velocity

Rotational inertial instability is caused by an imbalance between the pressure gradient force (PGF) and the Coriolis force (CF) in such a manner that the displaced parcel is accelerated from its origin as shown in the Fig. 7.

For rotational instability to exist the net force must be away from the original parcel position. This can not happen north of the jet axis because a northward displaced parcel (B to A) will become supergradient with CF overbalancing PGF and a southward displaced parcel (A to B) will become subgradient with PGF overbalancing CF. Both situations will tend to bring the parcel back to its original position, they therefore represent a stable condition. The situation is more complicated south of the jet axis. Stability will be controlled by the shear gradient. If a parcel is displaced southward (C to D) the tendency is for the parcel to become supergradient. However, as the parcel moves southward the value of  $f$  decreases helping to maintain a stable condition for certain weaker shear strengths. Similarly, a parcel displaced northward (D to C) the tendency is for the parcel to become subgradient but in this case  $f$  increases delaying instability. The critical value that determines instability is the

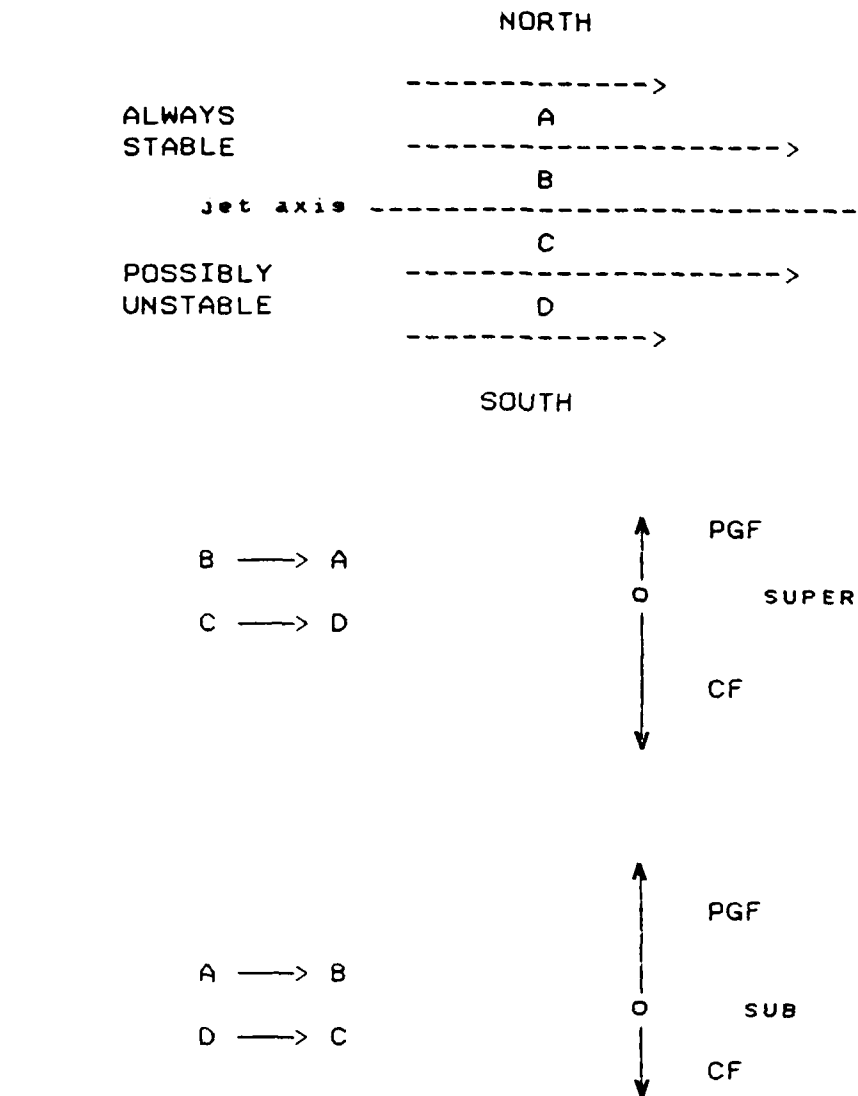


Fig. 7 The imbalance of forces of a jet streak.

value of relative vorticity which will in most instances be dominated by the shear term. If the value of  $f <$  the value of relative vorticity, or in other words negative values of absolute vorticity, instability occurs. With negative values of absolute vorticity, a displaced parcel south of the jet axis will experience an imbalance of forces in the direction away from the origin of the parcel. That is PGF will overbalance CF in the case of the northward displaced parcel and CF will overbalance PGF in the case of a southward displaced parcel. Such an environment is unstable and favorable for wave growth.

Rotational inertial instability is most likely to be found on the equatorward side of strong jet streaks with anticyclonic curvature in lower latitudes (Hess, 1959). A destabilizing mechanism that may link rotational inertial instability, gravity waves and jets can be tracked with the jet streak. Gravity waves are produced by the rapid upward (right rear and left front) and rapid downward (left rear and right front) motions associated with the secondary circulations around a jet streak as previously described. The gravity waves will tend to be unstable in the right front region that is generally associated with subsiding air because of the inertial instability (see Fig. 8a, 8b and 8c). Gravity waves have been observed to propagate in this area at speeds of 10 to  $60 \text{ m s}^{-1}$  with vertical amplitudes of 0.3 to 2.0 mb with  $Ri < 0.25$  and statistically stable conditions. Occasionally the vertical motions associated with the gravity waves may be strong enough to initiate organized convection. This is also dependent on the rate at which the jet streak itself is propagating as too rapid propagation would prevent enough time for the gravity waves to destabilize the atmosphere (McGinley, 1986). Rotational inertial instability is very likely occurring for some conditions run in the model and will be analyzed.

Barotropic instability is a form of inertial instability that requires discontinuities in the horizontal shear field as compared to rotational instability which required discontinuities in the wind field to produce specified wind shear values. The wind

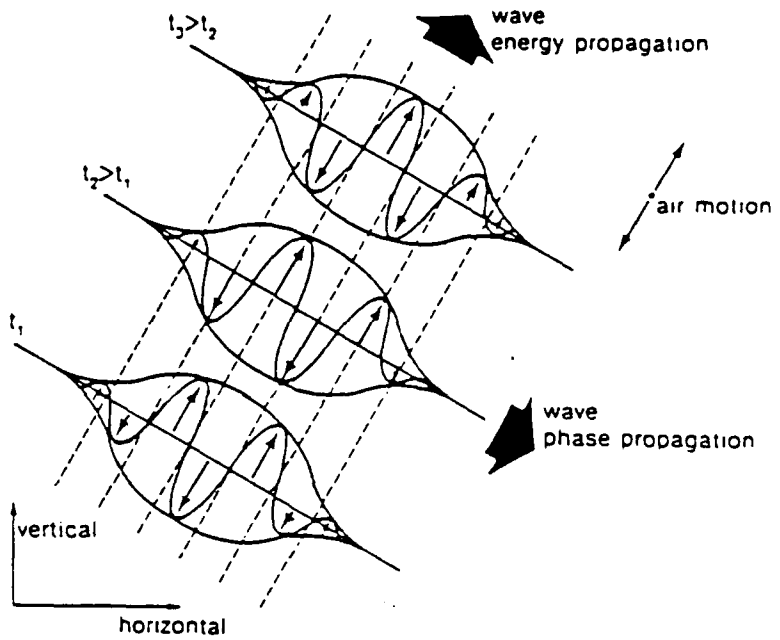


Figure 8a Gravity-wave energy and phase propagation. (Hooke, 1986)

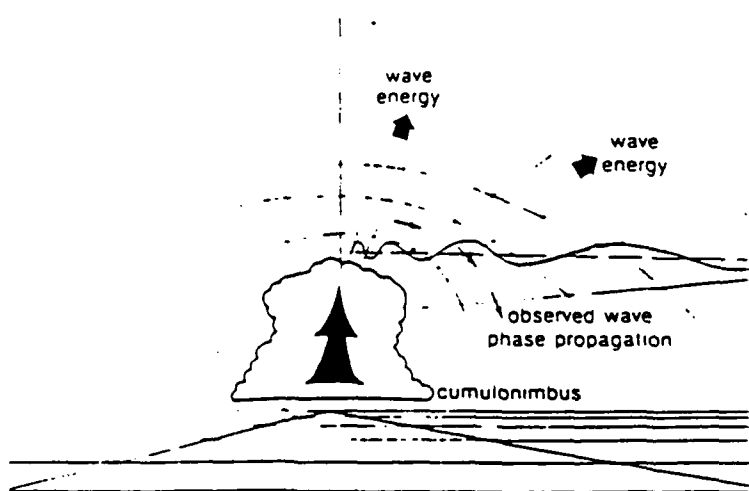


Figure 8b Gravity-wave generation by penetrative convection. (Hooke, 1986)

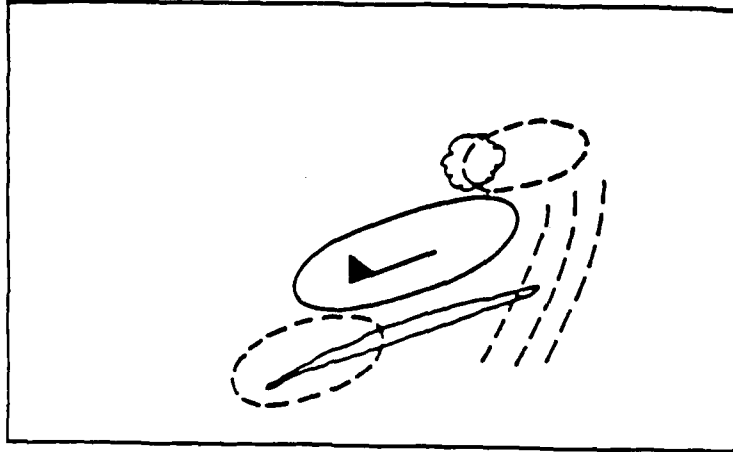


Figure 8c Areas of destabilization (dashed) relative to a jet maximum (solid). On the right-front quadrant, lift may be due to gravitational modes. Often cirrus streaks appear south of wind maximum and middle clouds on left-front side, as illustrated. (Hooke, 1986)

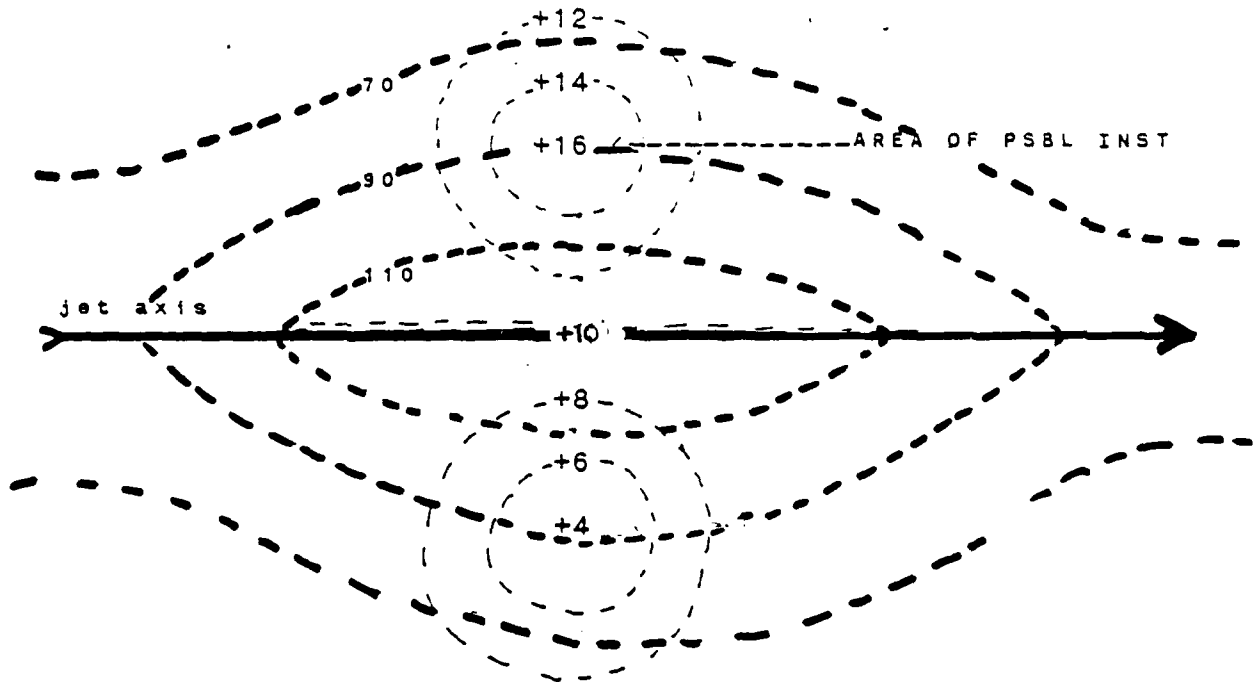


Fig. 9 Vorticity pattern for a straight-line jet streak.

----- Absolute Vorticity  $\times 10^{-5}$  sec $^{-1}$   
— — Isotachs in knots

shear discontinuities required for barotropic instability are such that the absolute vorticity gradient of the mean current must change sign. That is:

$$\frac{d\eta}{dy} = 0 \quad (13)$$

The above is a necessary condition for barotropic instability but does not guarantee barotropic instability.

As the name implies no vertical shear (thermal wind) is required for barotropic instability, it is completely independent of baroclinic instability. The vorticity pattern surrounding a straight-line jet streak and possible locations of barotropic instability are shown in Fig. 9.

Even though baroclinic instability is considered the more significant instability associated with midlatitude jet streams, barotropic instability will be considered when examining the jet streaks.

Baroclinic instability is a hydrodynamic instability that depends on the vertical shear (thermal wind) that is caused by the existence of a meridional (N-S) temperature gradient. For baroclinic instability to exist the atmosphere must be in quasi-geostrophic equilibrium and statically stable. Baroclinic instability is very different from the inertial forms of hydrodynamic instability in that it is the potential energy of the mean flow as stored in the thermal gradient that is converted to potential and kinetic energy of the disturbance.

Using Holton's (1979) description for a wave to exhibit baroclinic instability the phase speed ( $c$ ) is required to satisfy:

$$c = U_M - \frac{\beta(k^2 + \lambda^2)}{k^2(k^2 + \lambda^2)} \pm \delta^{1/2} \quad (14)$$

$$\delta = \beta\lambda^4/k^4(k^2 + 2\lambda^2)^2 - \frac{U_T^2(2\lambda^2 - k^2)}{(k^2 + 2\lambda^2)} \quad (15)$$

where  $U_M$  = vertically averaged zonal flow

$U_T$  = basic state thermal wind

$$\lambda_2 = f_o^2 / \sigma p^2$$

$$\sigma = -\alpha \partial \theta / \partial p$$

and have an imaginary part to the solution. For this to be true  $\delta$  must be  $< 0$ .

Examining the above phase speed relationship it is evident that for  $\delta$  to have an imaginary component there must be a thermal wind. It turns out that there are three factors for instability. (1) The magnitude of  $U_T$ , the wavelength ( $L$ ) or wavenumber ( $k$ ), and the amount of static stability ( $\sigma$ ).

Looking at a two-level baroclinic model and first setting the  $\beta$  plane to zero a critical wavelength ( $L_c$ ) develops.  $L_c$  turns out to be equal  $(2\pi)^{1/2} / \lambda$ ; so for a wave to be unstable  $L > (2\pi)^{1/2} / \lambda$  and  $d\eta/dy = 0$  (which is in accordance to Rayleigh's theorem for barotropic instability). Fjortort's theorem provides another necessary but not sufficient condition for barotropic instability namely,  $(du^2/dy^2 - \beta)(U - U_s)$  must be negative except at the point where  $(du^2/dy^2 - \beta) = 0$ . Thus for barotropic instability to occur the value of absolute vorticity of the primary flow must have a maximum in the domain of the flow. The consequence of the  $\beta$  term is to increase barotropic stability away from the equator. Also, the shear term indicates that troughs and ridges that tend to tilt opposite to the wind shear will be barotropically destabilized while troughs and ridges that tilt in the same direction to the wind shear will be barotropically stabilized. The addition of the  $\beta$  plane will require a minimum value of  $U_T$  such that  $U_T > \beta/2 \lambda^2$  for instability. Thus, the addition of the  $\beta$  plane stabilizes the very long wavelengths ( $k \rightarrow 0$ ). The impact of increasing static stability would be to stabilize the shorter wavelengths (Fig. 10a and 10b) (Holton, 1979).

Of particular interest, would be to find the wavenumber (wavelength) of maximum instability. This occurs when  $dU_T/dk = 0$ . Making  $dU_T/dk = 0$  gives the minimum  $U_T$  value required for instability. The minimum  $U_T$  value required for instability occurs when  $k_m^2 = (2 \lambda^2)^{1/2}$ . The value of  $k_m$  is the value of the

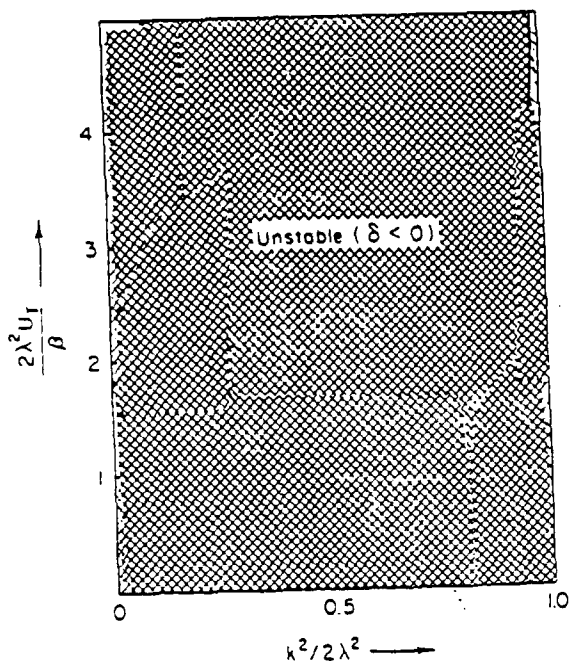


Fig. 10a Neutral stability curve for a two-level baroclinic model.  
 $\beta = 0$  (Holton, 1979).

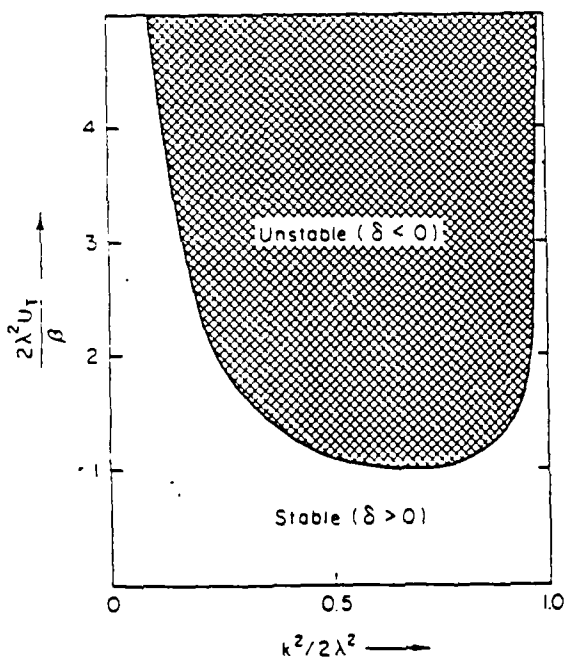


Fig. 10b Neutral stability curve for the two-level baroclinic model for  
 $\beta \neq 0$  (Holton, 1979).

wavenumber of maximum instability. These waves should amplify first and remove energy from the mean thermal wind thus stabilizing the flow. Therefore, one would expect to find that when disturbances with  $k = k_m$  dominate, baroclinic instability is at work.

For midlatitudes  $k_m \approx 4000$  km which fits very well with the average  $L$  for synoptic systems (Holton, 1979). Baroclinic instability is nearly ubiquitous poleward of 30 degrees (Emanuel, 1986) and should be very important around jet streaks with the associated strong thermal gradients and vertical wind shear

Some of the case studies include a thermal wind so evidence for baroclinic instability will be analyzed for. The various instabilities described all can influence the results by enhancing both the balanced and unbalanced motions. Of particular concern would be the growth of I-G wave produced by the adjustment process due to the presences of hydrodynamic instabilities. The hydrodynamic instabilities would likely alter the divergent and vertical motion patterns resulting in a different Rossby number vertical motion relationship. The most likely candidates for producing such changes are rotational inertial, barotropic and baroclinic instability.

#### e. Problems in Measuring Winds

Wind data fields with very small inherent error is required to analyze for divergent and vertical motion patterns. Errors on the order of 10% in the winds can produce 100% error in the divergence and vertical motion fields. There are two options for studying ageostrophy and vertical motion. One option is to use operational data; the other is to use model data.

The study of the jet streak adjustment process using operational data introduces the possibility of several systematic and random errors when using observed rawinsonde data from the U.S. (or any rawinsonde network). The inherent error therefore, the random errors due to the observational method is still a problem. Kurihara (1961)

found the random height errors of  $\pm 42$  gpm at 100 mb and wind speed 5.2 m/s above 500 mb for Japanese rawinsonde, Shapiro and Kennedy (1981) found random errors of 35 gpm at 300 mb and random wind direction errors of 10 degrees and speed errors of 20 m/s. Other studies have found similar rawinsonde error problem. So even though satisfaction results are possible there will always be an inherent uncertainty in the results when using rawinsonde data.

To avoid the uncertainty of rawinsonde data Keyser and Uccellini (1987) suggested using model generated data. Model data should eliminate the systematic and random errors. Belt and Fuelberg (1982) demonstrated that some computations are affected more significantly by wind errors than others. They determined that the resultant fields from a perturbed initial data field were still reliable for kinematic diagnostic computations. In addition, Moore (1985) determined that rawinsonde data was accurate enough to calculate ageostrophic wind components.

The rawinsonde network for North American (Fig. 11) provides upper air data. However, the equipment used is of the same technology as World War II with only minor technological upgrades in providing rawinsonde data. In this study the wind data will be generated by a two-level primitive equation model similar to a model initially developed by Houghton et al. (1981) and later used by Van Tuyl and Young (1982) to study the kinematics of upper-level straight jet streaks.

#### f. Numerical Models Useful for Jet Streaks

The classic definition of a jet streak from Reiter (1963) is an intense, narrow, quasi-horizontal current of wind that is associated with very strong wind shear. Bluestein (1986) further observes that the typical upper-level jet streak has a speed greater than 30 m/s, with its length being about an order of magnitude larger than its width.

Various numerical models can be used to study the jet streaks and avoid rawinsonde errors. To accurately evaluate the jet streak some form of a primitive equation

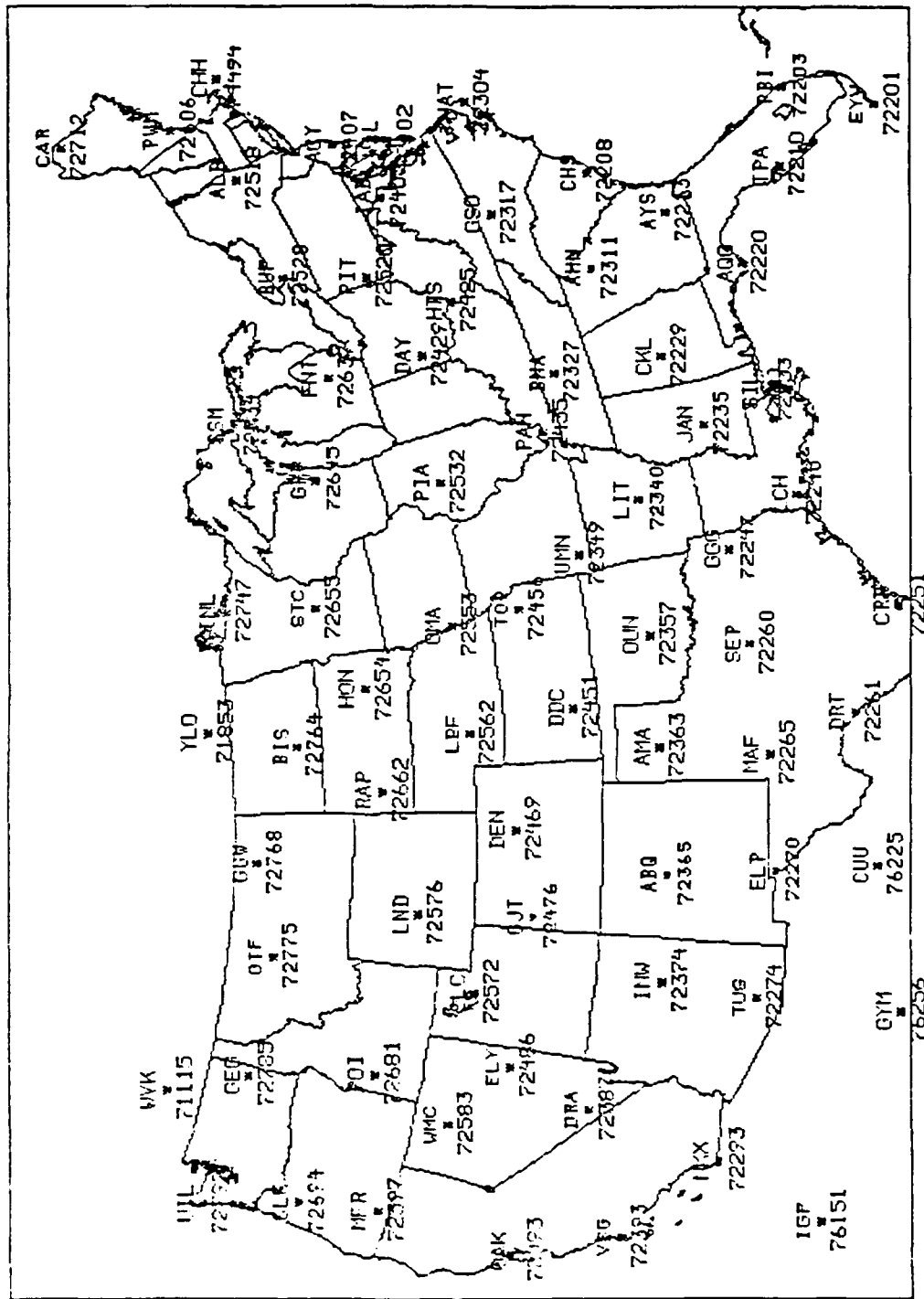


Fig. 11 Locations of U. S. and Canadian rawinsonde stations to be used in this study.

(PE) model must be used. If operational data were used the very complete nested grid PE model (NGM) would be used. The problem with using such a complex model in a diagnostic study is the difficulty in determining cause from effect. For example, increased vertical motions are caused by I-G waves. The I-G waves would increase the release of latent heat through convection. The latent heat increased vertical motions are caused by I-G waves. The I-G waves would increase the release of latent heat through convection. The latent heat release in turn increases vertical motion; in such a nonlinear relationship it is very difficult to distinguish the amount of increase in vertical motion due to the I-G from that due to latent heat release.

As an alternative, Houghton et al (1981) and Van Tuyl and Young (1982) used a simple two level PE model to simulate upper level jet streaks although such a model is not useful for producing operational prognostic data. It has a large advantage over the more complex models for diagnostic studies in that cause and effect are easier to determine. The PE model used in this research is similar to Houghton et al (1981) with the ability to produce curvature changes as well as speed changes.

#### g. Specific Research Objectives

The vertical motion and divergence associated with upper level jet streak patterns significantly influence the process of cyclogenesis and frontogenesis in both the upper and lower levels of the Troposphere. It is imperative that roles of curvature, speed and hydrodynamic instabilities be more fully understood in order to improve our understanding of the dynamics of jet streaks and other related phenomena, all of which are critical to both operational and theoretical meteorology.

Krishnamurti (1968) developed the mathematical balanced model that enabled Houghton et al. (1981) to develop a numerical model that could isolate the unbalanced vertical motions and I-G waves. Van Tuyl and Young (1982) used Houghton et al. (1981) numerical model to show that straight line jet streaks could produce unbalanced vertical motions as the result of I-G wave production. They developed a

relationship between the synoptic scale Rossby number and both the strength of the I-G waves and vertical motions. Molinaro (1988) demonstrated the important role curvature played in developing ageostrophy and unbalanced I-G waves. However, a general relationship between the magnitude of Rossby number and the vertical motion strength was never made. Also, no clear studies of the potential hydrodynamical instabilities and their effects were done.

The specific problems that this report will address are:

- (1) The role of the radius of curvature in  
the Rossby number magnitude and unbalanced  
vertical motion strength.
- (2) The role of the thermal wind (baroclinic) in  
the Rossby number magnitude and unbalanced  
vertical motion strength.
- (3) To examine the various forms of the Rossby  
number in order to find a general relationship  
between the magnitude of the Rossby number and  
the unbalanced vertical motion strength.
- (4) To examine for the three hydrodynamic instabilities  
(rotational, barotropic and baroclinic).

### 3. Methodology

#### a. Primitive Equation Model

##### 1) Description of the model

The model used in the jet streak experiments is a simple two level primitive equation model developed by Houghton et al (1981). The model is hydrostatic, frictionless, adiabatic and uses a constant Coriolis parameters over the entire 4000 km by 4000 km grid. Each individual grid distance is 200 km. The grid was made up of 21 columns by 21 rows of the 200 km grid spaces. The model uses a solid boundary condition on the North and South borders but uses a cyclonic condition for the East and West borders. The initial vertical motion field is computed using Krishnamurti's (1968) balanced omega equation. Thereafter, vertical motion is computed through a downward integration of the continuity equation.

The initial fields are calculated using Krishnamurti's (1968) complex diagnostic balance model which is based on a unique partitioning of the baroclinic terms into various forcing mechanisms. Houghton (1981) used a simplified version based on certain restrictive assumption to be discussed later to initialize the model and to be used as filtered reference data in the prognostic portion of the model.

The dynamical equations of Krishnamurti's (1968) balance model are only valid for small Rossby numbers. That is for values of  $\tilde{Ro} < 1$  where  $\tilde{Ro}$  is defined

$$\tilde{Ro} = \frac{U}{fL} \quad (7)$$

However, Krishnamurti (1968) shows that the model can be used to about 5 degrees latitude, where the critical values of the model are  $U = 10$  m/s,  $L = 1000$  km to keep  $\tilde{Ro} \approx .2$ . After the creation of a balanced initialized field the model is allowed to run forward in time for a desired period. The time step was set at 3 minutes with the model run out to 24 hours in most cases. The output data creates fields of  $\vec{V}, \vec{V}_{ag}$ ,

and heights at predetermined times. From the output data several diagnostic computations can be made in this research, various forms of vertical motion, vorticity, vorticity changes and Rossby number were calculated and plotted for analysis.

## 2) The Governing Equations

The main difference between this model and Houghton et al. (1981), Van Tuyl and Young (1982), Molinaro (1988) is the method of initialization used in some of the experiments. Each of the models variations use the same simulation of atmospheric structure, levels and variables (Fig. 12). In each case initialization of psi and omega fields is done through using a simplified version of Krishnamurti's (1968) diagnostic balance model. Table 2 lists the complete form of Krishnamurti's (1968) general balanced omega equation along with a scale analysis of each term. In the model used for this research only terms 1, 2, 3, 4, and 10 are used. The other terms are neglected due to the limitations of the model and scale analysis. Term 5 can be eliminated because the model is frictionless. Terms 6 and 7 are neglected because latent and sensible heat are ignored. Terms 8 and 9 are eliminated because vertical motion at both the top and bottom of the model are set to zero. Term 11 can be ignored because the divergent wind component is small at the models scale. Finally, Term 12 is neglected because the partial time derivative of psi and beta are small.

The balanced omega equation can be solved by using either the mass or velocity field. The velocity field must be used for some of the case studies in this research for the following reason. When solving for the balanced omega from the mass field an elliptical condition is required. The elliptical condition will be violated for anticyclonic jet streak cases in general as well as strong straight-line and cyclonic jet streaks. The initialization scheme in this model is after Molinaro (1988) which differs from Houghton et al. (1981) and Van Tuyl and Young (1982) in that curvature can be added. In addition this model initialization differed somewhat from Molinaro (1988) in that the vertical wind shear was varied for the same 400 mb wind. For the other

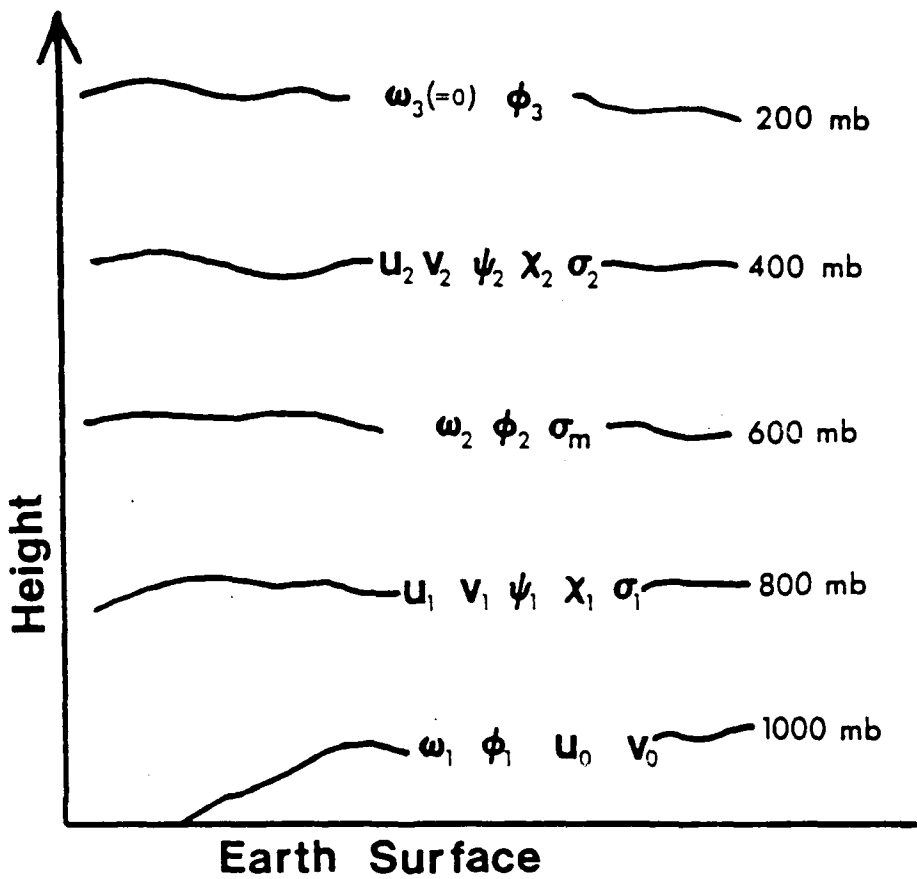


Fig. 12 Vertical structure and placement of variables in the model (Houghton et al., 1981).

1. $f \frac{\partial}{\partial p} J(\psi, \zeta_*)$	1.0e-16
2. $\pi \nabla^2 J(\psi, \theta)$	1.0e-16
3. $-2 \frac{\partial}{\partial t} \frac{\partial}{\partial p} J\left(\frac{\partial \psi}{\partial x}, \frac{\partial \psi}{\partial y}\right)$	1.0e-17
4. $-f \frac{\partial}{\partial p} (\zeta \nabla^2 x)$	1.0e-18
5. $f \frac{\partial}{\partial p} g \frac{\partial}{\partial p} \left[ \frac{\partial \tau_r}{\partial x} - \frac{\partial \tau_e}{\partial y} \right]$	1.0e-17
6. $-\frac{R}{c_p} \nabla^2 H_L$	1.0e-19
7. $-\frac{R}{c_p} \nabla^2 H_S$	1.0e-21
8. $f \frac{\partial}{\partial p} \left( \omega \frac{\partial}{\partial p} \nabla^2 \psi \right)$	1.0e-20
9. $f \frac{\partial}{\partial p} \left( \nabla \omega \cdot \nabla \frac{\partial \psi}{\partial p} \right)$	1.0e-17
10. $-f \frac{\partial}{\partial p} \left( \nabla x \cdot \nabla \zeta_* \right)$	1.0e-17
11. $-\pi \nabla^2 \left( \nabla x \cdot \nabla \theta \right)$	1.0e-17
12. $-\beta \frac{\partial}{\partial p} \frac{\partial}{\partial y} \frac{\partial \psi}{\partial t}$	1.0e-18

Table 2 Scale analysis for the forcing functions of the balanced omega equation for the synoptic scale.  
All terms are in units of Pa-l s-3. (Molinaro, 1988)

models this value was held constant.

To insert curvature into the initial jet streak data a modified psi field is used. The curvature of the jet streak is based on a cosine curve maintains the cyclonic east-west boundary conditions. The equation used for initialization is given by:

$$Y = y + \left[ 1 - \cos \left( \frac{\pi}{l} \right) \left( \frac{1}{2} - |x| \right) \right] \left[ \frac{D-y}{D} \right] AC \quad (16)$$

where  $x = y = 0$ ,  $l = 4000$  km,  $a = 833.3$  km  $b = 458.3$  km and  $D = 1900$  km and are held constant throughout the experiment.  $A$  is the amplitude of the jet streak's curvature which is set to zero for straight cases and varied between 600 to 900 km for the curved cases.  $C$  is the type of curvature ( $0 =$  straight,  $+1 =$  cyclonic,  $-1 =$  anti-cyclonic), and  $\psi_{800}$  is the stream function amplitude which is varied between  $3.75 e + 06$  and  $10.0 e + 06$  m<sup>2</sup>/s to control the magnitude of the jet streak (Table 3). After the initial psi field is computed the initial geopotential field is calculated using a "reverse" non-linear balance equation which is linearly interpolated to adjacent levels: Vertical motion is computed at 600 mb using the balanced omega equation. Then  $\chi$  is determined from the vertical gradient of  $\omega$ ,

$$\nabla^2 \chi = \frac{\partial \omega}{\partial P} \quad (17)$$

To simulate baroclinic condition the model was altered by Molinaro (1988) to be able to offset the upper and lower - level jet streak by a chosen number of grid points. The separation was varied by 1400 km to 2000 km. In addition Molinaro (1988) modified the model to allow the Coriolis parameter to vary linearly with latitude. This created a constant non zero value of  $\beta$  or a so called Beta Plane.

The center of the grid is selected to be 45 deg latitude with the northern and southern borders being at 63 and 27 deg latitude respectively (Fig. 13).

After initialization the prognostic portion of the model is performed using the following basic equations as described by Molinaro (1988) (a) The equation of motion

VALUES OF PSI AMPLITUDE FOR VARIOUS CASES      TABLE 3

SPEED M/S	STRAIGHT in	CYCLONIC $\times 10^6$ M	ANTICYCLONIC
26	5.0	3.75	3.75
37	7.5	5.0	5.0
52	10.0	7.5	7.5

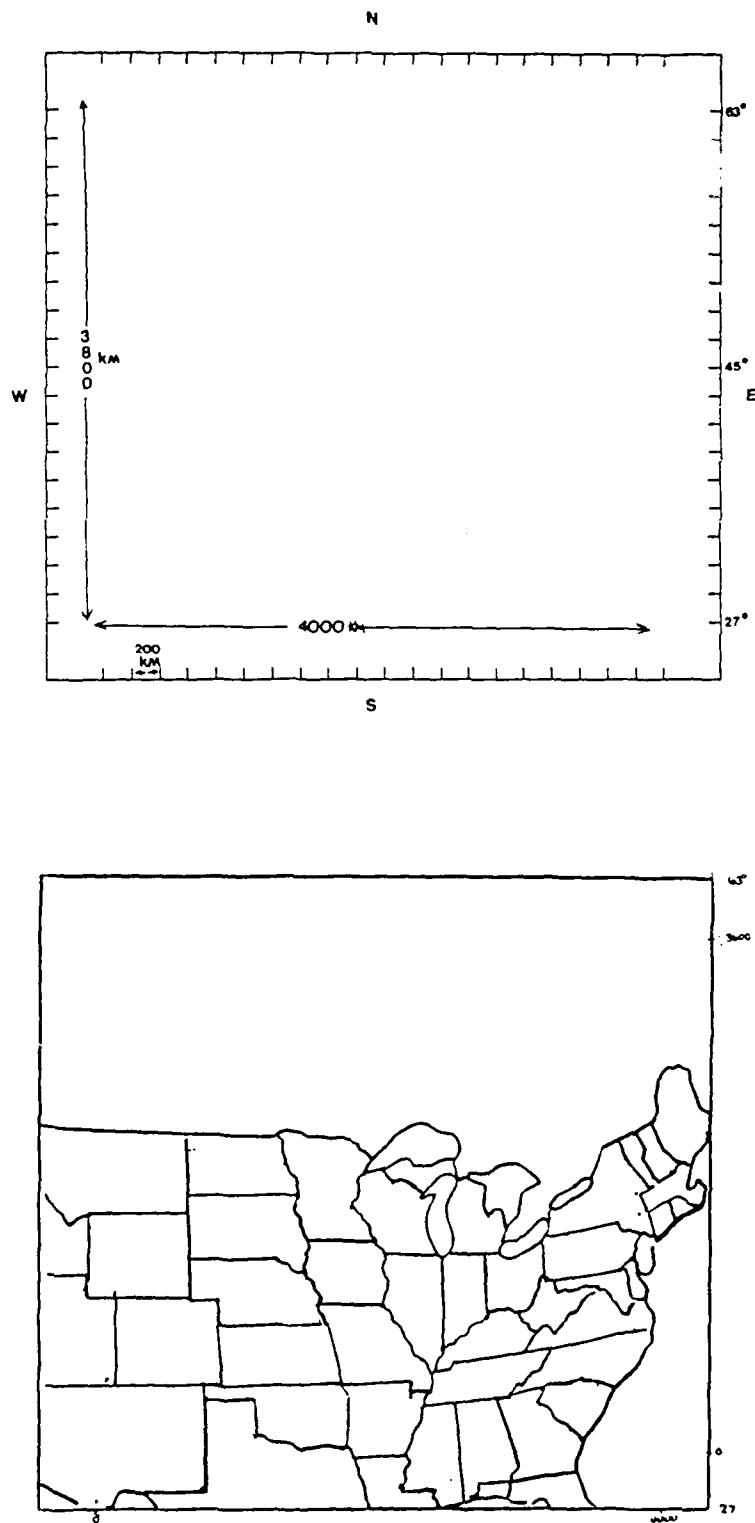


Fig. 13 Example of the gid values and corresponding area of U. S.

$$\frac{\partial \vec{V}_n}{\partial t} + \vec{V}_n \cdot \nabla \vec{V}_n + \left( \frac{\omega_n + \omega_{n+1}}{2\Delta P} \right) (\vec{V}_n - \vec{V}_{n+1}) + f \hat{k} \times \vec{V}_n = -\nabla [\frac{1}{2}(\phi_n + \phi_{n+1})] \quad (18)$$

(b) The thermodynamic "thickness" equation

$$\frac{\partial}{\partial t} (\phi_{n+1} - \phi_n) + \vec{V}_n \cdot \nabla (\phi_{n+1} - \phi_n) + \frac{1}{2}(\omega_n + \omega_{n+1}) \sigma_n \Delta P = 0 \quad (19)$$

(c) A special equation for the geopotential height of the lowest level derived from the integration of the hydrostatic relationship, the definition of omega and assuming that the mean values from the earth's surface to 1000 mb are given by values at 1000 mb.

$$\frac{\partial}{\partial t} \phi_1 + \vec{V}_0 \cdot \nabla \phi_1 = \frac{\omega_1}{\rho^*} - \phi_1 (\nabla \cdot \vec{V}_0) \quad (20)$$

where  $\rho^*$  is the mean density in the layer between the Earth's surface and 1000 mb.

(d) The continuity equation.

$$\omega_n = \omega_{n+1} - (\nabla \cdot \vec{V}_n) \Delta P \quad (21)$$

Because the model developed by Houghton et al. (1981) is a closed system additional relationships must be used:

$$\omega_3 = 0, \vec{V}_0 = \frac{3}{2} \vec{V}_1 - \frac{1}{2} \vec{V}_2 \quad (22)$$

$$\sigma_1 = \frac{1}{(\Delta P)^2} \left[ \frac{1}{2} \gamma^{-1} (\phi_2 - \phi_1) + B(\phi_3 - 2\phi_2 + \phi_1) \right] \quad (23)$$

$$\sigma_2 = \frac{1}{(\Delta P)^2} \left[ \frac{1}{2} \gamma^{-1} (\phi_3 - \phi_2) + A(\phi_3 - 2\phi_2 + \phi_1) \right] \quad (24)$$

where  $\nu$  is the ratio of specific heats of dry air and is calculated as the ratio of  $C_p / C_v$ .

The numeric value of  $\nu$  is 1.4. The constants A and B are coefficients used to offset truncation error and the uncentered nature of the second derivatives. The value of A is set at 1.745 and B at 0.472 to make the mean of  $\sigma_u$  agree the standard atmosphere.

$\sigma_n$  is the static stability parameter for a given level in the standard atmosphere. The values of  $\sigma_1$  ranged from  $1.9 \times 10^{-5} \text{ m}^2 \text{ Pa}^{-2} \text{ s}^{-2}$  to  $2.6 \times 10^{-5} \text{ m}^2 \text{ Pa}^{-2} \text{ s}^{-2}$  while  $\sigma_2$

ranged from  $2.6 \times 10^{-5} \text{ m}^2 \text{ Pa}^{-2} \text{ s}^{-2}$  to  $6.7 \times 10^{-5} \text{ m}^2 \text{ Pa}^{-2} \text{ s}^{-2}$ .

The basic prognostic equations are solved by using Grammeltvedt's (1985) explicit marching finite differencing method "F" of a quadratic conversion. After running the model numerous diagnostic fields can be computed from the basic field variables.

The first diagnostic program calculates Q-G vertical motion after Holton (1979). The Q-G program uses the geostrophic relationship to calculate the geostrophic wind velocity given by,

$$\vec{V}_g = \frac{\hat{k}}{f} \times \vec{\nabla} \phi \quad (25)$$

The geostrophic streamfunction is defined as:

$$\psi_g = \frac{\phi}{f} \quad (26)$$

vertical motion is defined from the Q-G. Omega equation as

$$\left[ \nabla^2 - \frac{2f^2}{\sigma_m(\Delta P)^2} \right] \omega_{QG2} = \frac{f}{\sigma_m(\Delta P)} \left[ J(\psi_{g1}, \nabla^2 \psi_{g1}) - J(\psi_{g2}, \nabla^2 \psi_{g2}) \right] \quad (27)$$

where  $J$  is the Jacobian operator and defined as:

$$J(a, b) = \frac{\partial a}{\partial x} \frac{\partial b}{\partial y} - \frac{\partial a}{\partial y} \frac{\partial b}{\partial x} \quad (28)$$

and  $\sigma_m$  is a constant static stability parameter at 600 mb ( $2.6 \times 10^{-5} \text{ m}^2 \text{ Pa}^{-2} \text{ s}^{-2}$ )

The second diagnostic program uses the simplified subset of Krishnamurti's (1968) balance model. The pressure - velocity relationship used is,

$$\nabla^2 \phi_B = f \nabla^2 \psi_B + 2J(u_B, v_B) \quad (29)$$

The vertical motion is computed from the same modified omega equation derived by Krishnamurti (1968):

$$\left[ \nabla^2 - \frac{2f^2}{\sigma_m(\Delta P)^2} \right] \omega_{B2} = \frac{f}{\sigma_m \Delta P} \left[ J(\psi_{B1}, \nabla^2 \psi_{B1}) - J(\psi_{B2}, \nabla^2 \psi_{B2}) \right] \quad (30)$$

The time derivatives required for this equation turn out to be the vorticity equation for the system and is given by:

$$\nabla^2 \frac{\partial \psi_B}{\partial t} = -J(\psi_B, \nabla^2 \psi_B) + \nabla \chi \cdot \nabla (\nabla^2 \psi_B) \quad (31)$$

The total vertical motion (omega PE) is derived from the intergration of the continuity equation,

$$\omega_n = \omega_{n+1} - (\nabla \cdot \vec{V}_n) \Delta P \quad (21)$$

in the vertical. The omega value obtained in this manner will be henceforth reffered to as PE omega. Holton (1979) outlines the basis for this kinematic method of calculating PE omegas. The primary disadvantage of the method is that small errors in the wind data will produce large errors in the divergence ( $\Delta V_n$ ) term. This is not a problem for the model generated data, but it is a problem for real case studies.

From the output of the PE model, various diagnostic computations can be performed. First the along and cross-contour vertical motion can be calculated using the kinematic omega equation. This is done by inserting the divergence created by the along- and cross-contour components of the ageostrophic wind instead of the total wind. Next, Rossby numbers are calculated by using the relationship  $Ro = V_{ag} / V$  and plotted on a grid. Third, vorticity fields and the vorticity derivative along the y axis is calculated to aid in identifying hydrodynamic instabilities. Finally, the effects of inertial-gravity waves can be described by the differences between the primitive equation vertical motion and either the quasi-geostrophic or balanced vertical motions.

#### b. Computations Using Rawinsonde Data

The data used to analyze actual jet streak cases was gathered from the U.S. and Canadian rawinsonde network as described by Molinaro(1988) (Fig. 11). It is received through the DDS+ data line network. The spatial resolution of the rawinsonde net-

work is on a macro-beta scale with a station spacing of 400 km. The temporal separation is 12 hours between observation, with observations being provided at 00 and 12 UTC. There are 92 upper air stations in North America that send data across the DSS+ dataline twice each day. The data is transmitted in three format types. TTAA - heights, winds and temperatures for the mandatory pressure levels TTBB - the temperatures for significant levels PPBB - the winds for significant levels. The data is archived and processed into a single complete upper air sounding at every observed pressure level for each station. Each parameter in every upper air sounding was checked for erroneous data. Seventy-three of the closest stations to the contiguous U.S. are used in the real jet streak case studies.

Objectively created analyzed fields of height, temperature and wind components were created at the surface and for 50 mb increments from 900 to 100mb. Rawindsonde drift cannot be systematically accounted for since information needed to accurately calculate the drift is unavailable. Rawindonde drift is generally neglected for the scales of motion drift within this research model.

## 2) Objective Analysis Method

The values of each basic variable have to be interpolated from the station points of the upper air data network to the grid points of the model. From the established grid fields of various selected kinematic parameters are created. An objective analysis scheme developed by Barnes (1973) is used to interpolate the sounding data to a 190.5 km grid system for each level. The Barnes (1973) technique is used because it is fast, requires only two passes per analysis, is widely used and allows for selection of the resolved wave amplitude.

The minimum possible wavelength which can be resolved through the Barnes (1973) analysis is 800 km. The minimum wavelength response is about 36.8% based on Koch et al. (1983) recommendations for analysis of synoptic scale weather systems.

In order to represent the large scale forcing on the macro-beta scale a c value of 82,000 km<sup>2</sup> and a g of 0.2 was used (Fig.14). These values allowed for the maximum amplitude gain to occur for a wavelength of 1,334 km.

The grid size for the rawinsonde data as described by Molinaro (1988) is 27 by 18 which allows for coverage of the U.S. except for northern Maine and southern Texas. The output display will be after Koch et al. (1983) as a 25 by 16 grid which will eliminate any border problems.

### 3) Method of Extrapolation

Finite differencing must be used to solve for certain first and second order derivatives to create the needed fields of Kinematic parameters. A problem arises in that the resultant field from finite differencing is smaller than the original field. In order to solve this problem the extrapolation equation,

$$d1=d2+(d2-d3) \quad (32)$$

will be used after each calculation of a first or second order derivative to enlarge the resultant grid to its original size as with Molinaro (1988). Smoothing of the gridded data fields during the objective analysis will minimize the impact on the border data. However, the extrapolated data will impact the border to some degree so caution must be used when interpreting data near the borders.

### 4) Analytical Procedures

Various meteorological parameters must be calculated to be used as input into the specific kinematic equations from the created data grids. The geostrophic wind components are computed from the created grids using second order finite difference with:

$$u_g = -\frac{1}{f} \frac{\partial \Phi}{\partial y} \quad (33)$$

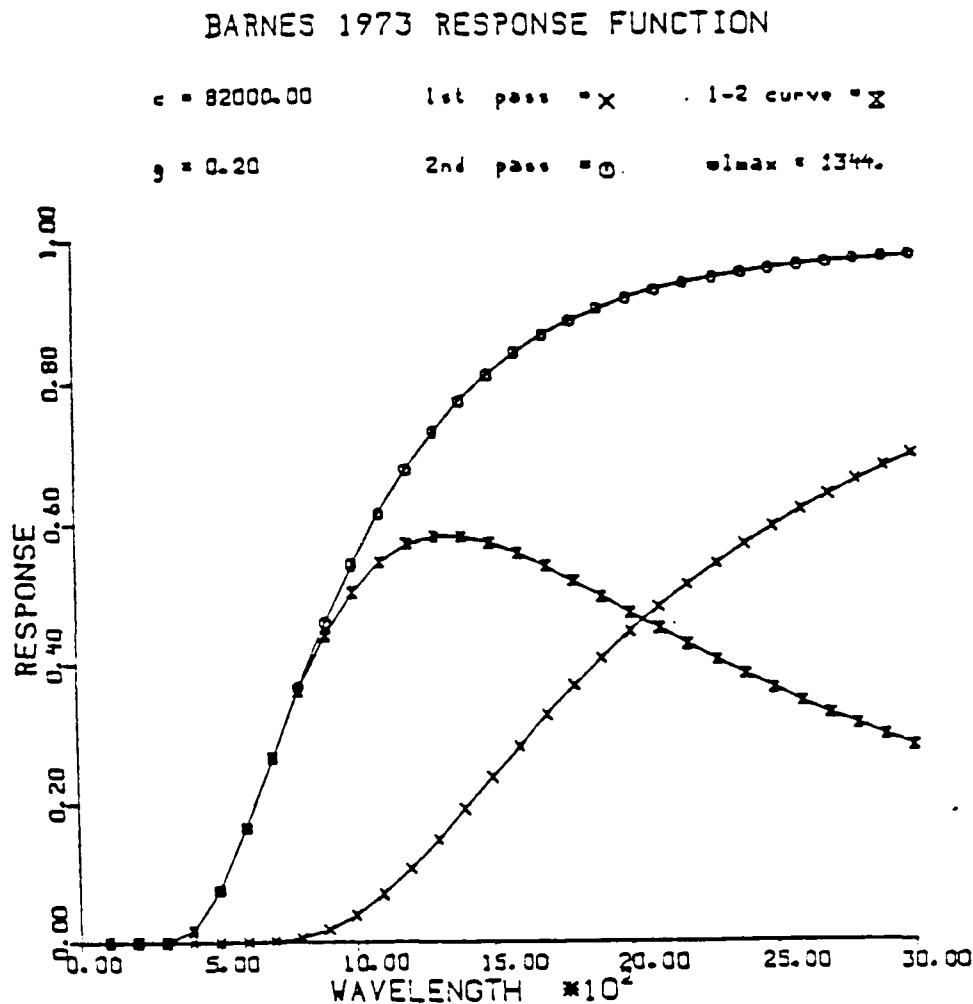


Fig. 14. Barnes (1973) response function for observational data set.

$$v_g = \frac{1}{f} \frac{\partial \Phi}{\partial x}$$

Where  $\Phi$  is geopotential.

As with the PE numerical model, the kinematic method will be used to calculate the total omega values. The kinematic method will use an integration of divergence in the vertical from

$$\nabla \cdot \vec{V}_2 = \frac{\partial u}{\partial x} + \frac{\partial v}{\partial y} \quad (34)$$

Where  $u$  and  $v$  are the observed wind components. The integrated divergence is then used to calculate omega values. The divergence is calculated from the isobaric form of the continuity equation:

$$\omega_p = \omega_{p+\Delta p} + \overline{(\nabla \cdot \vec{V}_2) \Delta p} \quad (35)$$

The surface omega is set to be zero, however the value of omega must be forced to be zero at the top of the model (100 mb). The O'Brien (1970) scheme as described by Molinaro (1988) is used to force the omega value at 100 mb to be zero by using,

$$\omega'_k = \omega_k - (\omega_k - \omega_T) \left[ \frac{k(k+1)}{K(K+1)} \right] \quad (36)$$

Where  $\omega_k$  is the original value of omega,  $\omega_T$  is omega assumed at the top level of the column,  $K$  is the total number of levels and  $k$  is the level number to which the divergence corresponds. The adjustment of the omega profile forces an adjustment to the divergence profile by using,

$$D'_k = D_k - \frac{k}{\frac{1}{2}(K(K+1)) \Delta p} (\omega_k - \omega_T) \quad (37)$$

Where  $D_k$  is the original divergence is the pressure difference between divergence levels.

### c. Parameterization and Model Operation

The PE model initializes using various initialization programs labled as initl\*, where the \* is either eb, qb, bc or ej.

Initleb runs the initialization program where the 400 mb wind is set equal to three times the 800 mb level. The wind directions are initially identical at both levels (upper trough or ridge directly over lower trough or ridge). This creates an equivalent barotropic condition.

Initlqb is identical to eb with the exception that the 400 mb winds are set equal to the 800 mb winds thus creating a nearly or quasi-barotropic condition. The initlbc program offsets the upper level wind maximums and trough or ridge axis. This creates a baroclinic condition.

Finally, initlej creates a lower level wind max in the opposite direction to the upper level wind max.

The PE program requires two answer files to be set up. The first called ANSIT is used in the initialization program. ANSIT provides the values of the parameters and variables of the model. ANSIT contains eleven variables on three lines. The first line contains six variables. The first two are Houghton et al. (1981) constants  $a = 833.3$  km,  $b = 458.3$  km. The third variable is the psi amplitude ( $c$ ) and is varied between  $3.75e +06$  and  $10.0e +06$  to vary the speed. The fourth variable is the grid distance ( $d$ ) and is constant at 200 km. The fifth variable is the amplitude of curvature ( $T_p$ ) which is set to zero for a straight jet and varied between 600 and 900 km for curved cases. The sixth and last term in the first line is the curvature function ( $C_r$ ),  $0 =$  straight,  $+1 =$  cyclonic,  $-1 =$  anticyclonic.

The second line consists of four variables. The first is the overrelaxation factor ( $\alpha_l$ ) and is set at 1.00. The second is the error criteria for overrelaxation ( $e$ ) and is set

FIRST LINE:	a	b	c	d	Tp	Cr
SECOND LINE:	a1	e	y6d		D	
THIRD LINE:	bc					

ANSIT DATA FOR A 400 MB 37 m/s STRAIGHT JET STREAK

833300.00	458300.00	75000000.00	200.00	770000.00	-1.00
1.00	20.00	000000.00	1900000.00		7

ANSIT DATA FOR A 400 MB 37 m/s CYCLONIC JET STREAK

833300.00	458300.00	75000000.00	200.00	770000.00	-1.00
1.00	20.00	000000.00	1900000.00		7

ANSIT DATA FOR A 400 MB 37 m/s ANTICYCLONIC JET STREAK

833300.00	458300.00	75000000.00	200.00	770000.00	-1.00
1.00	20.00	000000.00	1900000.00		7

Fig. 15 ANSIT file examples for various jet streak cases.

a	b	c	d
Time between printouts	No.of prinouts after initial	grid	time step
3	04	200.000	3.000

Note the total number of printouts = b + 1 and the total hours of the run is a times b. For the above example:  
Total printouts = 5. Total run time = 12 hours.

Fig. 16 Example of ANSPE file

at 20.00. Fourth is the north-south position of the axis (y6d). 000000.00 = centered at 45 degees latitude. Plus values move the axis north, minus values move the axis south. For example, 100000.00 moves the jet core south by 1/2 grid. The last variable in the second line is the constant D and it is set at 190000.00.

The third line consists of only of one variable (bc) that is used only in the baroclinic cases. The interger value will indicate the number of grid points the upper and lower level wind maxima will be seperated by (e.g. 7=1400km). An example of the types of ANSIT files are shown in Figure 15.

Note that the exact speed of the jet streak is a function of both the psi amplitude (c) and the curvature amplitude (Tp) so adjustments of both values are required for exact speed values. The running of the PE model can be done by running of the RUNPE\* shell programs. Where \* in this case stands for eb,qb,bc,ej,beta or init. The eb,qb,bc and ej versions are the same as in the initl\* programs. Beta stands for having  $df/dy =$  a constant creating a beta plane ; dnit is used when only the initial hour is required.

The basic RUNPE shell is as follows :

```
INITL* <ANSIT> OUTIT  
PEMODEL <ANSPE> OUTPE  
WINDAGV  
OMEGAB <ANSOB> OUTOB  
OMEGAQ > OUTOQ  
OMEGAC
```

The exact initl\* must be set in the beta and init versions. The second answer file must be set to use the RUNPE\* shells. It is called ANSPE and consists of four variables on one line. The first is the time between printouts in hours;the second is the total number of printouts after the initial printout; the third is the grid distance - constant at 200,000Km and the last is the time step set at three minutes. Fig. 16 gives

an example of ANSPE file.

There are several output files listed as \*.out created by the RUNPE. Init\* creates TEST.out and PE.dat. PE.dat can be used for height, wind and vorticity fields. However, ageostrophic winds cannot be created from this file. The PE model creates PE.out; the height, wind, vorticity and all of the omega programs can be run from this data. WINDAGV creates WIND.out from which the ageostrophic wind fields and Rossby number fields can be created. In addition, there are several omega programs: OMEGA.b creates OMB.out, OMEGA.q creates OMQ.out; OMEQ.ac creates OMAC.out and OMCC.out. Note that omega PE is the same for both omb.out and omq.out.

Each of the diagnostic parameters can be plotted using specific BOX\* plotting programs. To use these programs certain data files must be created all under the filenames of box\*.d. The \* represents various names such as plot, vort and baro. The box\*.d data files all have five lines of variables. Fig. 17 gives examples of various examples of box\*.d files.

The first line in the data files is the title you want for the output. The second line is the data file used, i.e. pe.out, wind.out or omb.out. The third line is the time to be printed on the plot. The actual time is selected in the BOX\* program. The forth line is the multiplier for heights and winds use 1.0e +00, for omegas use 1.0e + 05, for vorticity derivatives use 1.0e +11, and for Rossby numbers use 1.0e +02. The fifth line consists of 14 variables. The only variables not constant are the eleventh and twelfth in the line. The eleventh causes the pressure level to be printed out on the plot, while the twelfth controls the interval of the analysis.

The windplot program uses wind.out and has windplot.d as an answer file. This gives an output of the wind data as plotted arrows. Windplot.d consists of four lines. The first line consists of eight variables. The first gives the pressure level and the second gives the time as a printout on the plot. The fifth and sixth control the arrow

BOXPLOT.D EXAMPLE

```
wind  
pe.outebcm  
12.0  
1.0e+00  
19 21 4 0 1 31 1.0 1.0 2.0 2.0 0.0 400. 005.0 -1000.0 20000.0
```

BOXROSS.D EXAMPLE

```
ROSSBY NUMBER  
wind.outebcm  
00.0  
1.0e+02  
19 21 4 0 1 31 1.0 1.0 2.0 2.0 0.0 400. 020.0 -1000.0 20000.0
```

BOXBARO.D EXAMPLE

```
Y Derivative of Eta  
pe.out  
00.0  
1.0e+11  
19 21 4 0 1 31 1.0 1.0 2.0 2.0 0.0 400. 010.0 -1000.0 20000.0
```

WINDPLOT.D EXAMPLE

```
400. 00. 21 19 0.100 002.0 002.0 1.00 1.00  
REAL  
wind.out  
10 m s-1
```

Fig. 17 Plotting answer file examples.

length and magnitude equivalent. The second line gives the plot a title, the third line the needed output file and the forth line a legend for the arrows.

#### 4. Results

##### a. Types of Jet Streak Simulations and Case Studies

Forty five jet streak simulations were run using the PE model. All except the beta plane cases used a constant Coriolis parameter or f plane. There were seven cases that had the upper level winds (400 mb) equal to the lower level winds (800 mb) with jet streams and short waves in phase creating a quasi-barotropic condition. Twenty four cases maintained the superimposed relationships of the wind maximums and waves, but had the 400 mb winds equal to three times the lower level winds. These case simulated equivalent barotropic conditions. Four cases allowed the Coriolis parameter to vary by a constant amount creating a beta plane. These cases will be called beta plane cases. The remaining ten cases simulated baroclinic conditions with a constant value of f. One created a lower level (800 mb) easterly jet with an upper level westerly jet. The other cases displaced the upper wave from the lower wave creating a more typical baroclinic condition.

##### b. Velocity, Kinetic Energy and Momentum Changes

During each of the quasi-barotropic cases a consistent weakening occurred for both the 400 mb and 800 mb maximum wind velocity values over the 24 hours of the run. The equivalent barotropic case showed a general trend for larger velocity decreases at 400 mb and velocity increases at 800 mb. The addition of a beta plane reduced the decrease of the 400 mb winds slightly, while the baroclinic cases showed only very slight decreases or even increases at 400 mb.

The above kinetic energy changes can be the result of combinations of the following causes.

- 1) Dissipation due to truncation and round off error in the model.

- 2) Momentum transfer in the horizontal and/or vertical from areas of high to low momentum
- 3) Kinetic energy (KE) of the mean flow being transferred to the KE of the perturbation (LG waves)
- 4) Kinetic energy of the mean flow being transferred to the potential energy (PE) of the mean flow and/or perturbation. Each case will be examined for the possible cause of the momentum changes noted in (Table 4)

The weakest quasi barotropic case began with straight flow and the 400 and 800 mb maximum wind velocities set at 11.9 m/s. The drop in wind velocity over the twenty-four hours was less than 1% for both levels. The weak quasi barotropic case had the lowest values for Rossby numbers, ageostrophy and vertical motion. The low values listed in Table 4 suggest that very little momentum was transferred horizontally or vertically in this case. The low Rossby number and vertical motion (Table 5) with little change in the height fields suggest little or no production of LG waves (perturbations) (Fig. 18). This would seem to indicate that the amount of KE transferred to KE', PE or PE' was very small. The small decrease also suggests the magnitude of model dissipation due to truncation or round off error is very small. The results of this run would suggest that changes in the other runs were primarily due to dynamical processes and not model error.

The three other straight quasi barotropic cases showed progressively larger decreases in wind speeds over twenty-four hours as the initial maximum wind speed was increased (Table 4). As the initial wind maximum was increased, both the corresponding large scale Rossby number ( $Ro = U/fL$ ) and the mesoscale Rossby number ( $Ro = V_{ag} \cdot V$ ) increased significantly while the balanced vertical motion showed only a small increase. The highest wind speed case had a minimum absolute

## SUMMARY OF PE MODEL RUNS TABLE 4

TYPE	400/800		S CHANGE	BIN SIZE	TEST SQUARE x100-1 n-1
	V <sub>0</sub>	V <sub>24</sub>			
<b>**QBAR0**</b>					
ST QB	11.9	11.8	-00.8	9	0.0
	11.9	11.8	-00.8		
ST QB	25.5	24.4	-04.3	3	0.0
	25.5	23.9	-08.2		
ST QB	35.8	33.0	-07.3	3	0.0
	35.8	32.3	-07.3		
ST QB	38.2	35.2	-07.9	3	0.0
	38.2	34.8	-08.9		
ST QB	50.8	45.3	-10.8	-1	0.0
	50.8	44.8	-11.8		
CY QB	34.7	32.1	-07.4	3	0.0
	34.7	31.7	-08.8		
AC QB	34.5	33.1	-04.0	0	0.0
	34.5	33.1	-04.0		
<b>**EQBAR**</b>					
ST EB	28.0	24.1	-07.3	5	3.3
	08.7	09.5	+09.2		
ST EB	38.8	33.8	-12.9	3	4.9
	12.9	14.3	+10.8		
ST EB	52.0	43.0	-17.3	3	6.6
	17.3	19.3	+11.8		
CY EB	28.0	24.0	-07.7	0	1.3
	08.7	09.8	+10.3		
CY EB	34.2	30.6	-10.5	3	4.1
	12.9	14.1	+09.3		
CY EB	37.0	32.3	-12.7	4	4.9
	12.3	13.7	+11.4		
CY EB	52.0	41.0	-21.2	3	6.6
	17.1	20.4	+19.3		
CY EB	68.9	53.1	-22.8	-1	7.8
	28.9	40.1	+59.8		
AC EB	28.0	24.0	-07.8	1	3.3
	08.7	09.1	+04.8		
AC EB	35.8	31.2	-12.3	0	4.8
	10.4	11.0	+05.8		
AC EB	52.0	44.0	-13.5	-4	6.6
	17.2	20.4	+18.6		

AC EB	74.0 20.0	63.5 28.2	-14.2 +41.0	-10	10.3
BETA EB ST	38.6 12.9	32.6 14.0	-15.5 +08.5	3	4.3
BETA EB CY	35.8 12.3	30.3 14.0	-14.9 +13.8	3	4.7
BETA EB AC	35.7 11.9	32.1 13.1	-10.0 +10.0	0	4.8
BETA AC UMST	73.4 19.5	58.7 27.8	-20.0 +41.5	-10	10.2
**BAROC**					
ST BC (8)	38.6 12.9	36.5 17.0	-05.4 +24.1	3	4.7
ST BC (14)	38.5 12.8	37.3 17.1	-03.1 +33.6	3	4.9
ST BC (20)	38.5 12.8	38.4 18.2	-00.3 +44.4	3	5.3
CY BC (8)	35.0 12.0	34.7 16.1	-00.9 +34.1	3	5.0
CY BC (14)	35.0 11.9	35.4 15.1	+01.1 +28.9	3	5.2
CY BC (20)	35.1 11.8	35.9 14.3	+02.3 +21.1	3	5.5
AY BC (8)	35.7 11.5	33.0 16.7	-07.6 +48.4	0	5.2
AY BC (14)	35.8 11.7	31.8 15.3	-11.2 +30.1	0	5.4
AY BC (20)	38.0 12.0	31.8 15.1	-12.2 +24.1	0	5.8
EJ BC	34.5 -11.2	32.5 -14.9	-05.6 +33.0	3	8.7

## SUMMARY OF PE MODEL RUNS TABLE 5

TYPE	V <sub>B</sub> 400mb	$\tilde{R}_0$	R <sub>0</sub>	24HR VM 600 mb MAX	PE	IG
ST QB	11.9	0.12	0.05		0	0
ST QB	25.5	0.26	0.10		1	1
ST QB	35.8	0.35	0.20		5	2
ST QB	38.2	0.38	0.20		5	3
ST QB	50.8	0.50	0.30		25	20
CY QB	34.5	0.35	0.25		6	3
AC QB	34.5	0.35	0.20		5	2
ST EB	26.0	0.26	0.15		4	2
ST EB	38.6	0.38	0.20		10	6
ST EB	52.0	0.52	0.50		16	9
CY EB	26.0	0.26	0.80		22	15
CY EB	34.2	0.34	1.30		28	17
CY EB	36.2	0.36	1.40		30	19
CY EB	52.0	0.52	1.90		60	40
CY EB	68.9	0.70	2.10		120	75
AC EB	26.0	0.26	0.40		12	8
AC EB	35.8	0.35	0.80		16	12
AC EB	52.0	0.52	0.70		30	16
AC EB	74.0	0.74	1.05		80	50
BETA ST	38.6	0.39	0.05		8	3
BETA CY	35.6	0.36	1.20		25	10
BETA AC	35.7	0.36	0.50		12	4
BETA UNST	73.4	0.73	0.95		70	40
ST BC (8)	38.6	0.39	0.25		15	8
ST BC (14)	38.5	0.39	0.35		30	18
ST BC (20)	38.4	0.39	0.40		35	24

CY BC (8)	35.0	0.35	1.50	70	35
CY BC (14)	35.0	0.35	1.40	90	37
CY BC (20)	35.1	0.35	1.30	95	40
AC BC (8)	35.7	0.36	1.40	35	25
AC BC (14)	35.8	0.36	1.00	40	30
AC BC (20)	36.0	0.36	0.80	40	30
EJ BC	34.5	0.35	1.50	95	40

Fig. 18 STR PE VERT MOT VS. ROSSBY NUMBER

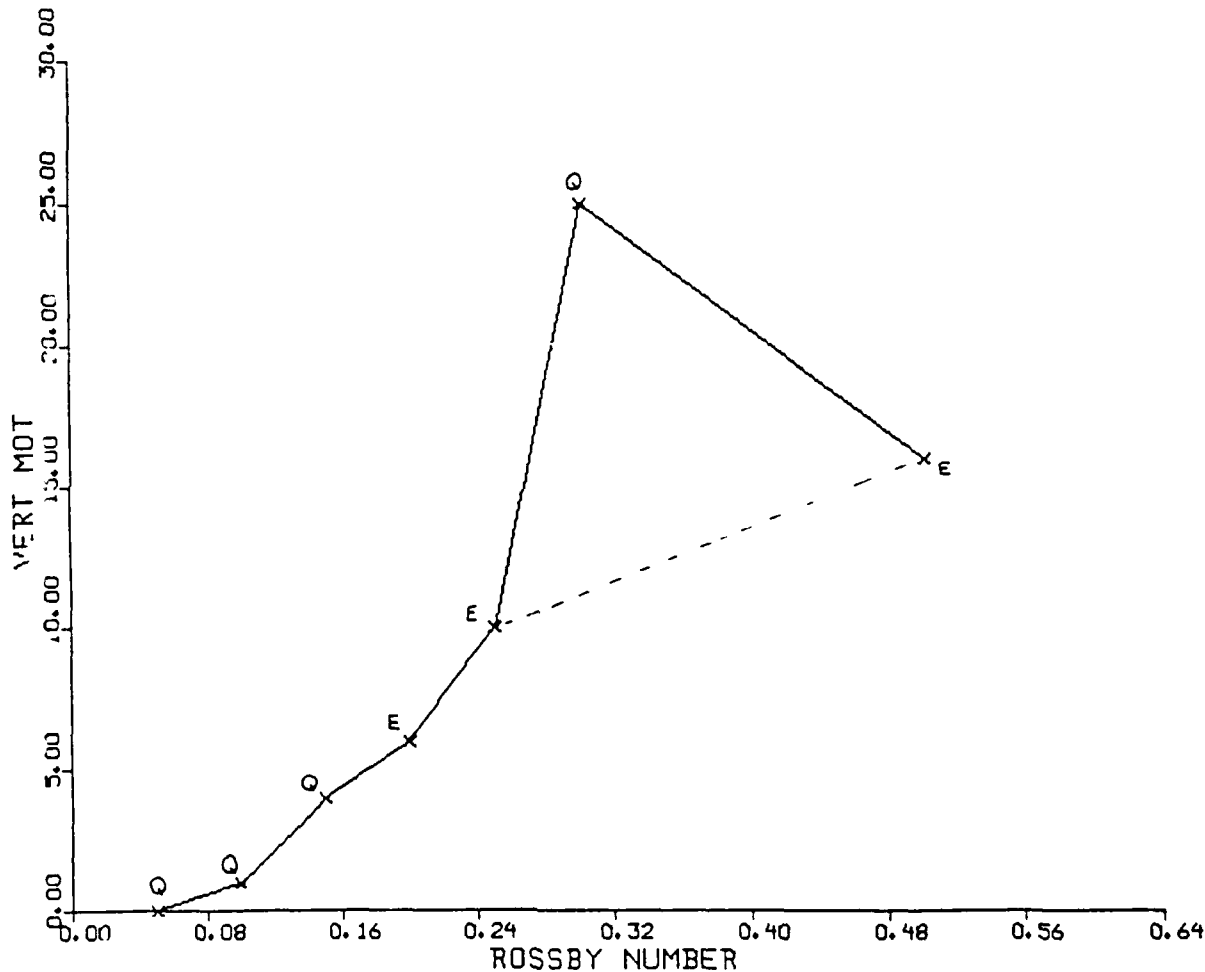


Fig. 18 Plot of PE vertical motion versus Rossby number ( $Ro$ ) for straight jet streaks. Q indicates a quasi-barotropic condition; E indicates equivalent barotropic condition. The Q that does not show the linear relationship (dashed line) displayed rotational inertial instability.

vorticity of zero which suggests the possibility of (rotational) inertial instability. These results suggest that at least some of the loss in KE was due to the transfer KE to KE' as I-G vertical motion increased. Vertical momentum transfer did not seem to play a significant role in the quasi-barotropic cases, but there was some horizontal transfer of momentum associated with the development of the I-G waves. Even though there was KE loss the values of vertical motion were less than half those of the equivalent barotropic and baroclinic cases. This suggests that vertical wind shear (a thermal wind) is very important in establishing vertical motions as the jet streak adjustment process proceeds.

The addition of cyclonic curvature did not change the results significantly. However, the addition of anticyclonic curvature halved the velocity drop and greatly lowered the PE vertical motions as well as the IG vertical motions. This observation suggests that the introduction of anticyclonic curvature somehow stabilized the jet streak geostrophic adjustment process. The stabilization reduced the production of I-G waves which reduced the amount of KE transferred to KE'.

The equivalent barotropic cases differed from the quasi-barotropic cases in three significant ways. First, the equivalent barotropic cases produced much larger PE and IG vertical motions, while the balanced motions remained about the same. Second, there were larger upper level (400mb) velocity drops and 800 mb velocity increases (Table 4). Finally, the addition of curvature significantly altered the resulting vertical motion fields and mesoscale Rossby numbers (Ro). The velocity changes suggest a vertical momentum transfer from the upper level to the lower level. Also the increased vertical motion suggested an increase in the transfer of KE to KE'. The addition of cyclonic curvature produced the largest vertical motion increases while the higher speed straight and anticyclonic cases showed negative absolute vorticity values. In these cases an abrupt increase in the magnitude of the vertical motion values occurred suggesting the presence of rotational inertial instability.

The cases that added a beta plane showed a slightly smaller drop in the 400 mb wind speed. However, the most significant difference from the constant f cases was the increase in the balance vertical motion values. The total PE vertical motion increased slightly, while the I-G vertical motions decreased slightly. This suggests that the addition of the beta plane stabilized the jet streak adjustment process. The result of the stabilization was an increase in KE as well as reduction of the production of the I-G waves and KE'.

The addition of baroclinicity to cases with a constant f was done by displacing the upper and lower level waves. The baroclinic cases produced a smaller weakening and in some cases small increases to the 400 mb winds over 24 hours. On the other hand, vertical motions increased slightly. This suggests that baroclinic instability may enhance both KE and KE'.

#### c. Rossby Number - Vertical Motion Relationships

As previously described for the straight quasi-barotropic jet streak cases, there was a general positive correlation between the magnitudes of the Rossby number and the magnitude of the maximum vertical motion. The following procedure was used to further evaluate the Rossby number - vertical motion relationship. The basic definition of the Rossby number as the dimensionless ratio of inertial forces to the Coriolis force can be written:

$$Ro = \frac{\left| \frac{\partial \vec{V}}{\partial t} \right|}{f \left| \vec{V} \right|} \quad (9)$$

The large scale (macro B) the Rossby number reduces to the form:

$$\bar{Ro} = \frac{U}{fL} \quad (7)$$

where  $U = \text{max wind speed of jet streak}$

$L = 10^6$  meters

For the smaller scale (meso  $\alpha$ ) it seems more appropriate to use the more basic form:

$$Ro = \frac{|\vec{V}_{ag}|}{|\vec{V}|} \quad (10)$$

The two Rossby numbers were compared to the maximum vertical velocity associated with a given jet streak.  $Ro$  is taken as the maximum value on the grid excluding any values near the northern (poleward) or southern (equatorward) boundaries. This prevents any values of the Rossby number to be misrepresented because of boundary condition problems. Table 5 summarizes the Rossby number results.

The quasi-barotropic and equivalent barotropic straight-line cases showed basically a linear relationship between vertical motion and either type of Rossby number ( $\tilde{Ro}$  or  $Ro$ ) with the exception of the cases involving negative absolute vorticity values (Figs. 18 and 19). The most noted relationship is the increase in the unbalanced vertical motion with increased Rossby numbers. The unbalanced vertical motion is taken to be that of the I-G waves as described Houghton et al. (1981). The linear relationship breaks down between the large scale Rotilte and the magnitude of the vertical motion when curvature is added. Table 6 outlines the difference between the magnitudes of  $\tilde{Ro}$  and  $Ro$  for a given jet streak condition. However, the linear relationship is maintained for all cases if  $Ro$  is used instead of  $\tilde{Ro}$ . The most noted exceptions are cases involving negative absolute vorticity values. This indicates that ageostrophy is greatly influenced by curvature. Since  $Ro$  is better at evaluating ageostrophy than  $\tilde{Ro}$ , a more fundamental relationship between  $Ro$  and vertical motion is established (Figs. 20-22).

When varying the radius of curvature for jet streaks that are equivalent barotropic and have a maximum 400 mb wind speed of 38 m/s the relative importance of curvature can be examined. Increases in curvature (decrease in radius of curvature) increased the vertical motion and the Rossby numbers for both cases. The 38 m/s

Fig. 19 STR IG VERT MOT VS. ROSSBY NUMBER

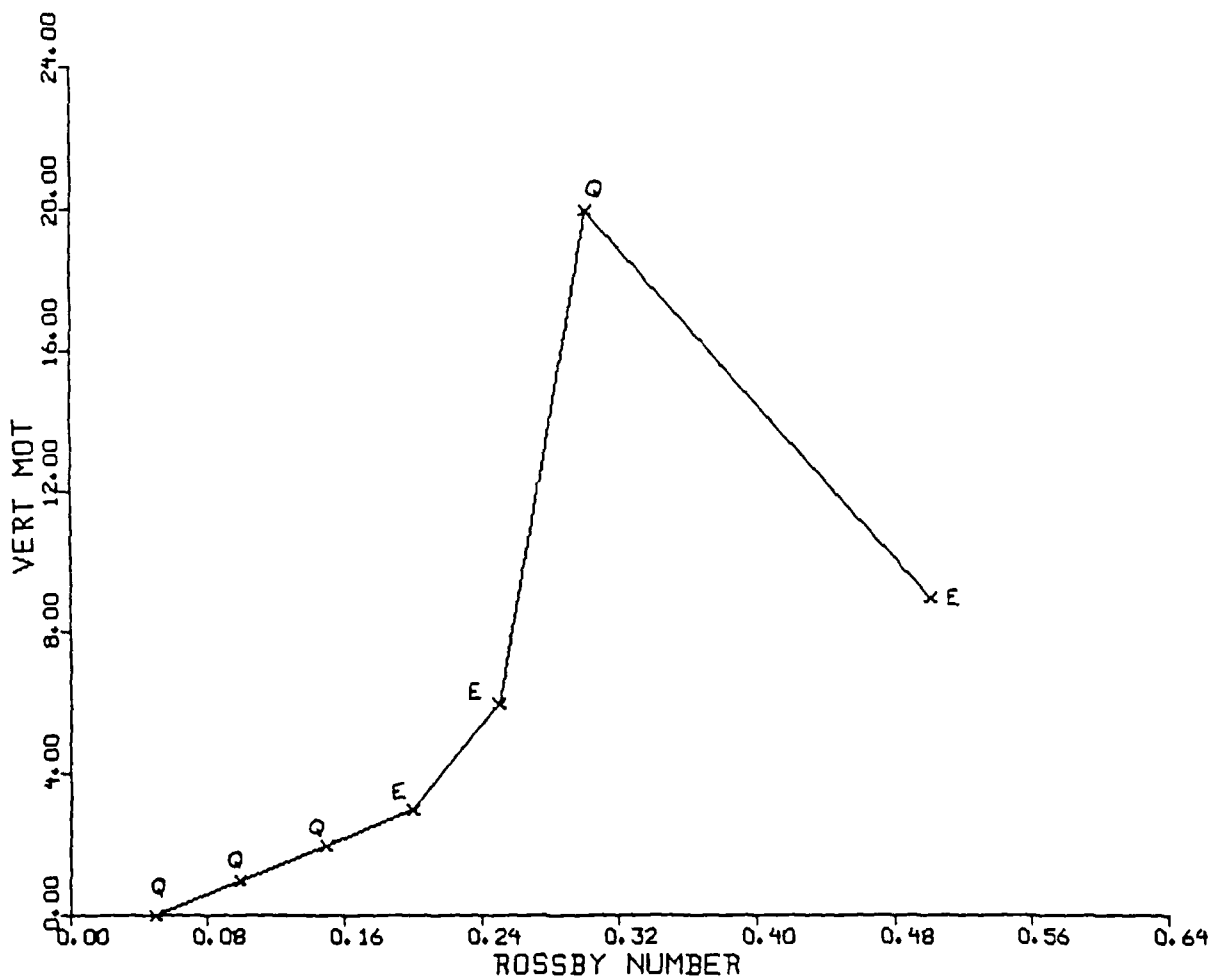


Fig. 19 Plot of IG vertical motion versus Rossby number ( $Ro$ ) for straight jet streaks. Q indicates a quasi-barotropic condition; E indicates equivalent barotropic condition. The Q that does not show the linear relationship displayed rotational inertial instability.

Fig. 20 EB PE VERT MOT VS. ROSSBY NUMBER

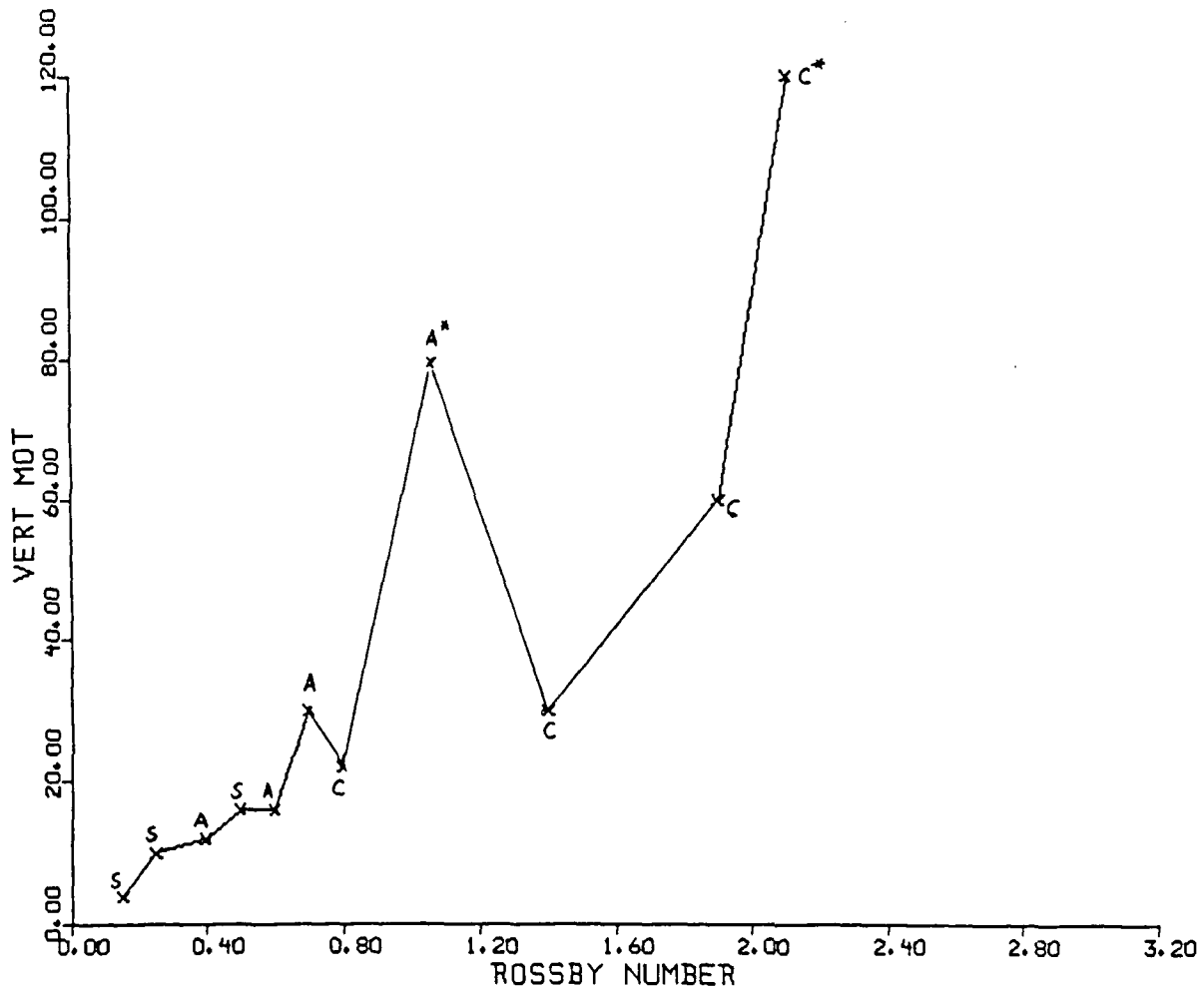


Fig. 20 Plot of PE vertical motion versus Rossby number ( $Ro$ ) for all equivalent barotropic cases. S indicates straight; A indicates anticyclonic; C indicates cyclonic. The anticyclonic ( $A^*$ ) and cyclonic ( $C^*$ ) case which fall outside the linear relationship display rotational inertial instability.

Fig. 21 EB IG VERT MOT VS. ROSSBY NUMBER

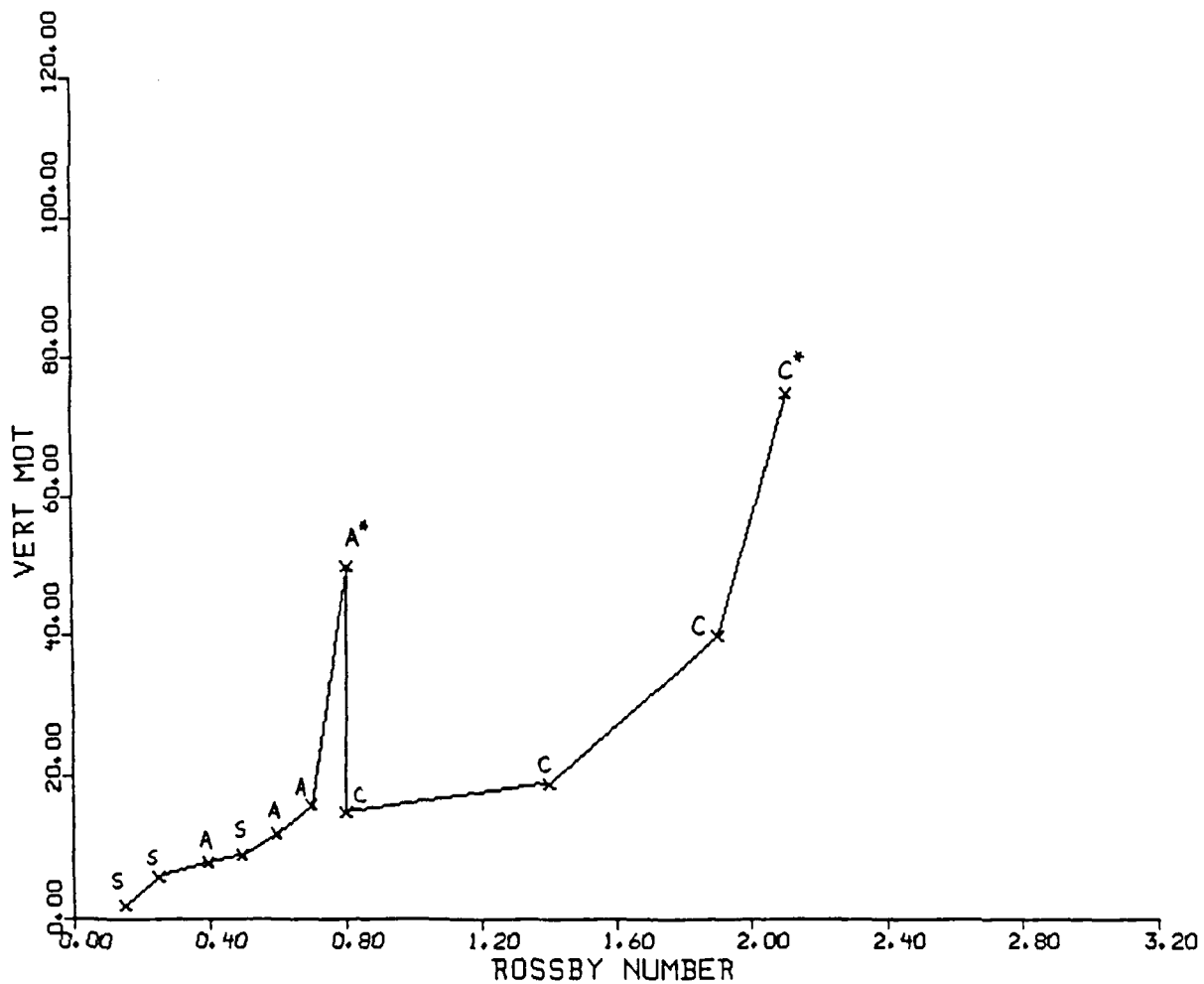


Fig. 21 Plot of equivalent barotropic I-G vertical motion. A\* and C\* displayed rotational inertial instability.

Fig. 22 EB BAL VERT MOT VS. ROSSBY NUMBER

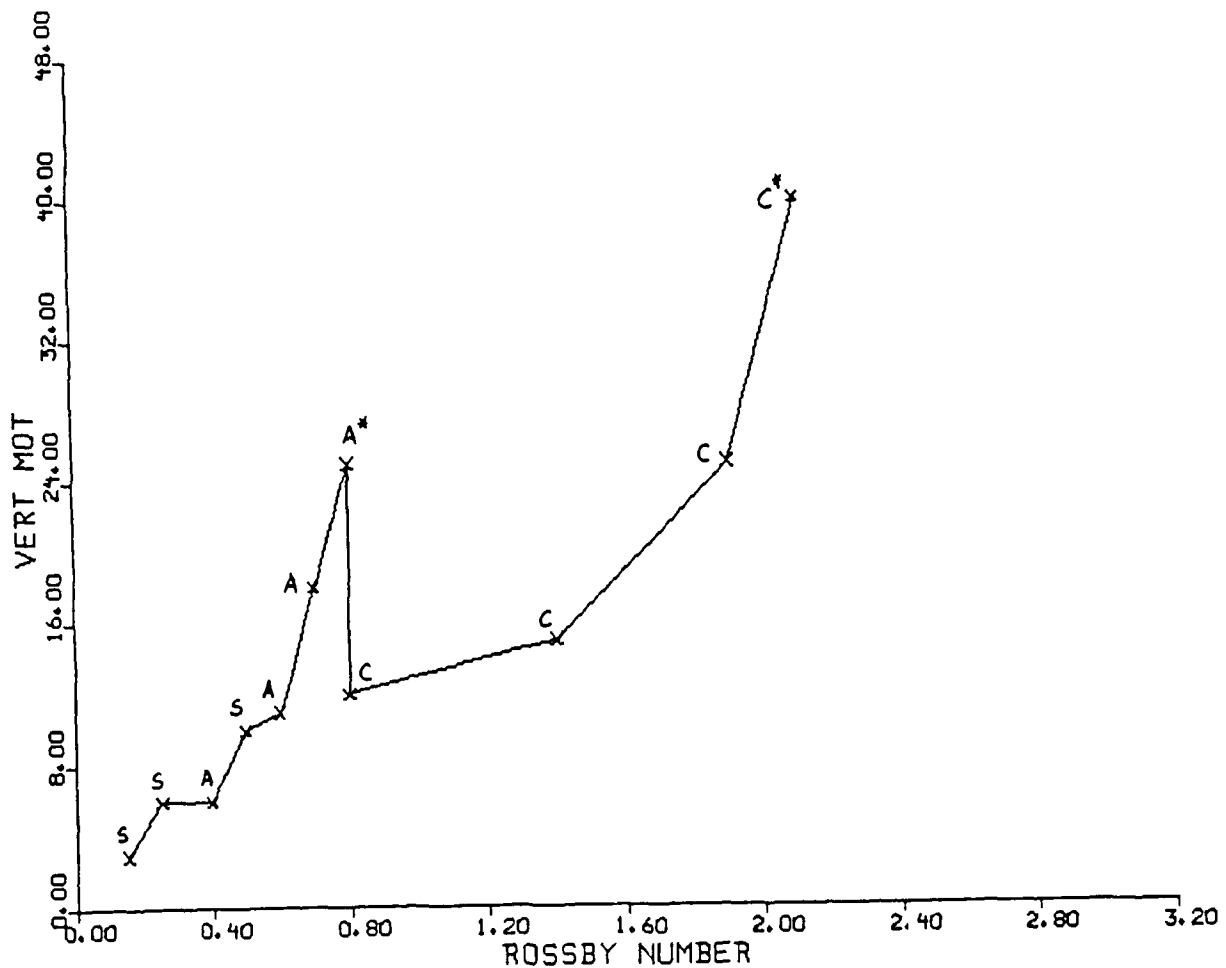


Fig. 22 Same as Fig. 20 for balanced vertical motion.

case was picked to insure that rotational inertial instability was avoided (Table 6 - 8 and Fig. 23). The data indicated that cyclonic curvature was more effective in increasing ageostrophy than anticyclonic curvature. Caution must be given to the interpretation of the results of the curvature variation cases because of the subjectivity involved in measuring the radius of curvature. However, the general trends would seem to be reliable.

The baroclinic cases served to increase the vertical motion somewhat over the equivalent barotropic cases for the same Ro value. The introduction of the beta plane served to increase the balanced and decrease the I-G vertical motions for the same Ro value.

A similar relationship was noted between the magnitude of the Rossby number and the magnitude of the vertical wind shear (Tables 4 and 5 and Fig. 24). This indicates the direct relationship between the vertical wind shear and the magnitude of the ageostrophic wind.

#### d. Hydrodynamic Instabilities

As already discussed, it seems fairly certain that rotational inertial instability occurs with negative absolute vorticity values. As support for this, the linear relationship between Ro and vertical motion breaks down when absolute vorticity is negative.

Barotropic inertial instability is a possibility because the necessary conditions of  $d(\eta)/dy = 0$  ( $\eta$  changes sign) occurs in areas of maximum vorticity values. However, a definitive answer as to the actual role of barotropic inertial instability is very difficult to make.

Baroclinic instability appears to be playing a role in the baroclinic cases. Baroclinic instability seems to be impacting both the larger scale waves and the smaller scale waves as both the balanced and unbalanced vertical motions increase with the introduction of baroclinicity through vertical directional wind shear.

Fig. 24 EQ BAROT VERT MOT VS. VERT SHEAR

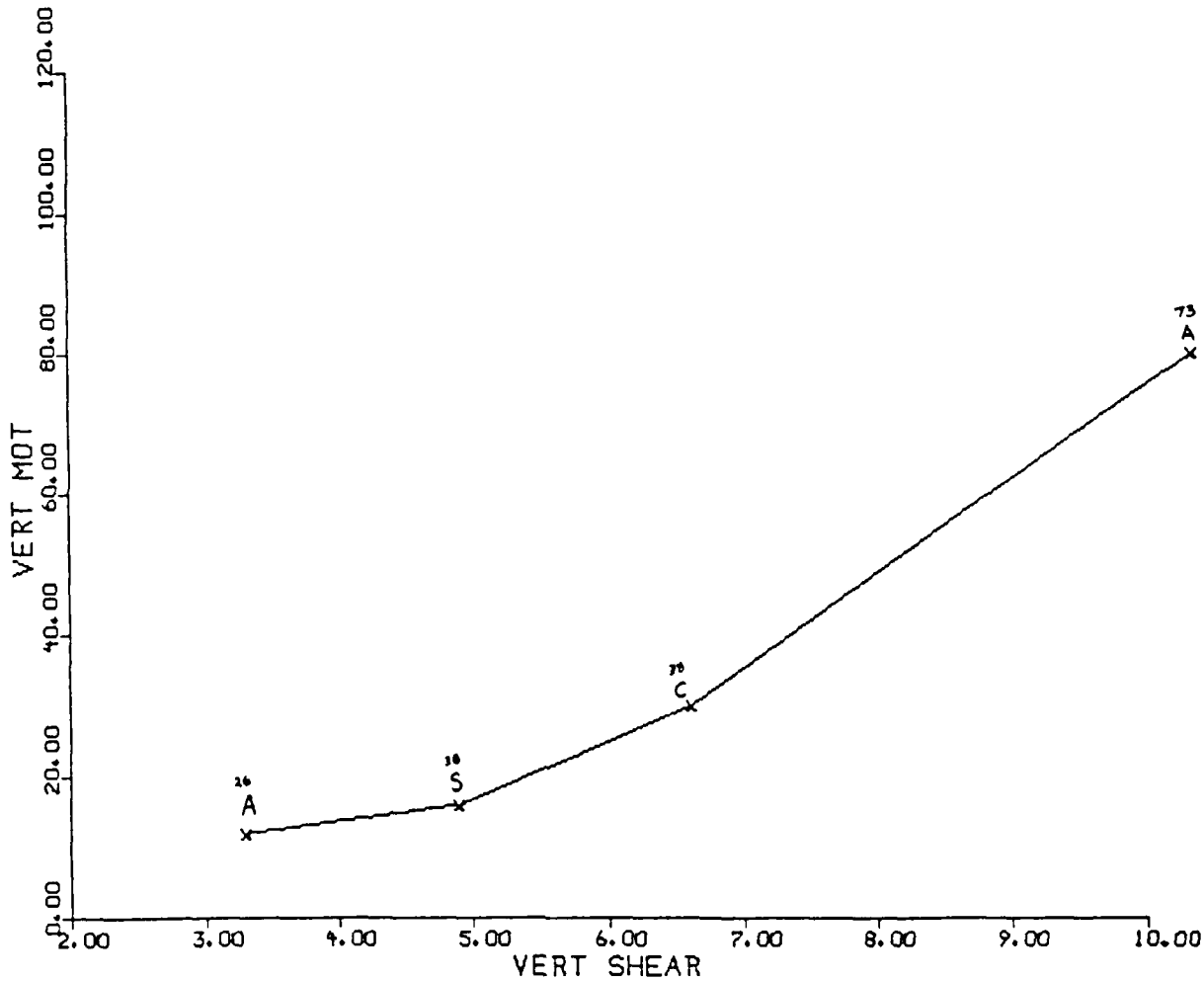


Fig. 24 Vertical motion versus maximum vertical shear for equivalent barotropic cases.

(Molinaro, 1988)

Fig. 23 EQ BARO PE VERT MOT VS.  
CURVATURE

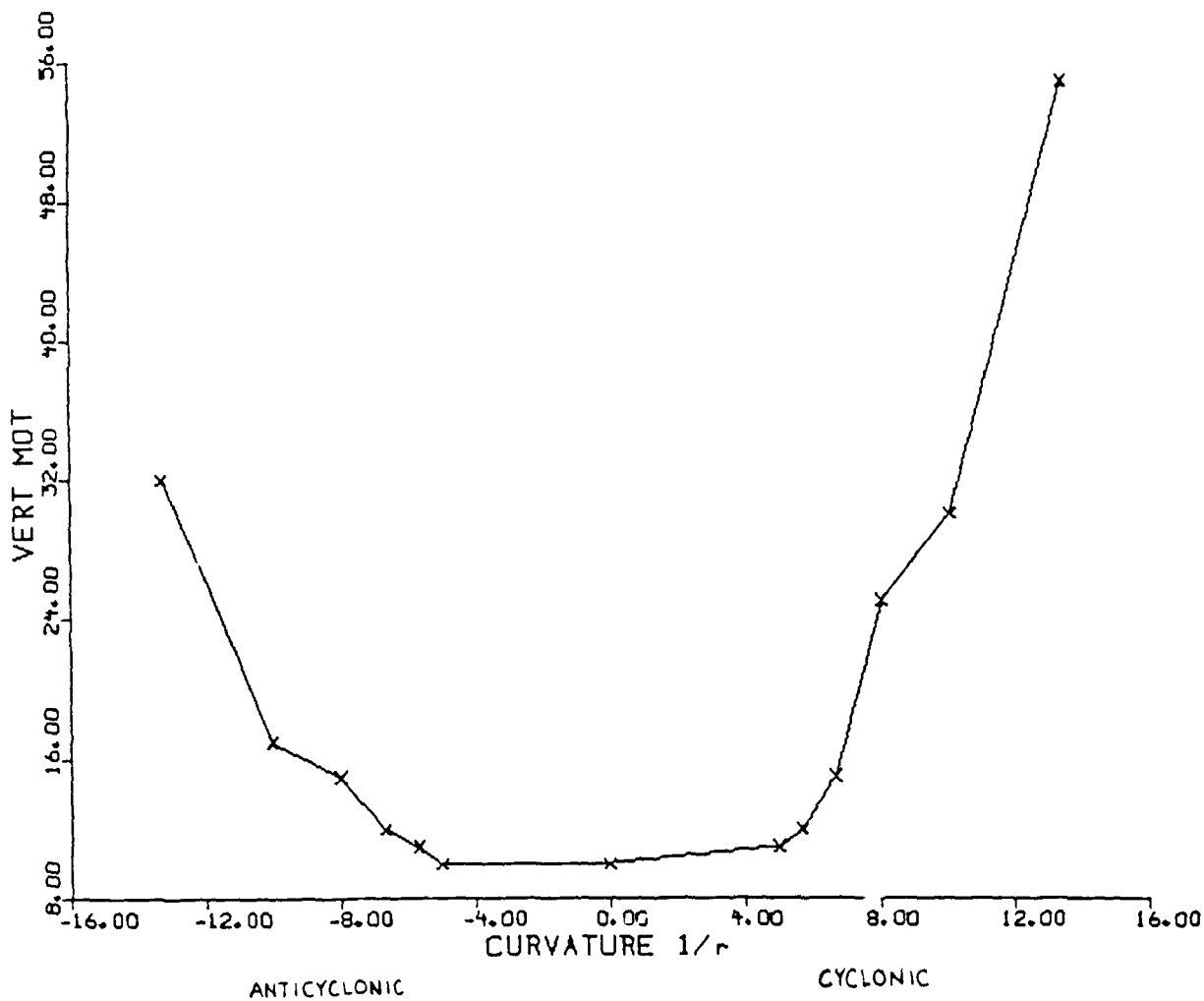


Fig. 23 Vertical motion versus curvature for a 12  
hour 38 m/s jetstreak maximum.

CYCLONIC CURVATURE VARIATION 38 m/s TABLE 6

Rad of Curv. $\times 10^6 \text{m}$	+2.00	+1.75	+1.50	+1.25	+1.00	+0.75	0
$1/r$ $\times 10^{-7}$	+5.00	+5.70	+6.67	+8.00	+10.00	+13.30	0
$\widetilde{Ro}$	0.38	0.38	0.38	0.38	0.38	0.38	0.38
Ro	0.27	0.30	0.45	1.10	1.40	1.70	0.25
PE VM	11	12	15	26	30	55	10
IG VM	7	8	11	15	19	37	6

ANTICYCLONIC CURVATURE VARIATION 38 m/s TABLE 7							
Rad of CURV. $\times 10^6$	-2.00	-1.75	-1.50	-1.25	-1.00	-0.75	0
$1/r$ $\times 10^{-7}$	-5.00	-5.70	-6.67	-8.00	-10.00	-13.30	0
$\tilde{Ro}$	0.38	0.38	0.38	0.38	0.38	0.38	0.38
$Ro$	0.25	0.30	0.40	0.50	0.60	0.70	0.25
PE YM	10	11	12	15	17	32	10
IG YM	6	7	8	10	13	15	6

ROSSBY NUMBER COMPARISON STRAIGHT JET STREAK TABLE 8							
$\gamma_0$	QB 12	QB 26	QB 38	QB 50	EB 26	EB 38	EB 52
$\tilde{Ro}$	.12	.26	.38	.50	.26	.38	.52
$Ro$	.05	.10	.20	.30	.15	.20	.50
ROSSBY NUMBER COMPARISON CYCLONIC AND ANTICYCLONIC							
$\gamma_0$	CY 27	CY 36	CY 52	CY 89	AC 26	AC 36	AC 52
$\tilde{Ro}$	.27	.38	.52	.89	.26	.38	.52
$Ro$	.80	1.40	1.90	2.10	.40	.60	.70

Three specific cases are included to more fully examine the instability problem. One straight-line, anticyclonic and cyclonic case is examined. Each case will look at the first 12 hours of the run. The following information is useful in evaluating the case studies plotted data.

- 1) Isotachs are in 5 m/s intervals.
- 2) Vertical motions are in  $10^1$  microbar/s with negative (dashed) values indicating upward motion.
- 3) Vorticity is in  $10^{-5} \text{ s}^{-1}$  at  $2 \times 10^{-5}$  intervals.
- 4)  $d(\eta)/dy$  is in  $10^{-11} \text{ s}^{-1} \text{ m}^{-1}$ .
- 5) Rossby numbers are in  $10^{-2}$  (e.g. a value of 20 is a  $\text{Ro} = 0.20$ ).

e. Model Case Studies

1) Straight-Line Equivalent and Quasi-Barotropic

The wind data indicates the weakening of the 400 mb maximum over 12 hours. The weakening was somewhat less for the quasi-barotropic than equivalent barotropic case (Figs. 25 - 27).

The vertical motion plots show an initial hour classic four cell straight-line jet streak vertical motion pattern for the equivalent barotropic case (Fig. 28). The quasi-barotropic case shows a weak, unorganized vertical motion pattern throughout the model run (Fig. 29). The 12 hour equivalent barotropic plots (Fig. 30 - 32) show the development of significant unbalanced (I-G) vertical motion pattern which cause the PE vertical motion to deviate from the classic quasi-geostrophic (Q-G) pattern. The main influence of the I-G vertical motions is to increase the magnitude of the total PE vertical motion over the more classic balanced pattern.

The presence of any hydrodynamic instability appears to be small as the overall PE pattern remains quite close to the classic Q-G four cell pattern. There are no

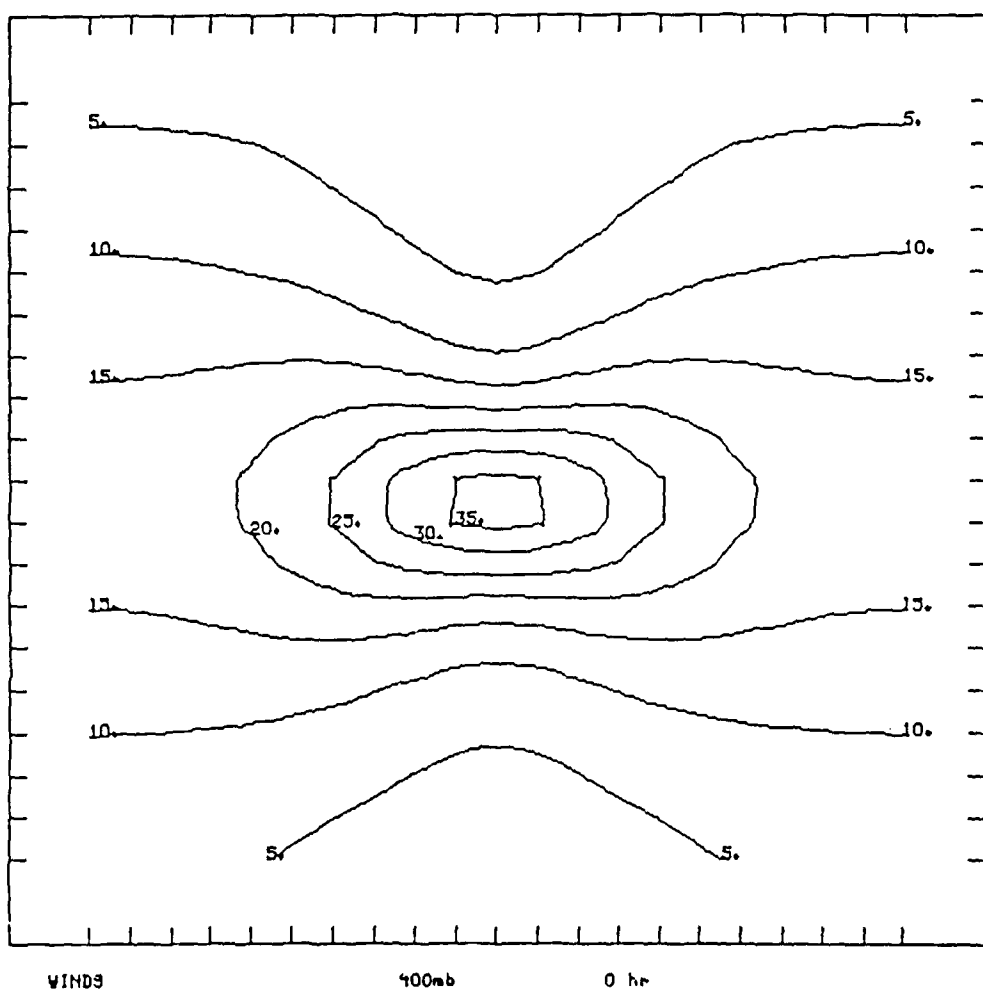


Fig. 25. Initial 400 mb winds. Quasi and equivalent barotropic conditions.

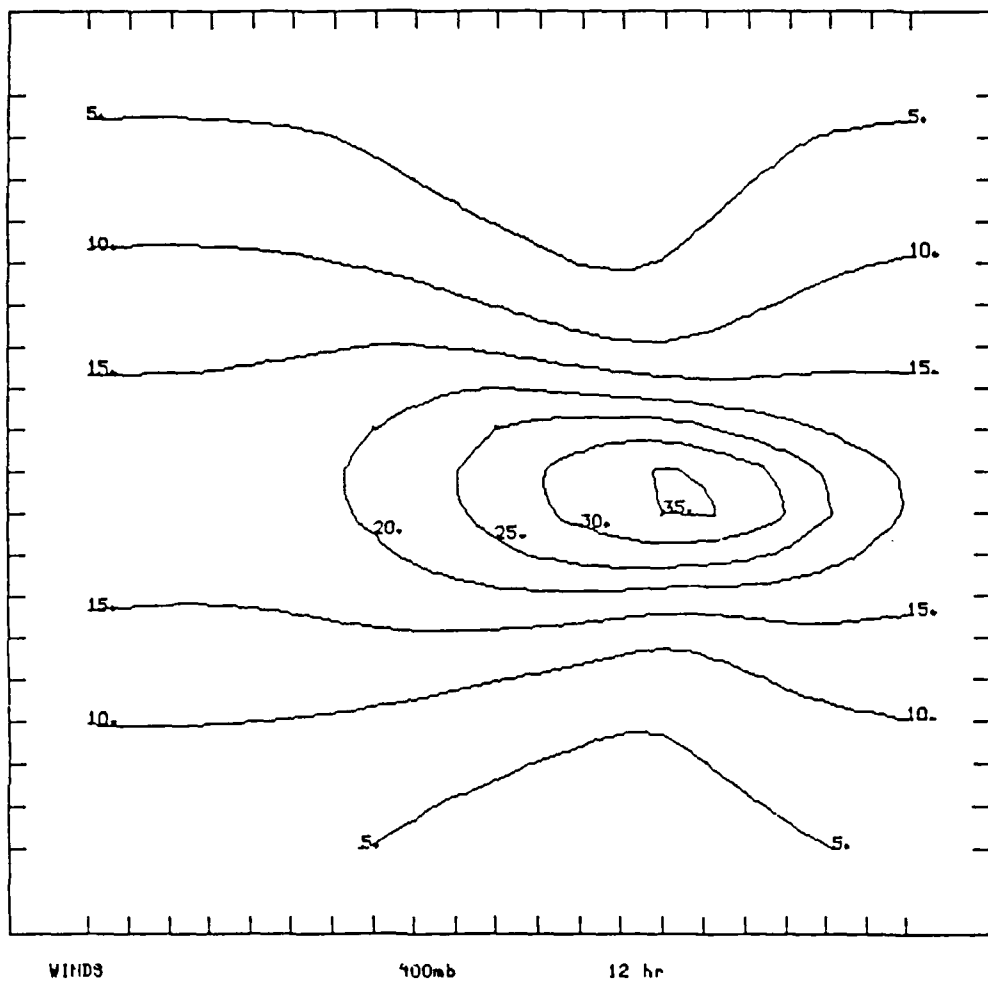


Fig. 26. 12 Hour 400 mb winds. Straight-line equivalent barotropic conditions.

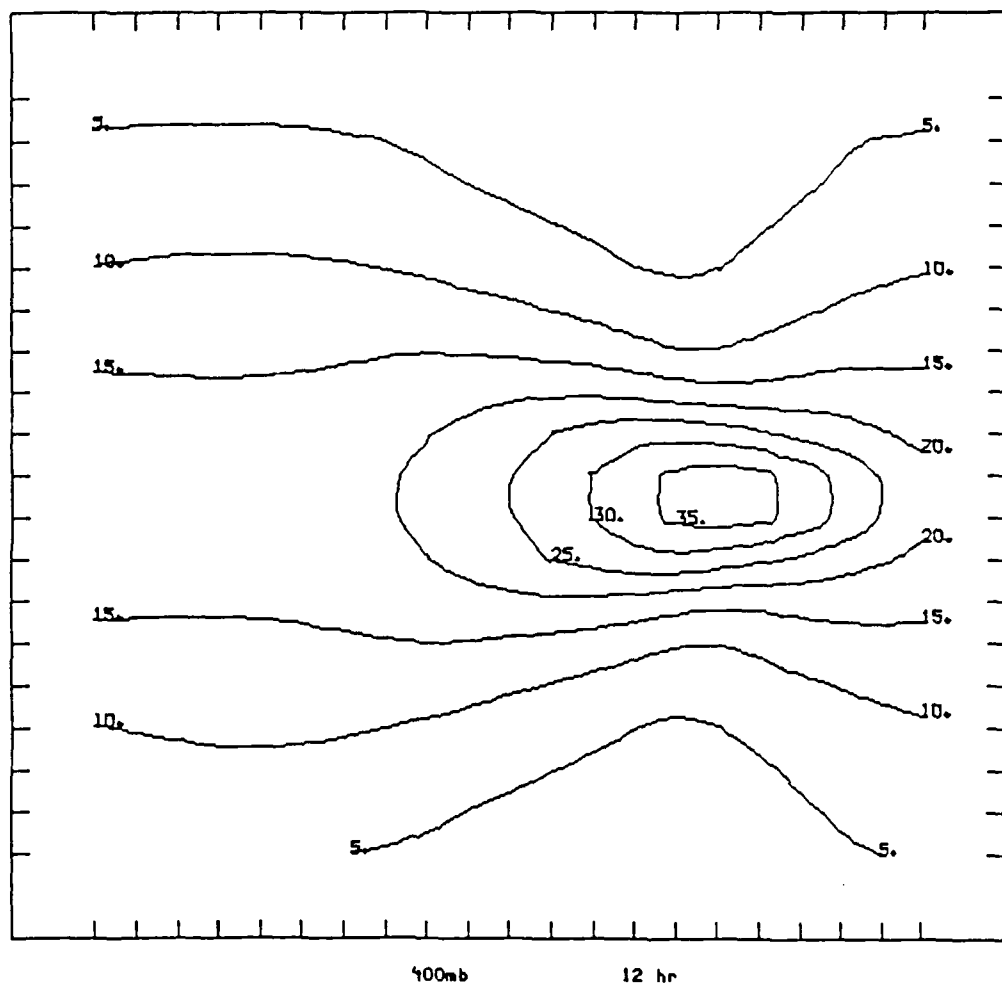


Fig. 27. 12 Hour 400 mb winds. Straight-line quasi barotropic conditions.

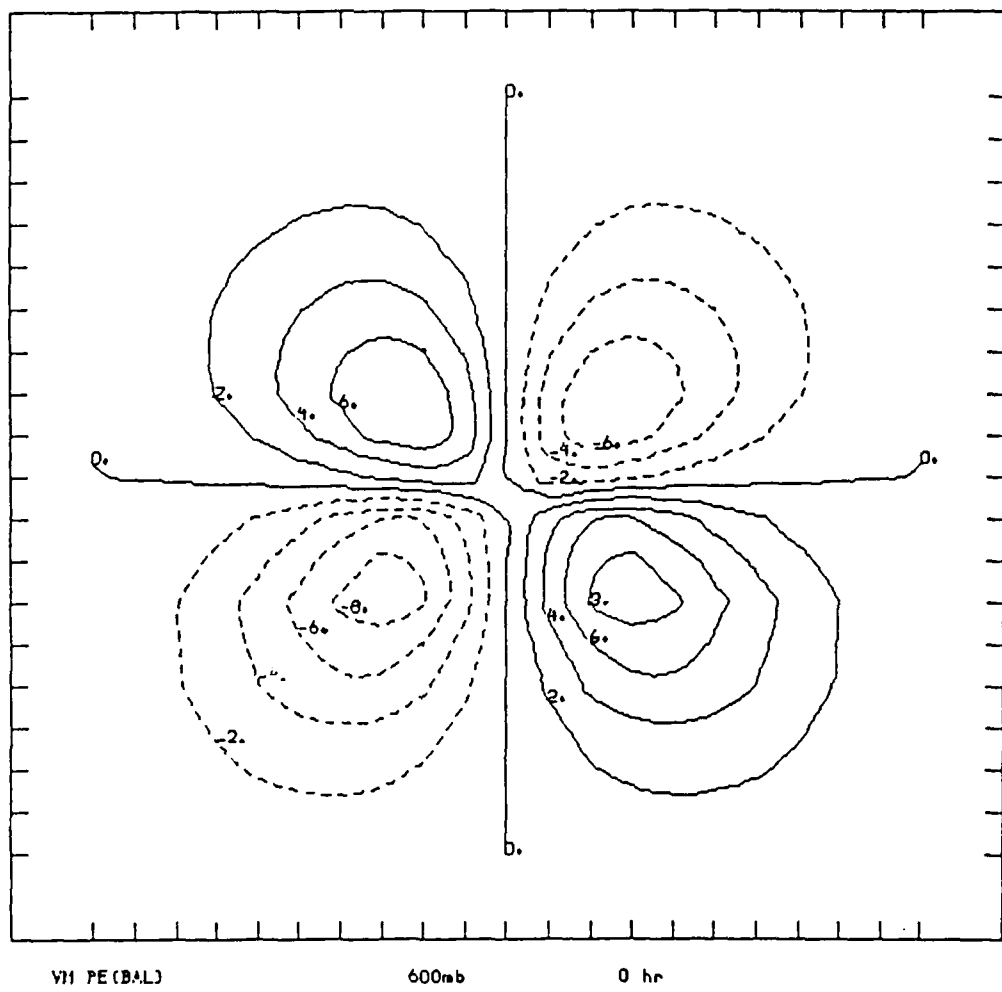


Fig. 28 Initial hour balanced and PE Eq Barotropic vertical motion.

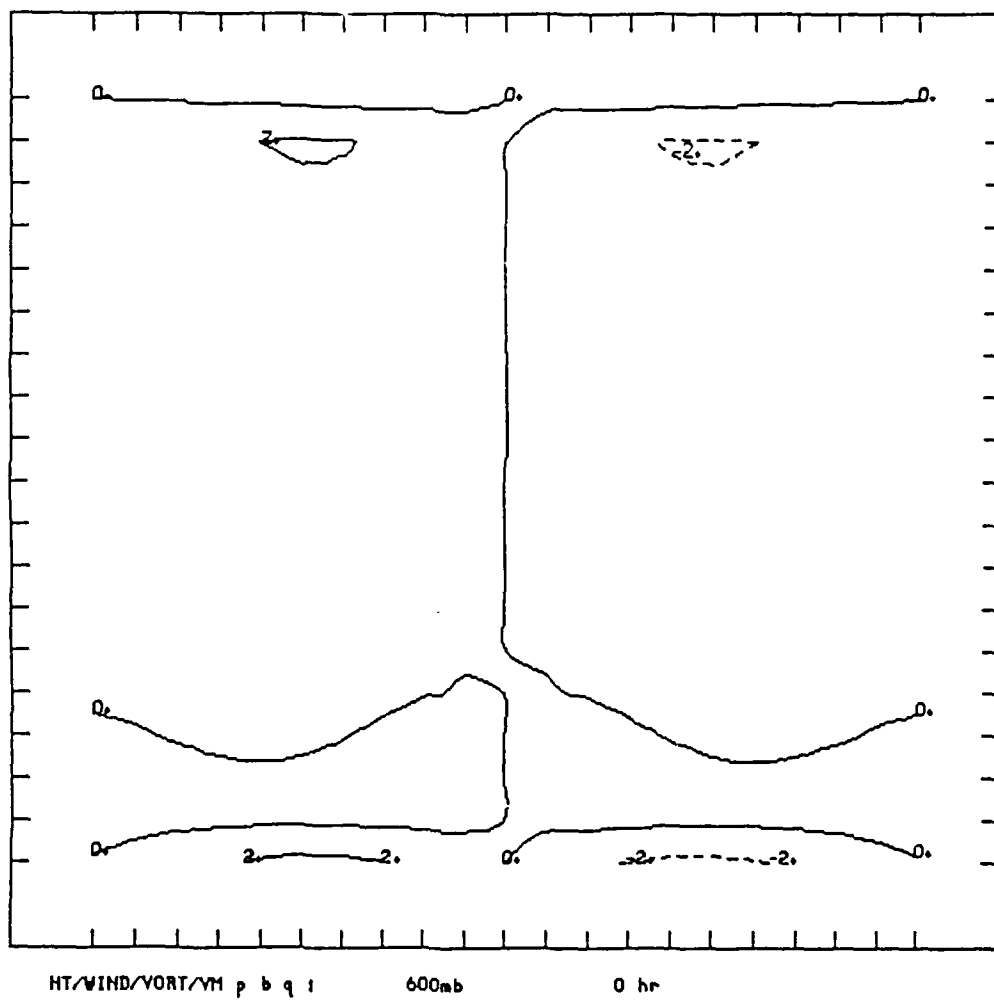


Fig. 29. Initial and 12 hour balanced and PE  
quasi barotropic vertical motion.

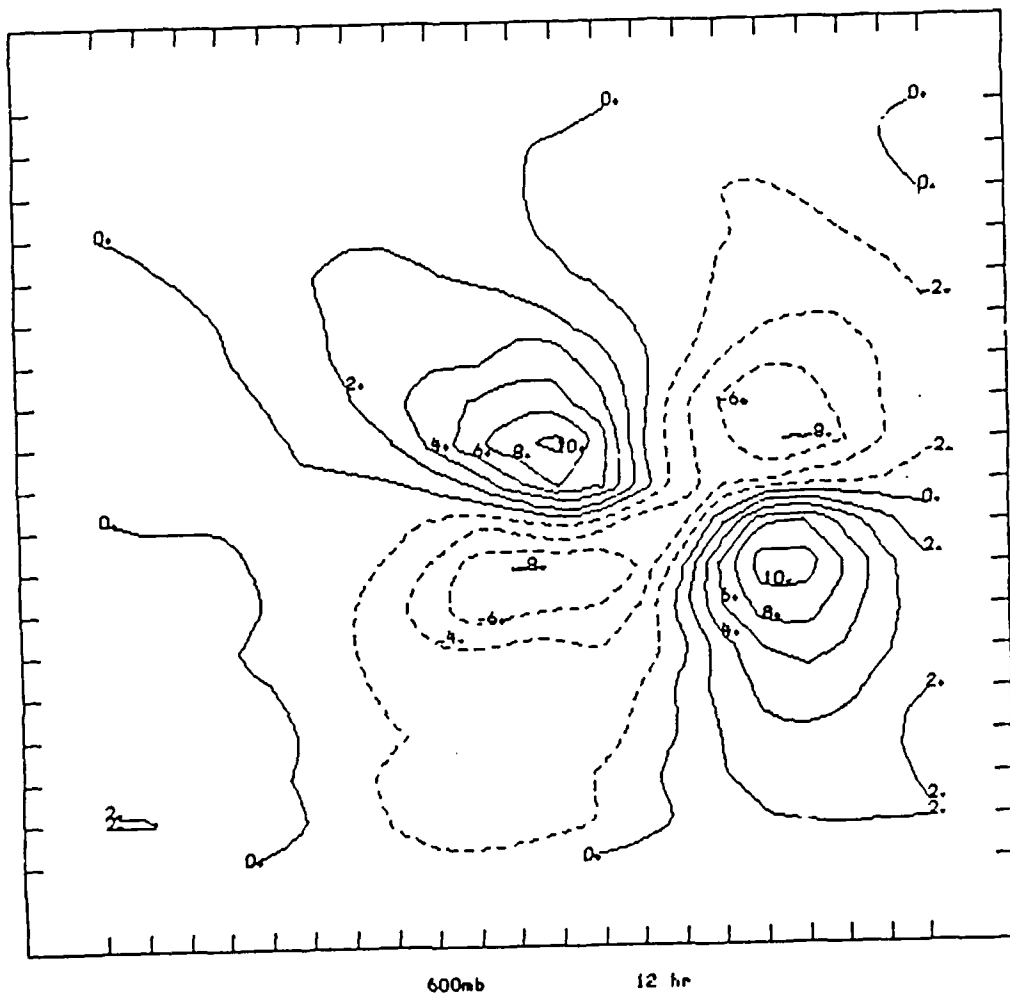


Fig. 30. 12 Hour vertical motion PE Equivalent Barotropic.

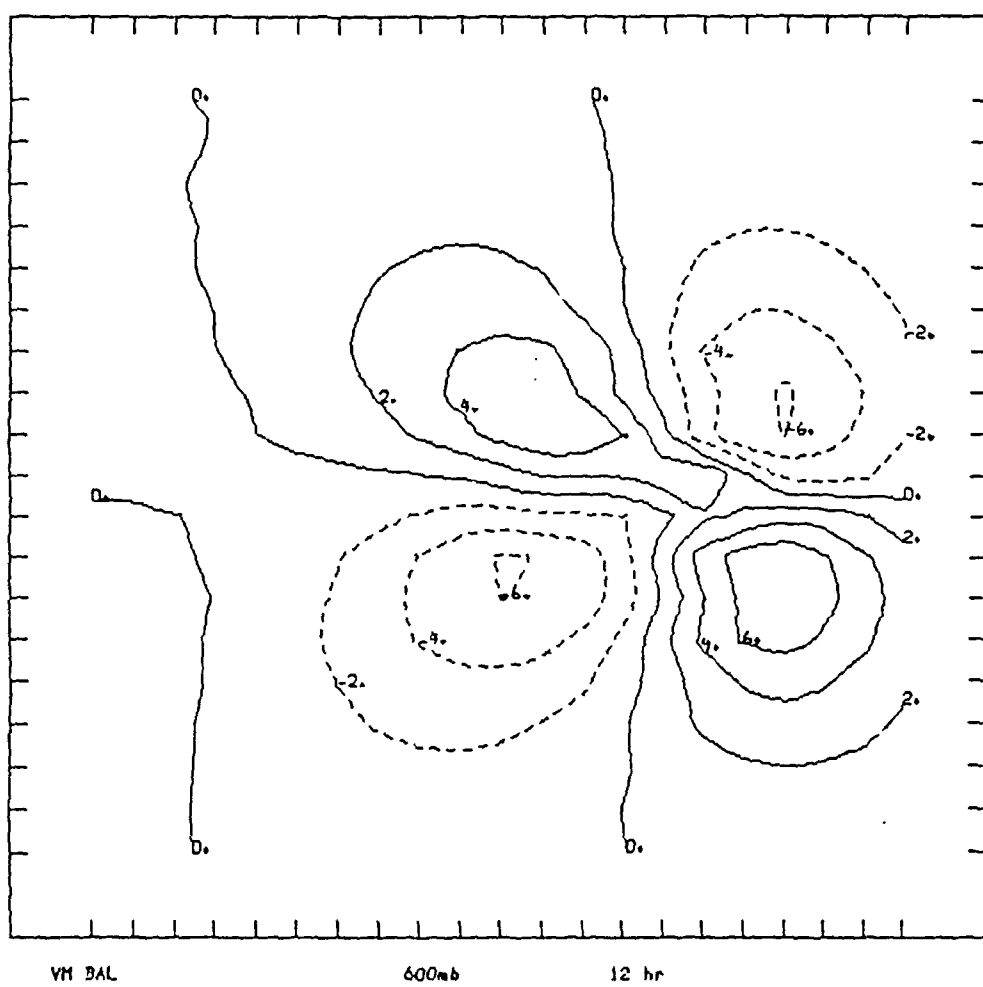


Fig. 31. 12 Hour balanced eq barotropic vertical motions.

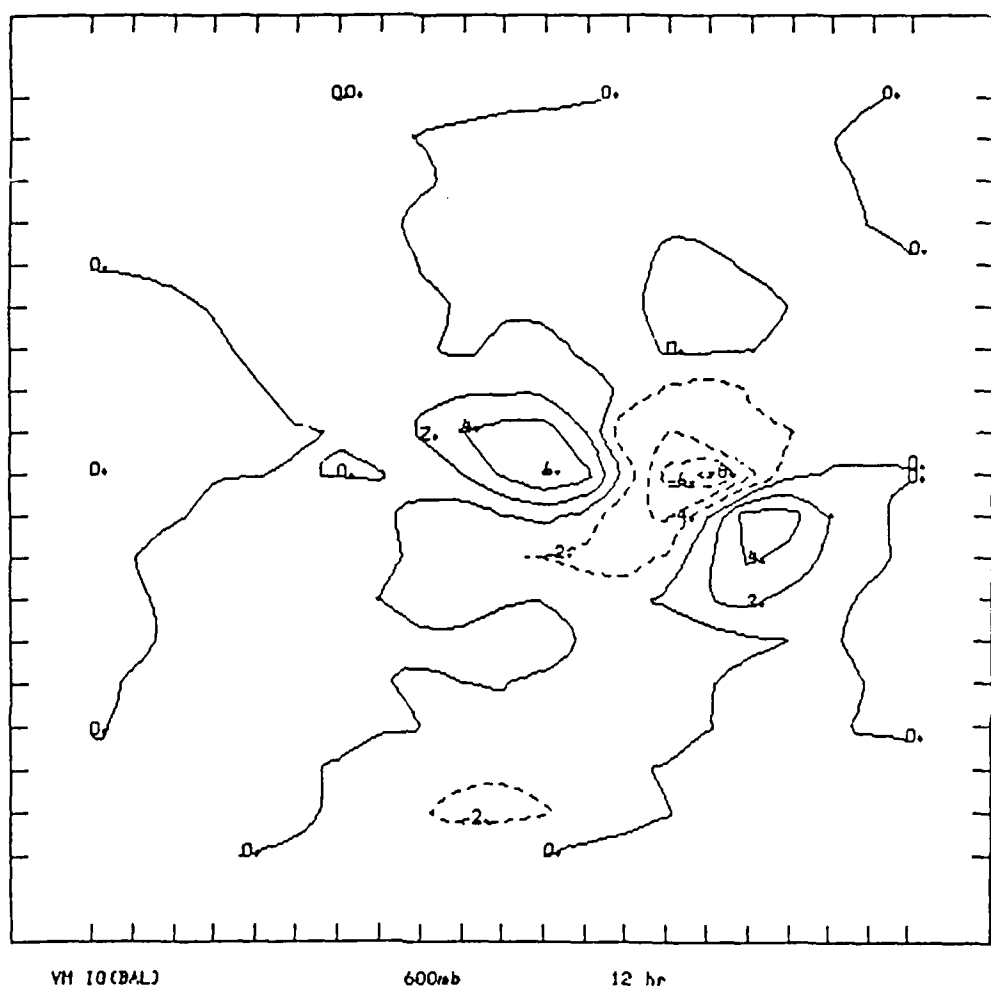


Fig. 32. 12 Hour vertical motion IG Equivalent  
Barotropic.

negative values on the absolute vorticity plots, thus no indication of rotational inertial instability. The vertical motion patterns for straight-line jet streaks associated with negative absolute vorticity values deviated much more from the classic vertical motion pattern than this case.

There seems to be no evidence for barotropic inertial instability. However, the  $d\eta/dy = 0$  isopleth intersects the vorticity maximum polward of the jet streak axis which would seem to allow for barotropic instability (Figs. 33 to 36).

The possibility of baroclinic instability exists in the equivalent barotropic model case. As Holton (1979) points out the addition of a thermal wind to the model with a constant  $f$  value should be baroclinically unstable. However, the growth rate due to baroclinic instability appears to be quite small. In the cases adding a beta plane, the balanced component of the vertical motion increased, while the I-G component decreased for the same conditions. Holton (1979) describes how replacing a constant  $f$  with a beta plane should increase baroclinic stability. This would seem to suggest that both the balanced and unbalanced vertical motions should decrease with the addition of a beta plan.

Figures 37 and 38 show the values of  $Ro$ . The value of  $\tilde{Ro}$  for this case is 0.38. The plots indicate a lower maximum value of  $Ro = 0.2$ . The lower  $Ro$  value indicates that the geostrophic approximation is even better for this case than the large scale Rossby number would indicate. This goes along with the fact that aside from the magnitude differences the general pattern of the total PE vertical motion resembles quite closely the pattern predicted by the quasi-geostrophic approximation. Also, it would be seen that the real atmosphere would tend to smooth out the differences in magnitude of the vertical motions due to compensating motions in the vertical. Such compensating motions are not possible in the two layer model.

The results of the straight line model run with initial negative values of absolute vorticity differed substantially from those with all positive absolute vorticity values.

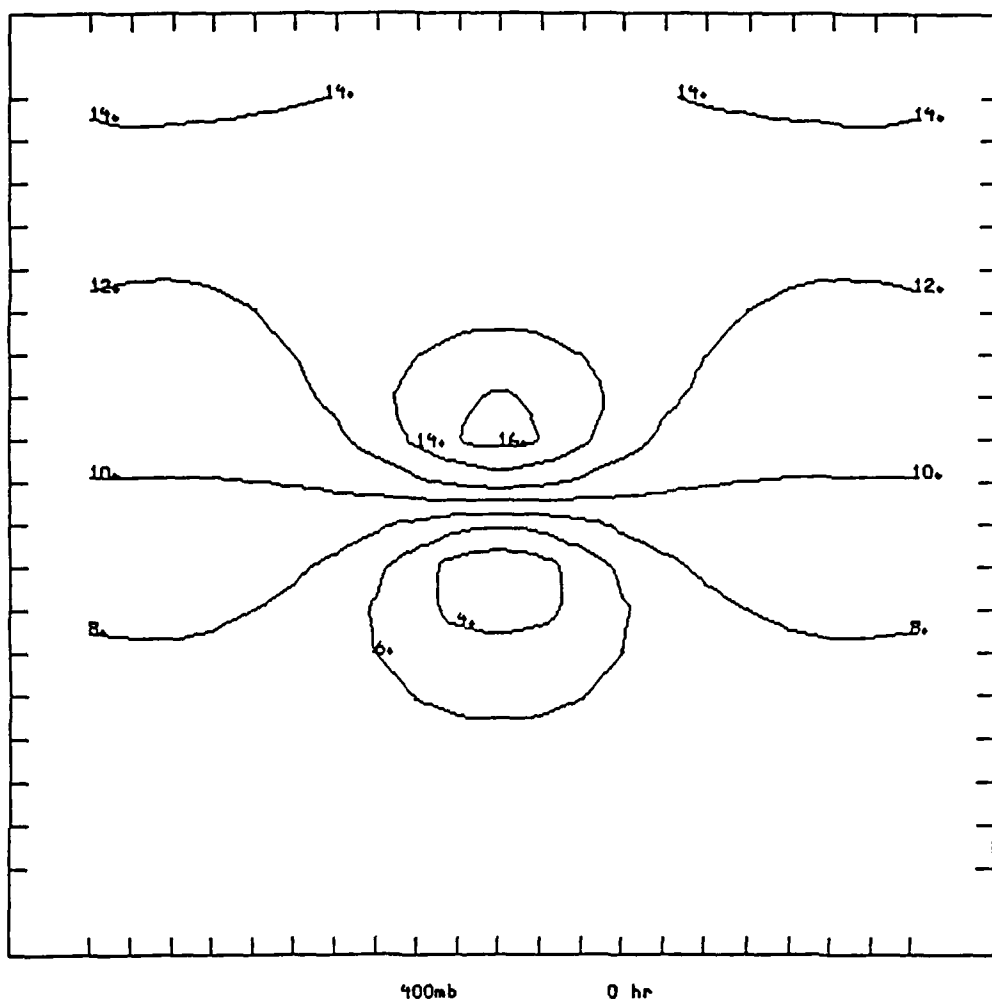


Fig. 33. Initial hour equivalent barotropic absolute vorticity.

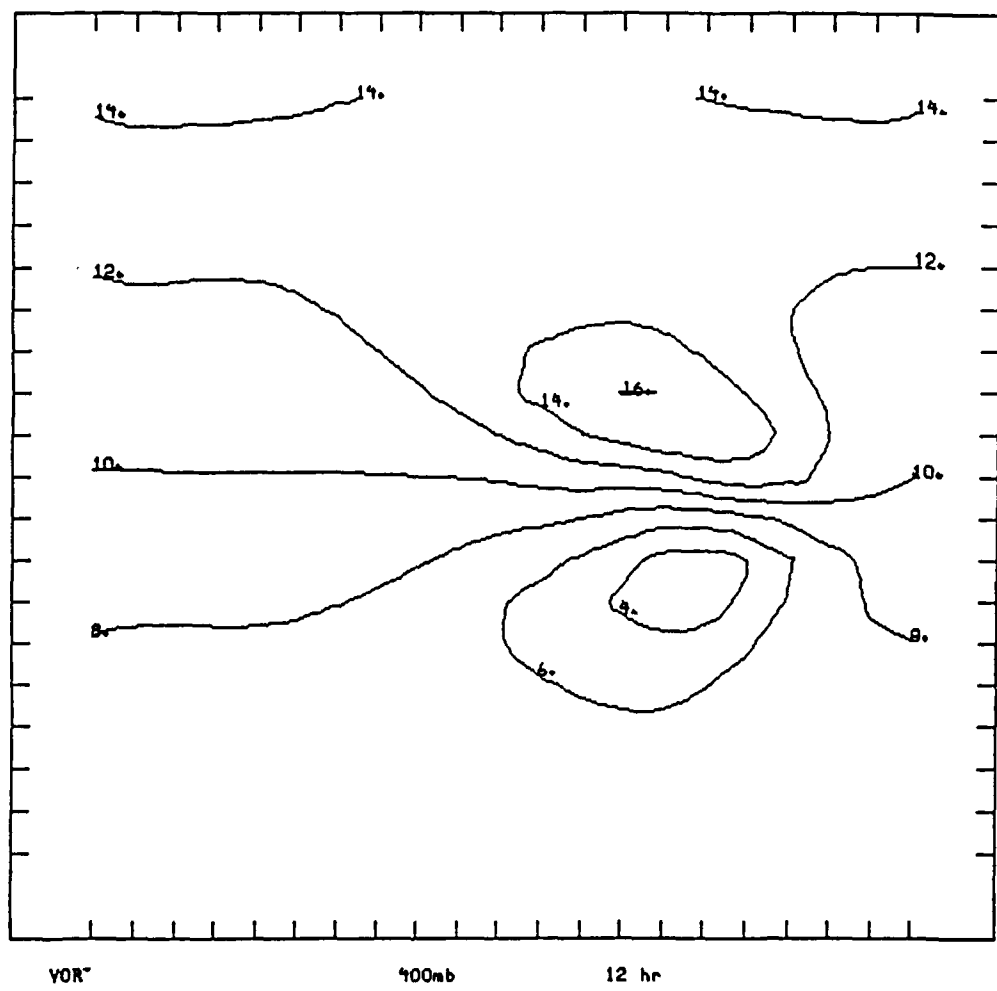


Fig. 34. 12 hour equivalent barotropic absolute vorticity.

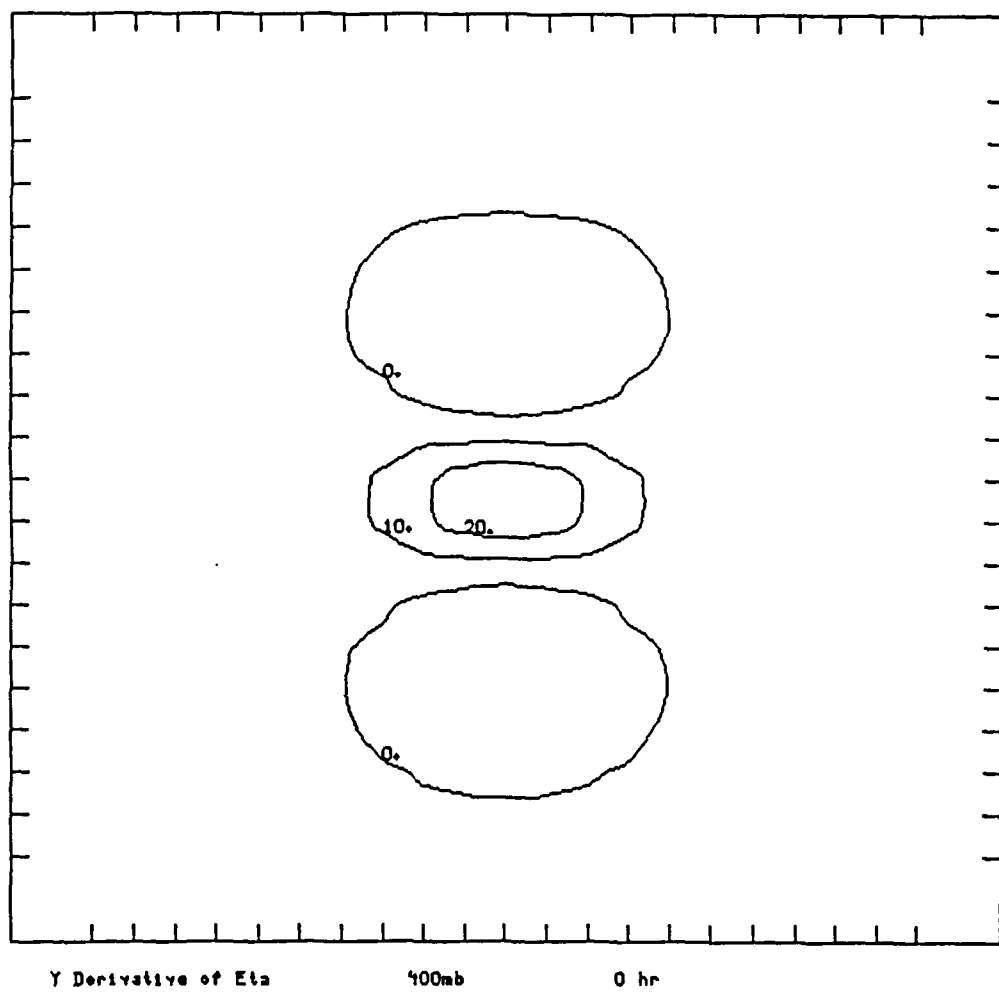


Fig. 35. Initial hour equivalent barotropic absolute vorticity variation with latitude.

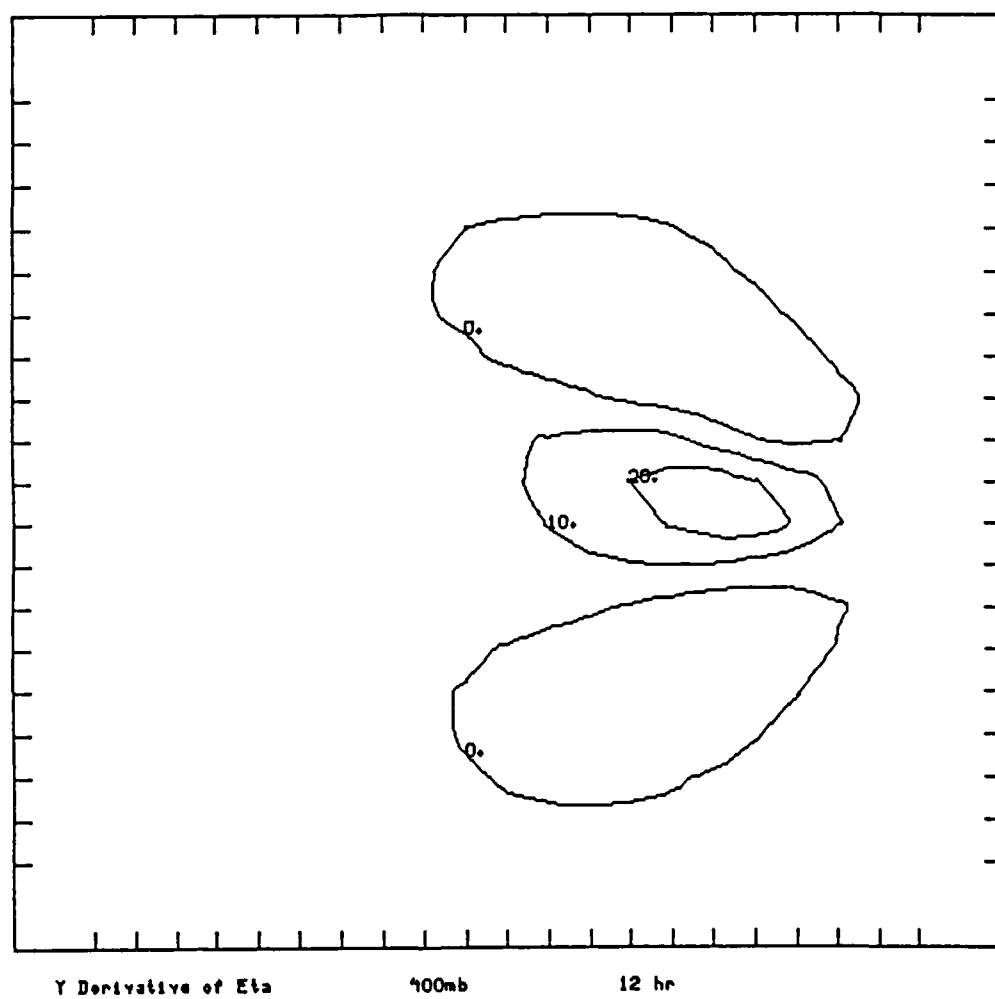


Fig. 36. 12 hour equivalent barotropic absolute vorticity variation with latitude.

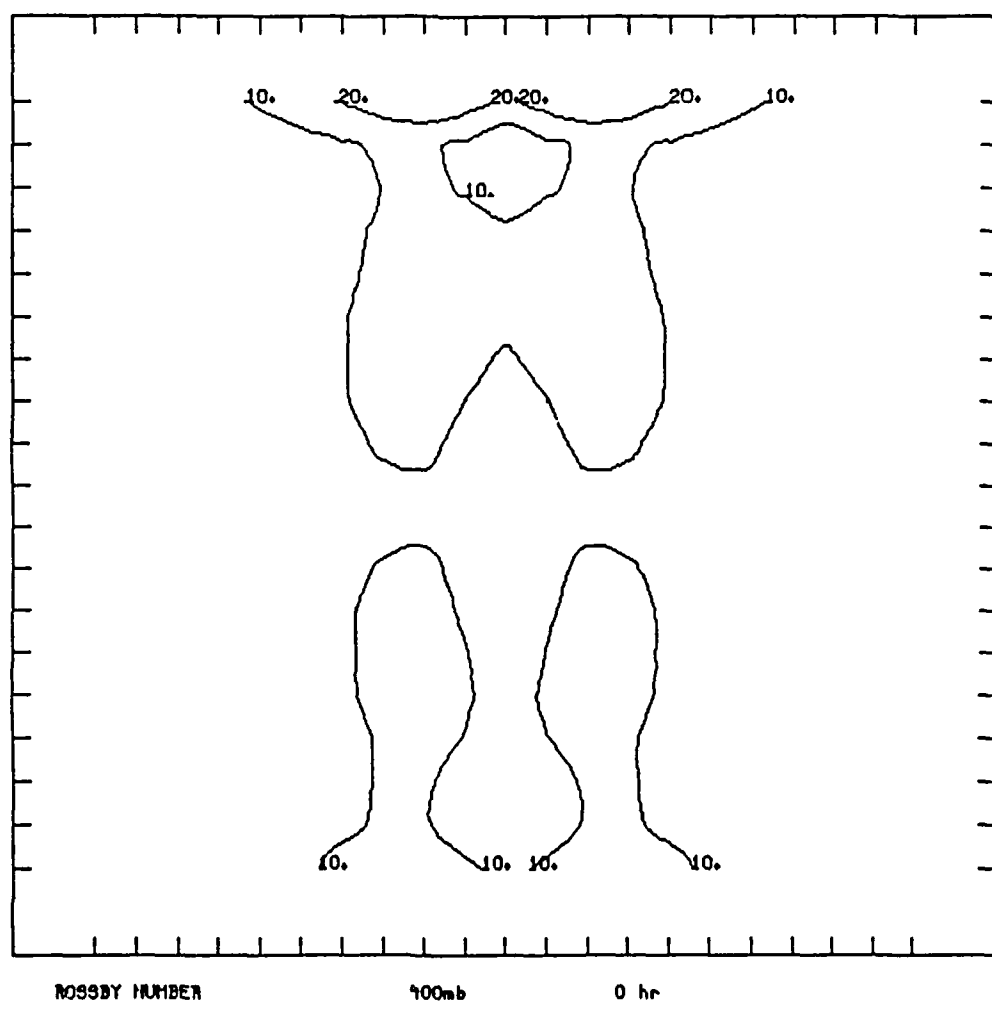


Fig. 37. Initial Hour Rossby Number (Ro) Eq Barotropic.

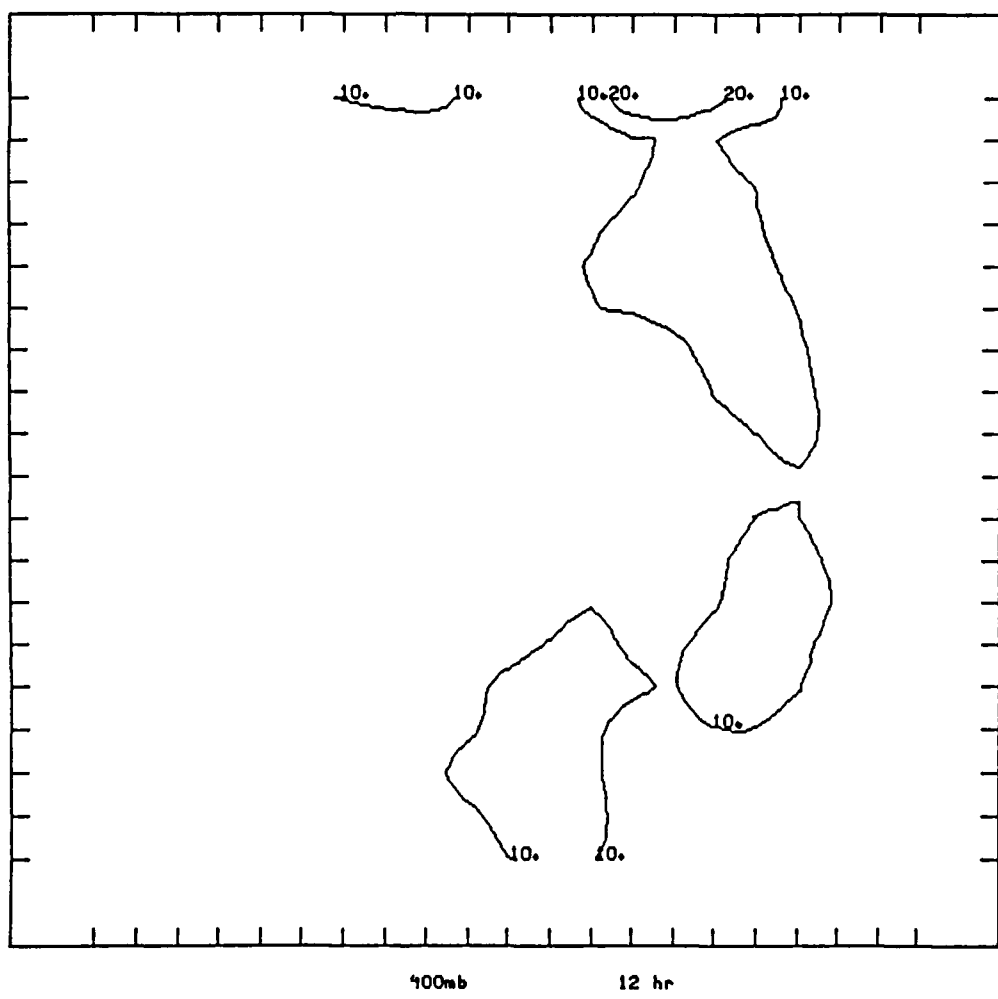


Fig. 38. 12 Hour Rossby Number (Ro) Eq Barotropic.

The negative values were located exclusively equatorward of the jet streak axis (Fig. 39). This resulted in rotational inertial instability and dramatically increased the vertical motion values (Fig. 40). The increase in vertical motion outside the area of inertial instability suggests that non-linear interactions are enhancing vertical motions.

The general conclusion that can be made from the straight - line cases is that the quasi-geostrophic assumption is reasonable for straight-line jet streaks without rotational inertial instability.

## 2) Anticyclonic Equivalent and Quasi-Barotropic

The quasi-barotropic anticyclonic cases showed little changes in the vertical motion strength and only slight increases in Rossby number when curvature was added. The low Rossby numbers suggest that the geostrophic adjustment process taking place is weak resulting in little vertical motion.

By contrast, the equivalent barotropic case shows vertical motion about three times as large as the corresponding quasi-barotropic case. The Rossby number-vertical motion relationship maintains a fair linear relationship until inertial instability is present. In the case where the initial 400 mb speed max is 74 m/s inertial instability dominates the vertical motion. The most significant feature of this case was the production of highly negative absolute vorticity values. The likely result was rotational inertial instability.

Initial wind speed is 74 m/s (Fig. 41 shows 65 m/s due to smoothing by the plotting program) and decreases to about 68 m/s in 12 hours. The initial hour organized isotach pattern becomes quite complex in 12 hours. Several secondary wind maxima are created upstream from the main jet streak maximum (Fig. 42). The resulting PE vertical motion is strong but fairly well organized in the initial hour with an extremely strong complex pattern by the 12 hour (Figs 43 and 44).

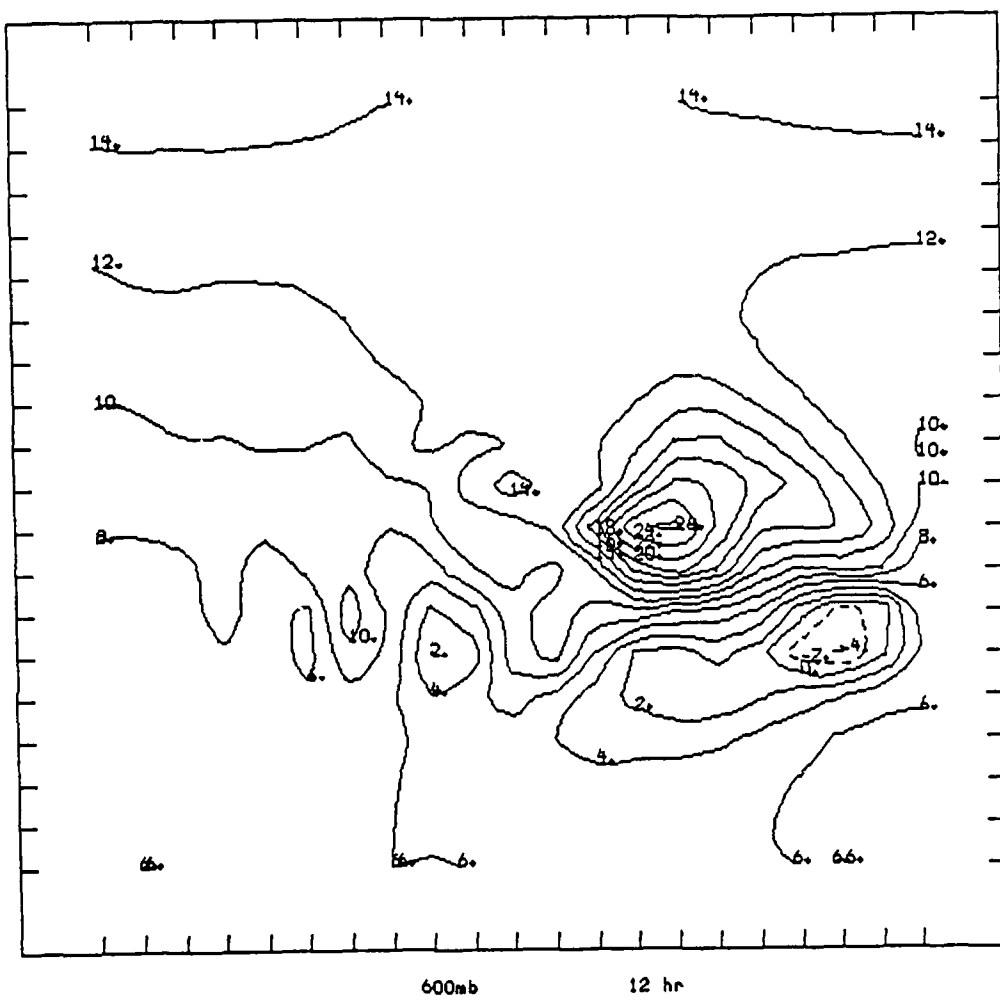


Fig. 39. Inertial unstable absolute vorticity values.

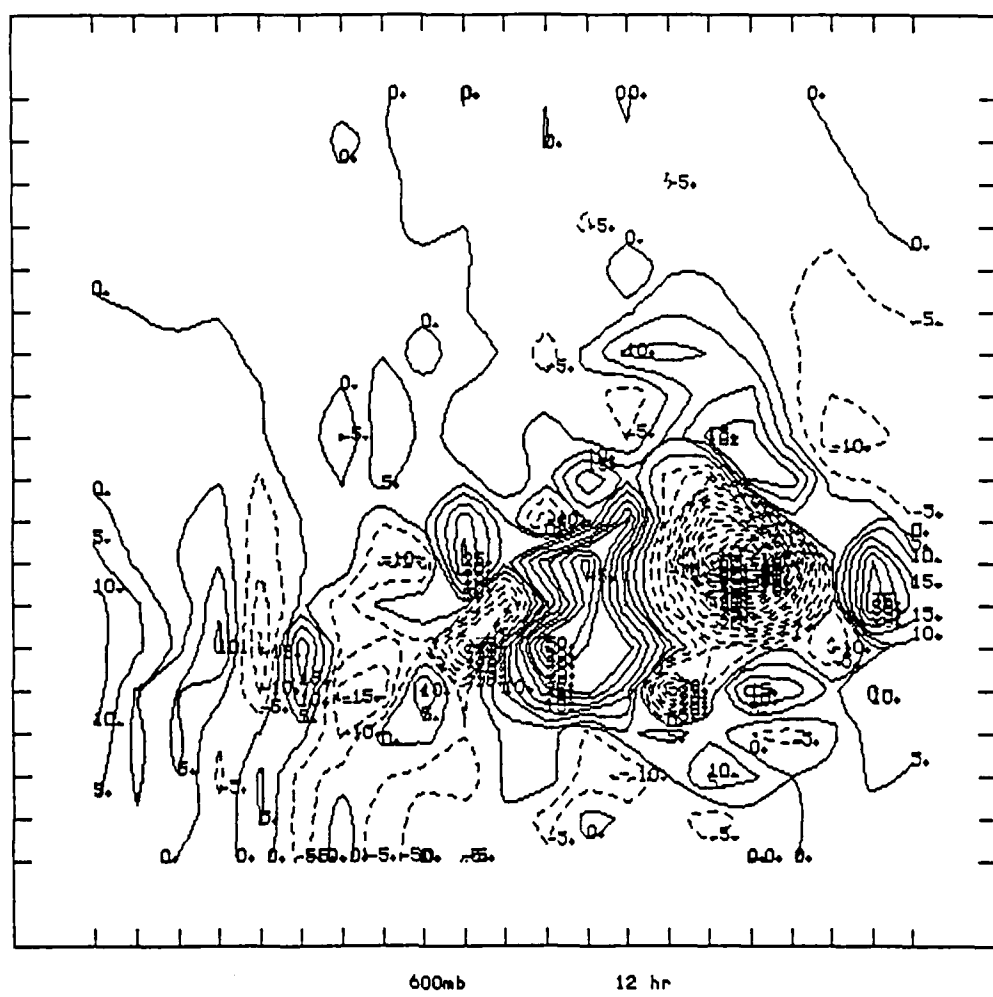


Fig. 40. Inertial unstable PE vertical motion.

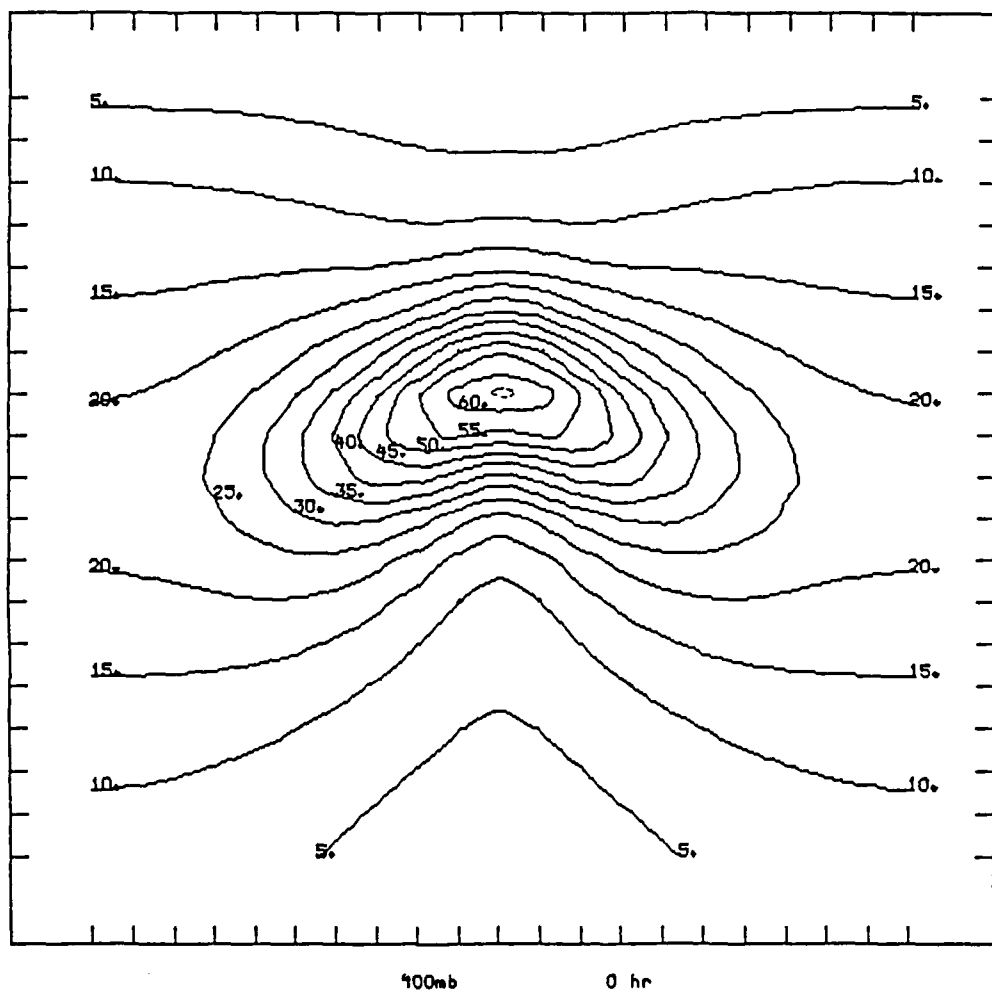


Fig. 41. Initial Hour Anticyclonic 400 mb wind speed.

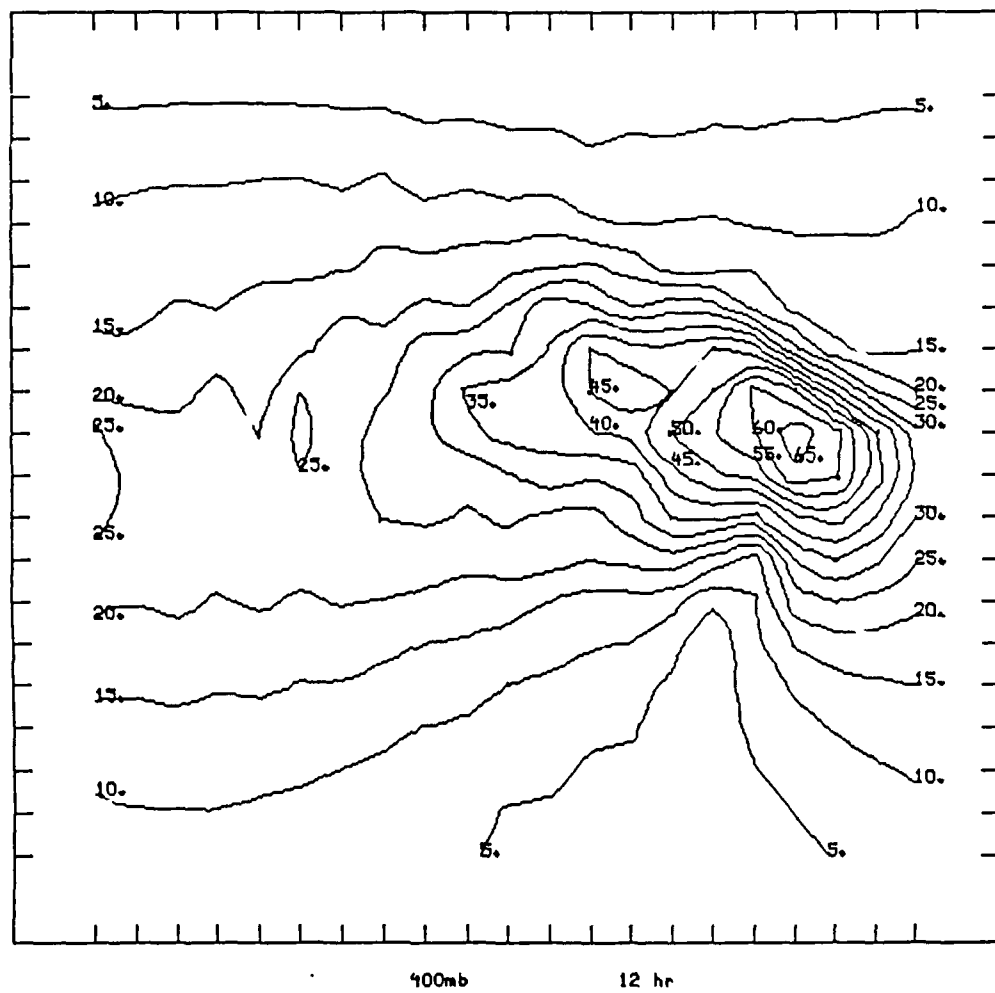


Fig. 42. 12 Hour Anticyclonic 400 mb wind speed.

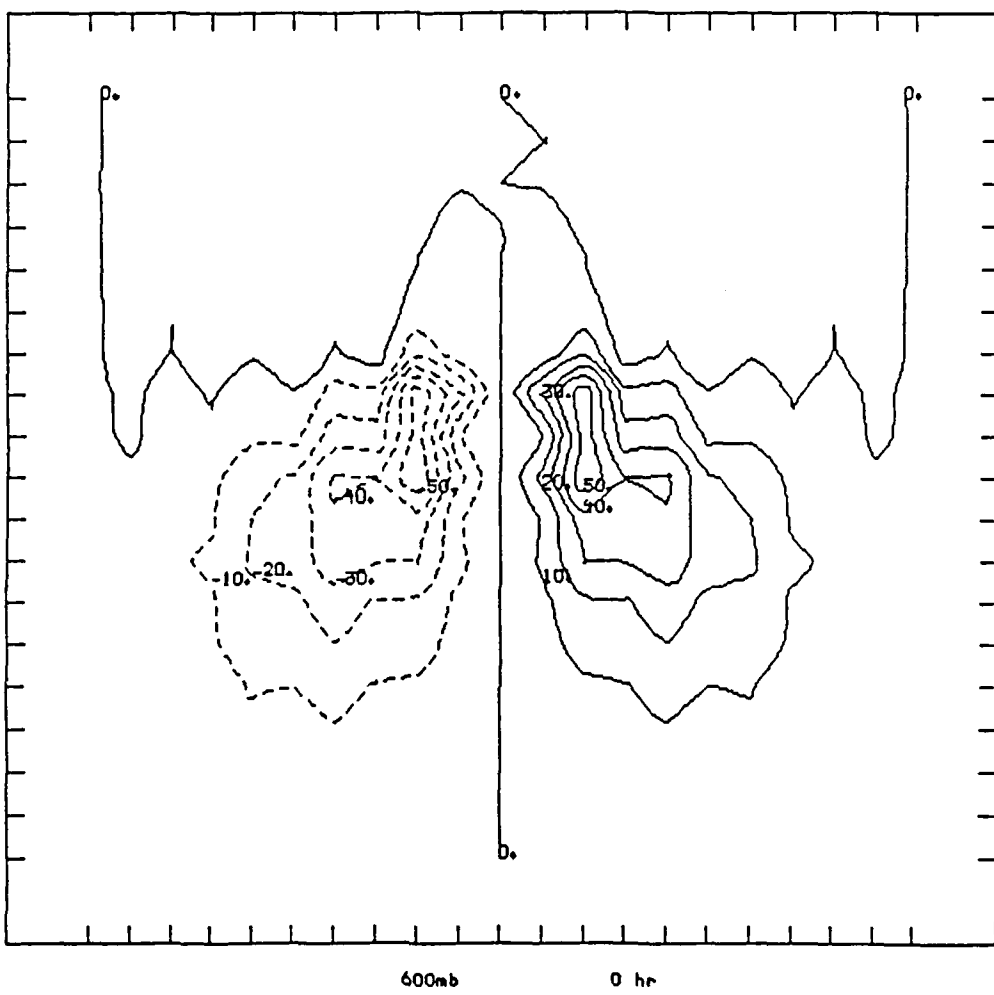


Fig. 43. Initial hour PE vertical motion.

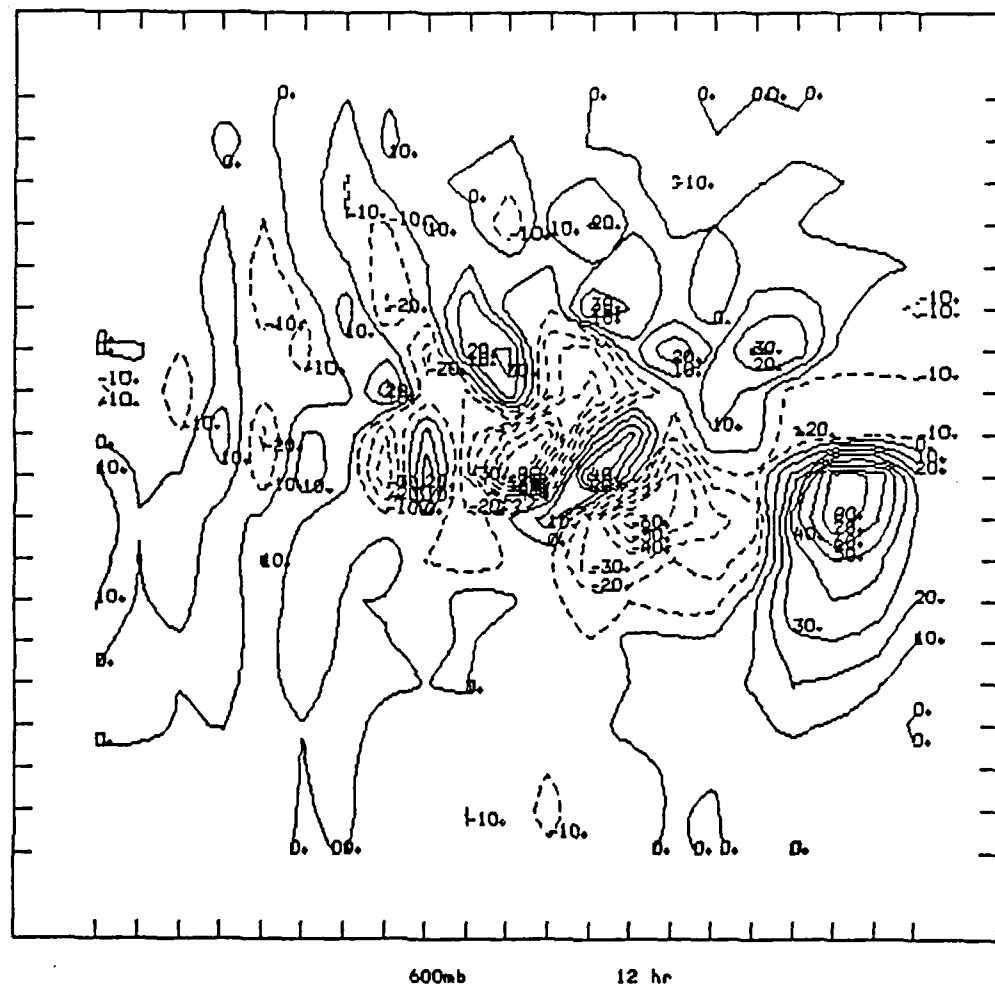


Fig. 44. 12 hour PE vertical motion.

Rotational inertial instability seems to be certain in this case with negative absolute vorticity values as low as -10 (Figs. 45 and 46). Barotropic inertial and baroclinic instabilities have the same possibility of occurring as discussed in the straight line Case A (Figs. 47-48). In addition, some form of computational instability may be possible with the very high wind speeds causing very high wave speeds. However the model does not "blow up" completely which would be expected in a case of severe computational instability.

The initial value of  $\tilde{Ro}$  is a relatively high 0.74, but a much higher  $Ro$  of 1.00 is observed. During the 12 hours of the model run  $\tilde{Ro}$  decreases to about 0.65 indicating a progression back to geostrophic balance. However, the  $Ro$  value increases dramatically to about 1.7 indicating a large increase in ageostrophy (Figs. 49 and 50). The overall results certainly support the indication of increased ageostrophy as indicated by  $Ro$ .

The major conclusion for the anticyclonic cases are that the geostrophic approximation is poor for anticyclonic vertical motion in general and is very poor for high wind speed cases because of the production of rotational inertial instability; also  $Ro$  is a much better indicator of the true Rossby number.

### 3) Cyclonic Equivalent and Quasi-Barotropic

The quasi-barotropic cyclonic case showed slightly higher vertical velocity values. However the equivalent barotropic cases showed dramatic increases in both the Rossby number and the vertical velocities. The only case that had vertical velocities comparable with the cyclonic values were the anticyclonic cases that exhibited rotational inertial instability.

First, examining the results from a cyclonic case with an initial 400 mb speed maximum of 36 m/s. The main feature evident from this case is the deviation from the classic quasi-geostrophic vertical motion pattern due to the addition of cyclonic

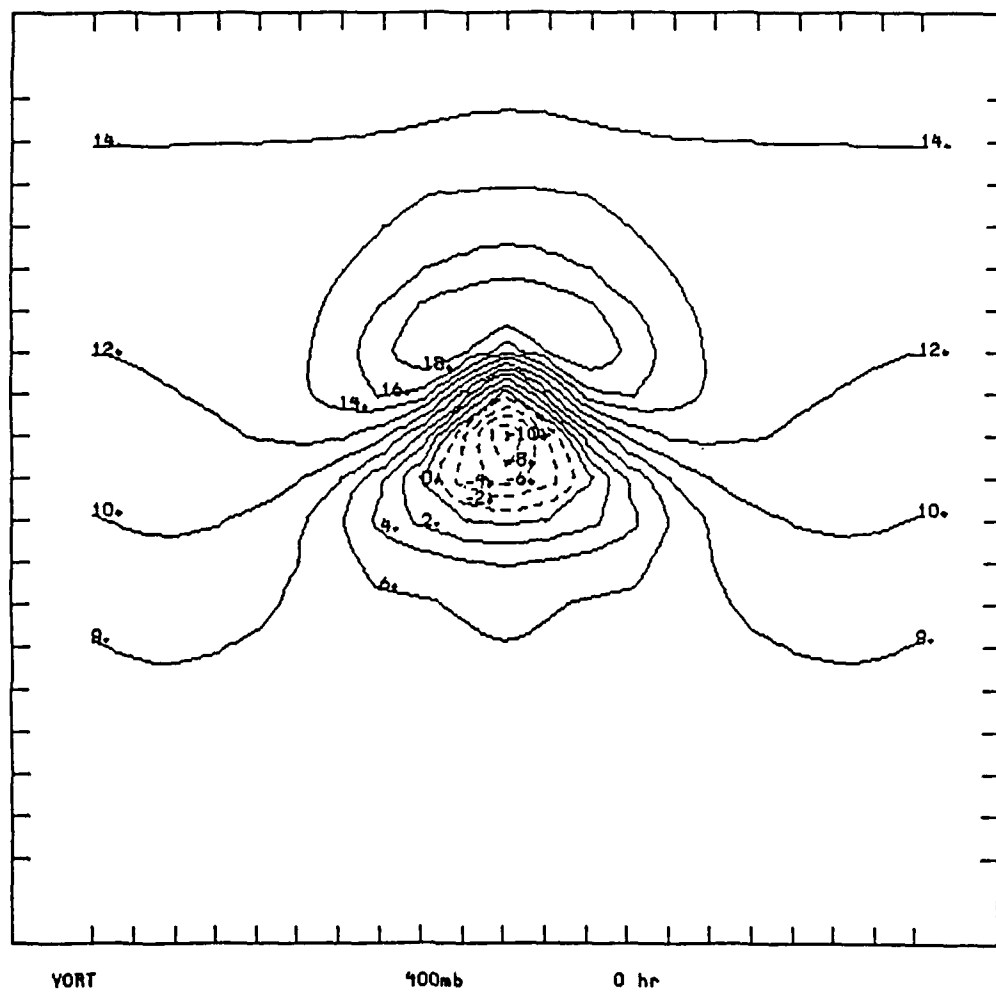


Fig. 45. Initial hour absolute vorticity.

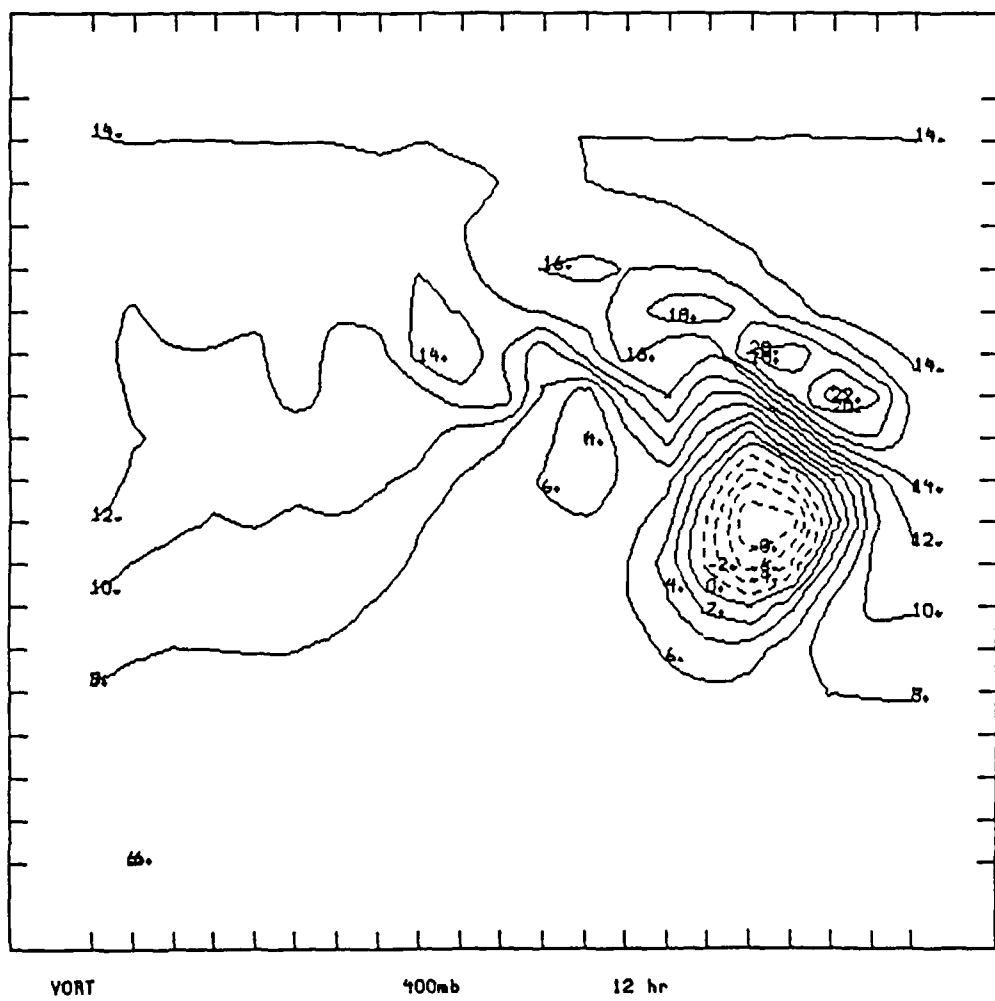


Fig. 46. 12 hour absolute vorticity.

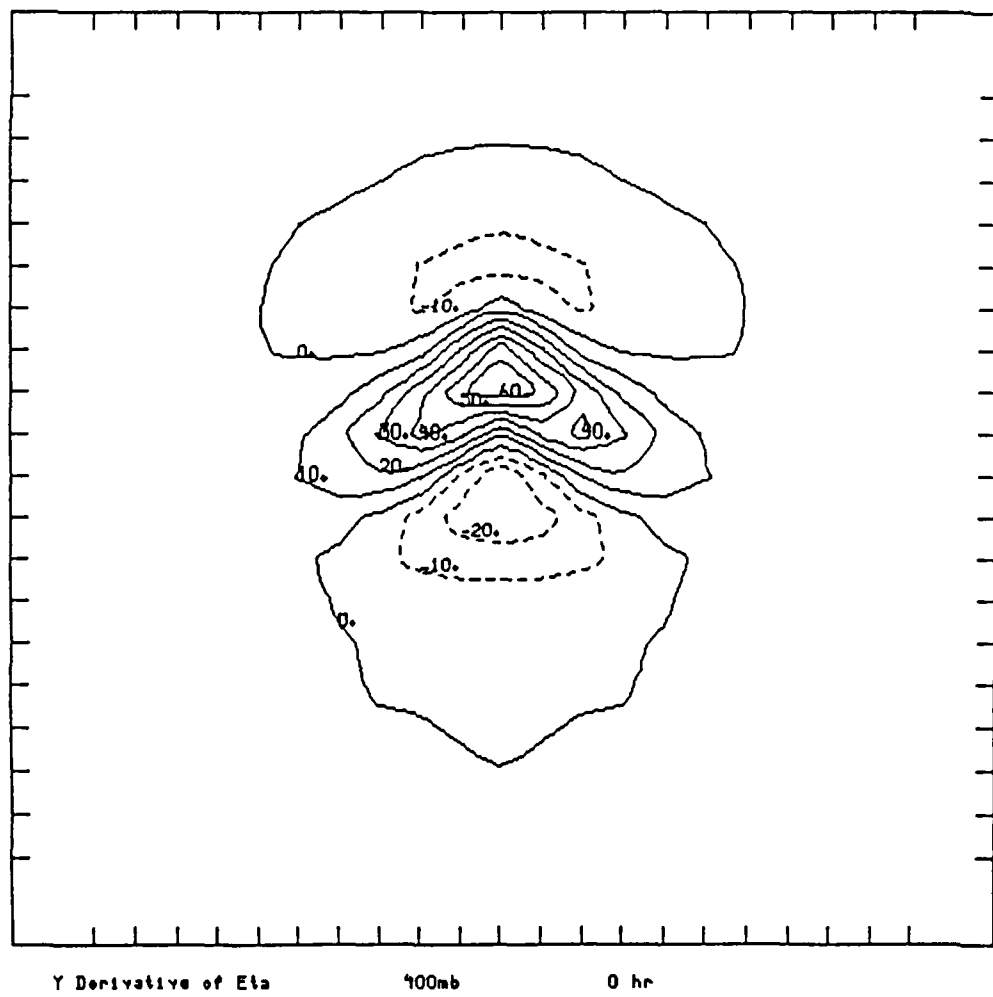


Fig. 47. Initial hour absolute vorticity variation with latitude.

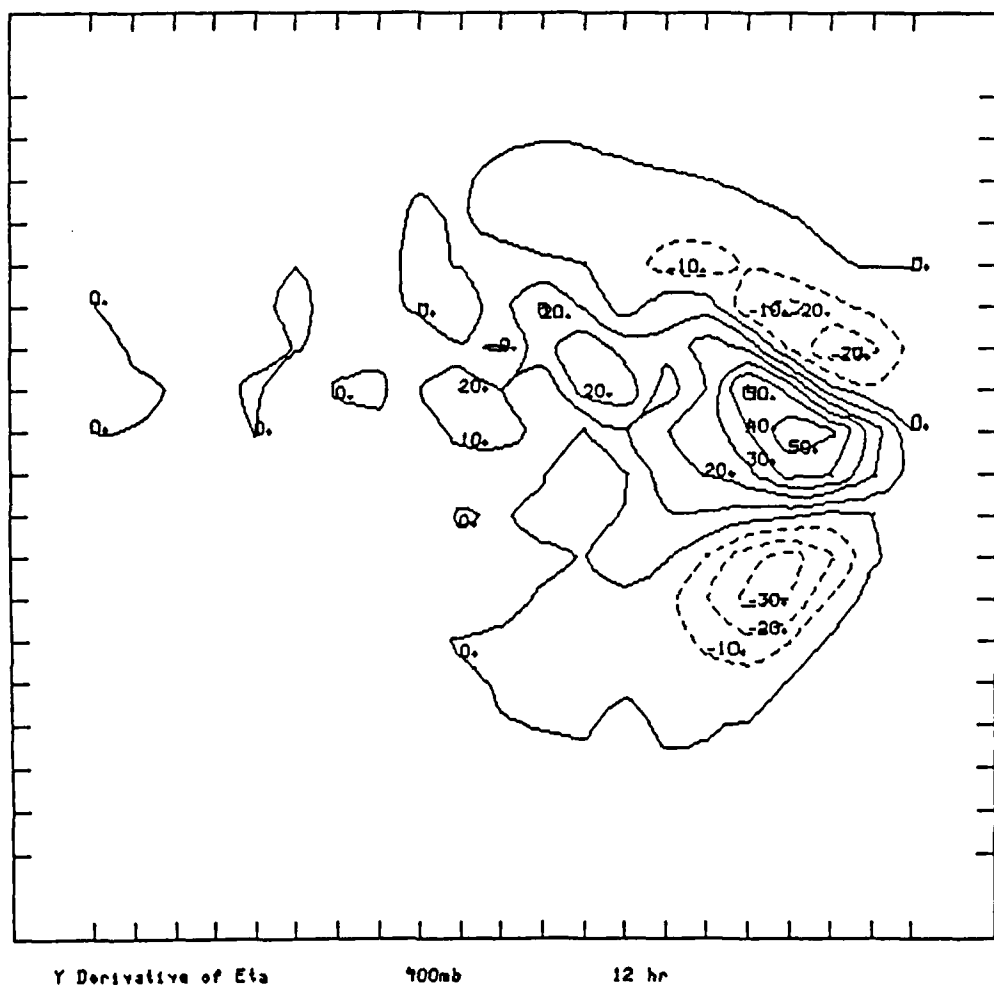


Fig. 48. 12 Hour absolute vorticity variation with latitude.

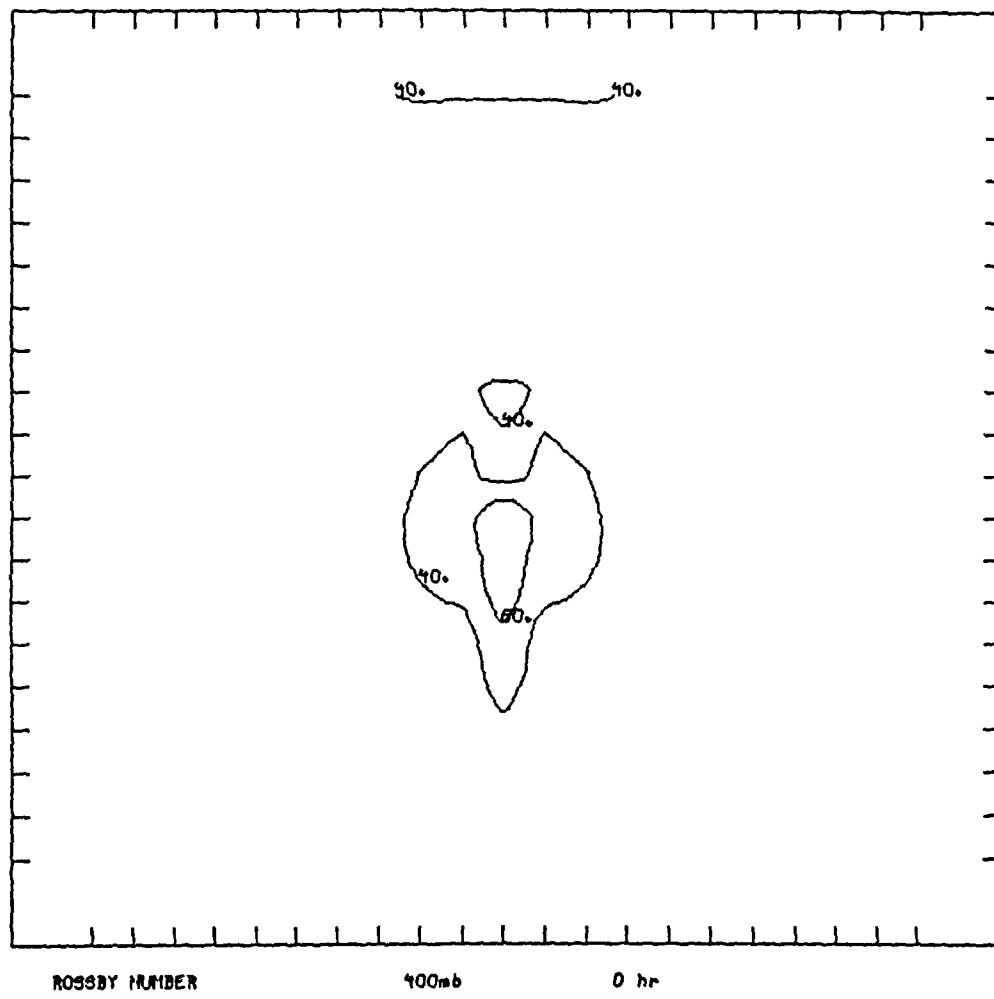


Fig. 49. Initial Hour Rossby Number (Ro) Eq Barotropic.

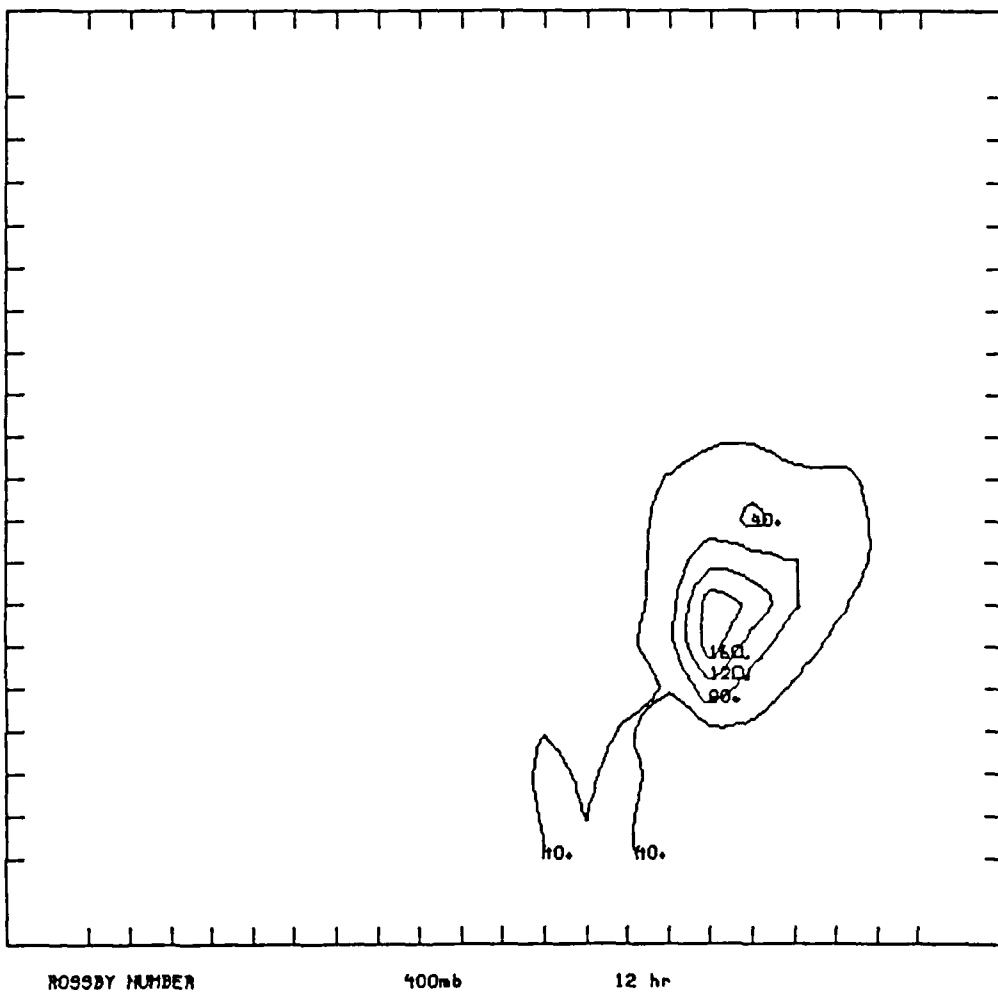


Fig. 50. 12 Hour Rossby Number (Ro) Eq Barotropic.

curvature.

The wind data indicated a trend for the jet streak maximum to propagate slightly faster than the short wave height trough axis resulting in the speed maximum to be slightly ahead of the height trough axis by 12 hours. In addition, the trough axis shifts from a neutral to a slightly negative tilt with time. This resembles what one observes in real jet streams with low level cyclogenesis (Figs. 51 - 53). The 1000 mb height field developed significant cyclonic circulations giving confidence that the model is simulating the real atmosphere reasonably well.

The initial equivalent barotropic motion pattern is quite organized and symmetrical. However, the vertical motion is stronger and organized into a two cell pattern as compared to the corresponding straight-line case. As in the straight-line case the quasi-barotropic vertical motion remains near zero. The increased strength of the initial vertical motion field shows that in this case the along-contour ageostrophy due to the curvature effect is strong enough to neutralize the cross-contour ageostrophy due to the speed effects equatorward of the jet streak axis as well as to intensify the vertical motions into a concise two cell pattern (Figs. 54 - 56). This can be understood and predicted qualitatively by the quasi-geostrophic approximation. However, the 12 hour equivalent barotropic vertical motions deviate considerably from the quasi-geostrophic theory. The most noted deviation is a secondary upward vertical motion maximum that is caused by a strong unbalanced (I-G) vertical motion component. This secondary upward vertical motion maximum is as strong as the primary maximum in the corresponding straight-line case. This pattern seems to resemble the occurrence of a secondary upward vertical maximum behind a short wave trough. This pattern is quite common as indicated by a primary and secondary comma cloud field (Fig. 57).

When looking at hydrodynamic instabilities, rotational instability can be ruled out because all absolute vorticity values remain positive (Figs. 58 and 59). The argument for barotropic inertial instability and baroclinic instability remains the same as

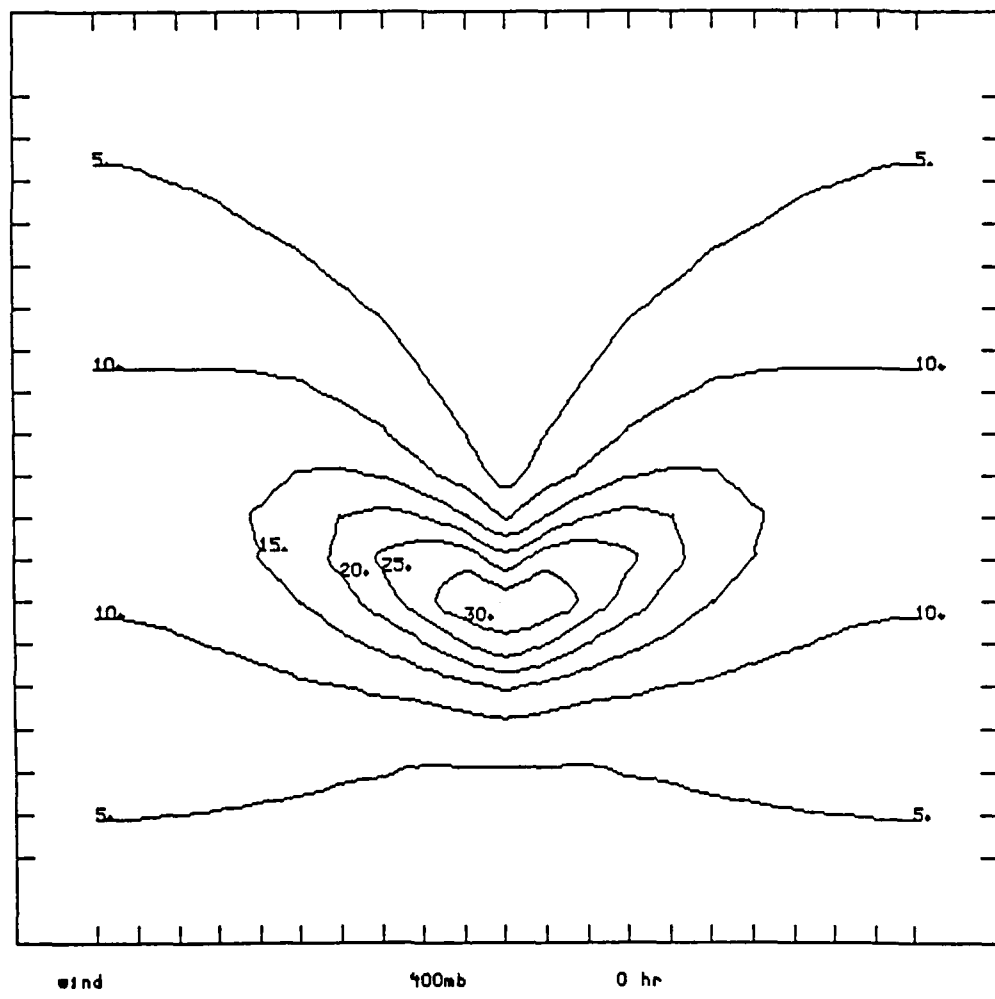


Fig. 51. Initial Hour Cyclonic 400 mb wind speed.

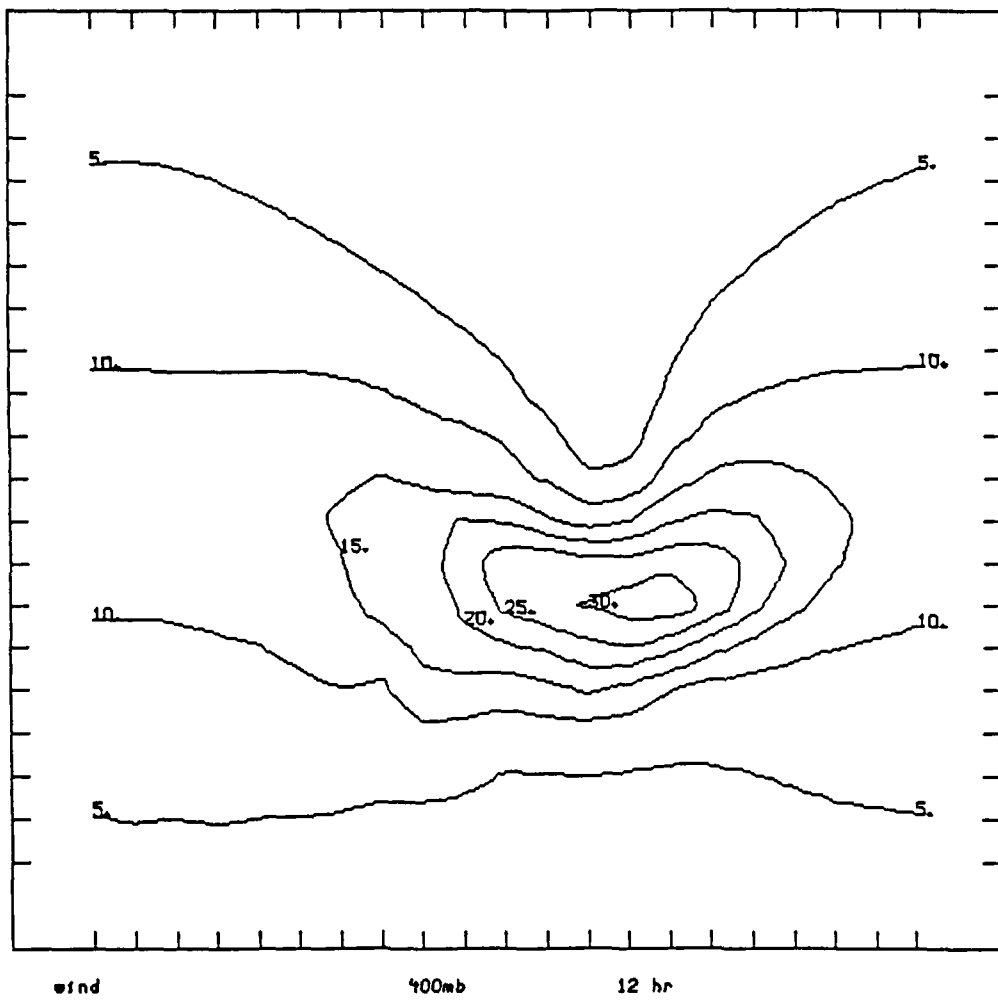


Fig. 52. 12 Hour Cyclonic 400 mb wind speed Eq Barotropic.

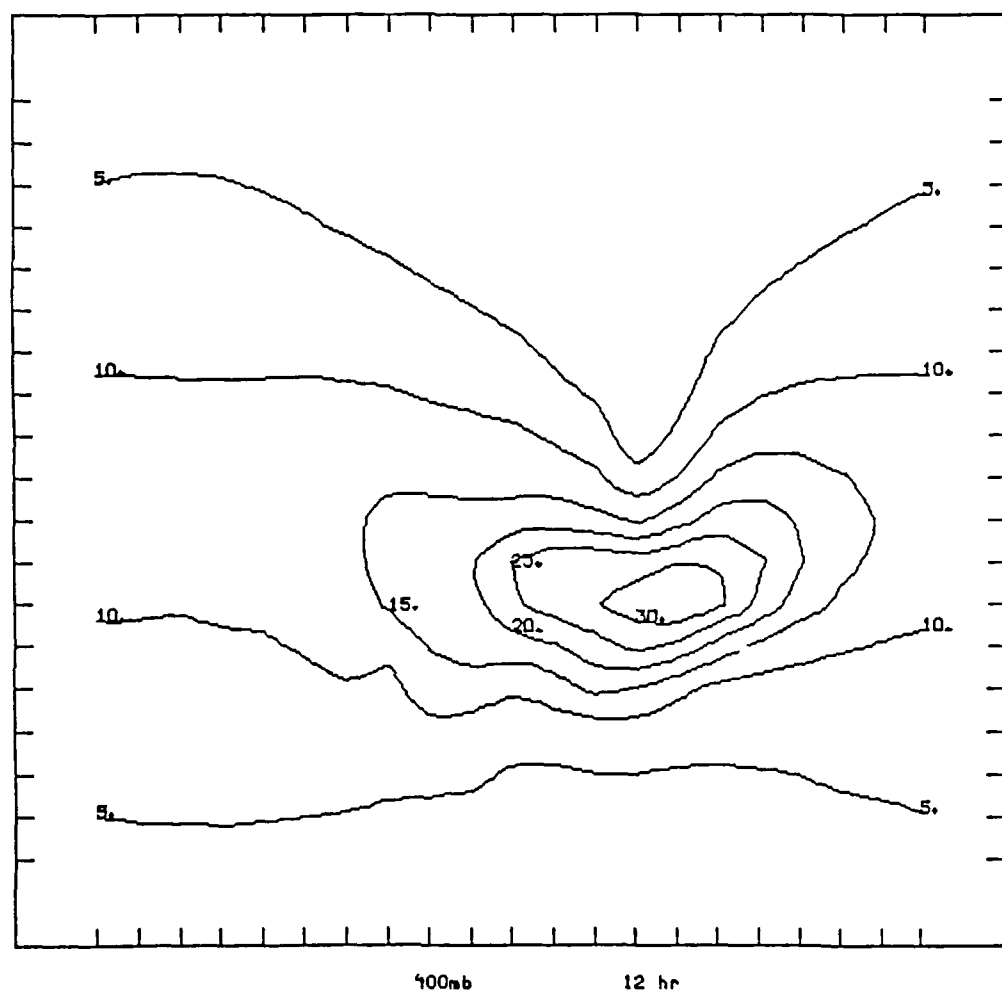


Fig. 53. 12 Hour Cyclonic 400 mb wind speed Quasi Barotropic.

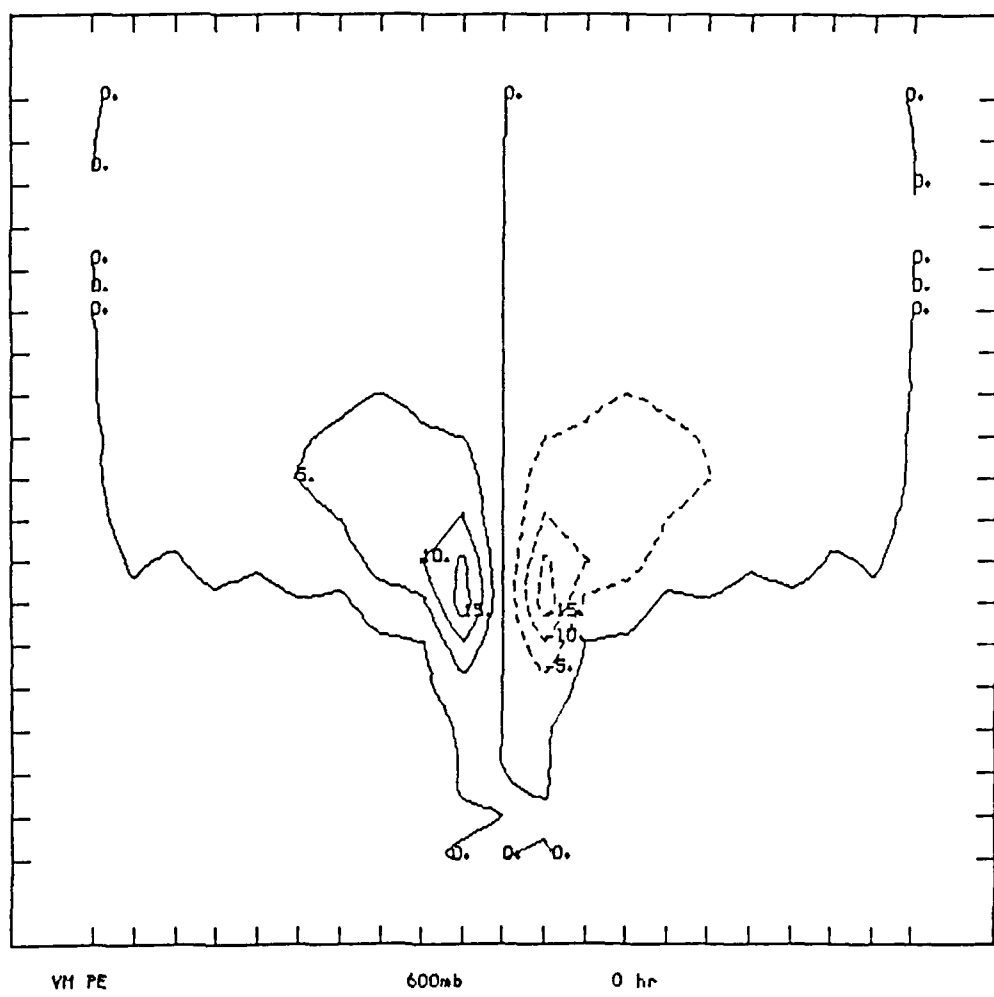


Fig. 54. Initial hour PE vertical motion EB.

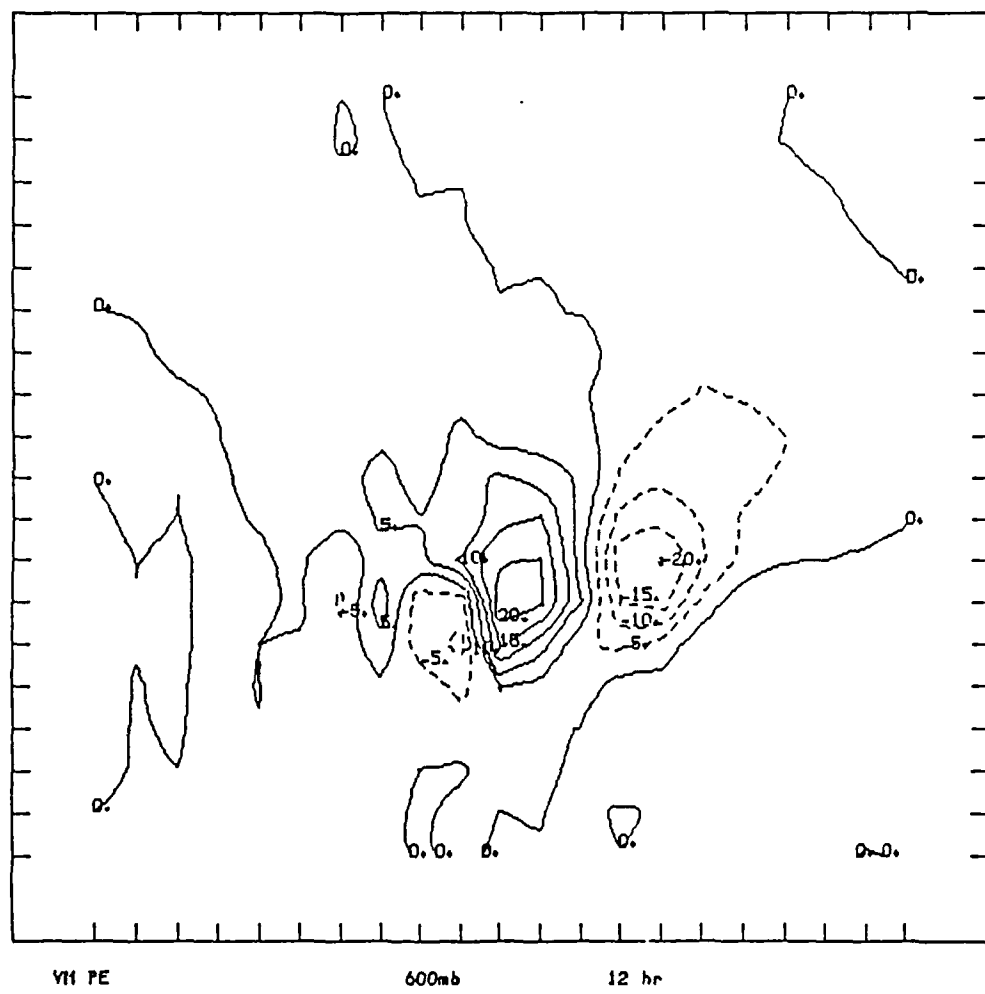


Fig. 55. 12 Hour PE vertical motion EB.

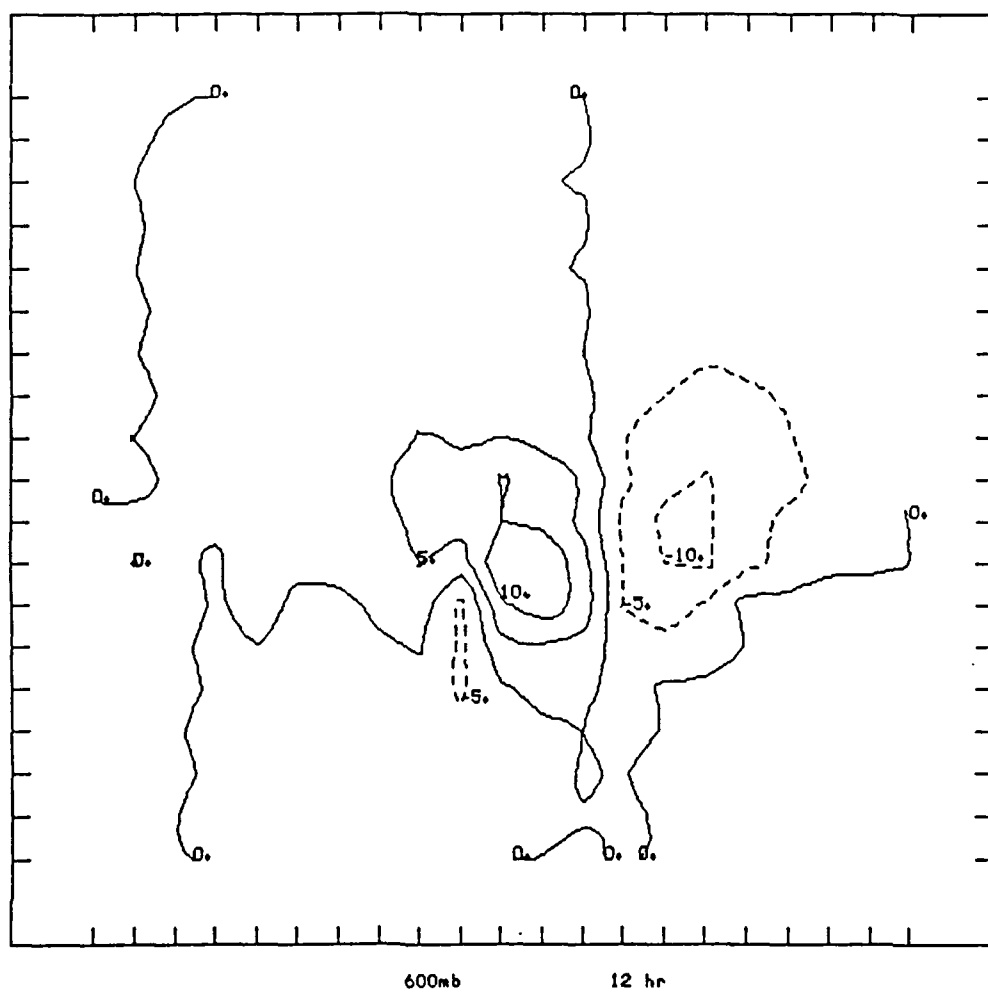


Fig. 56. 12 Hour BAL vertical motion EB.

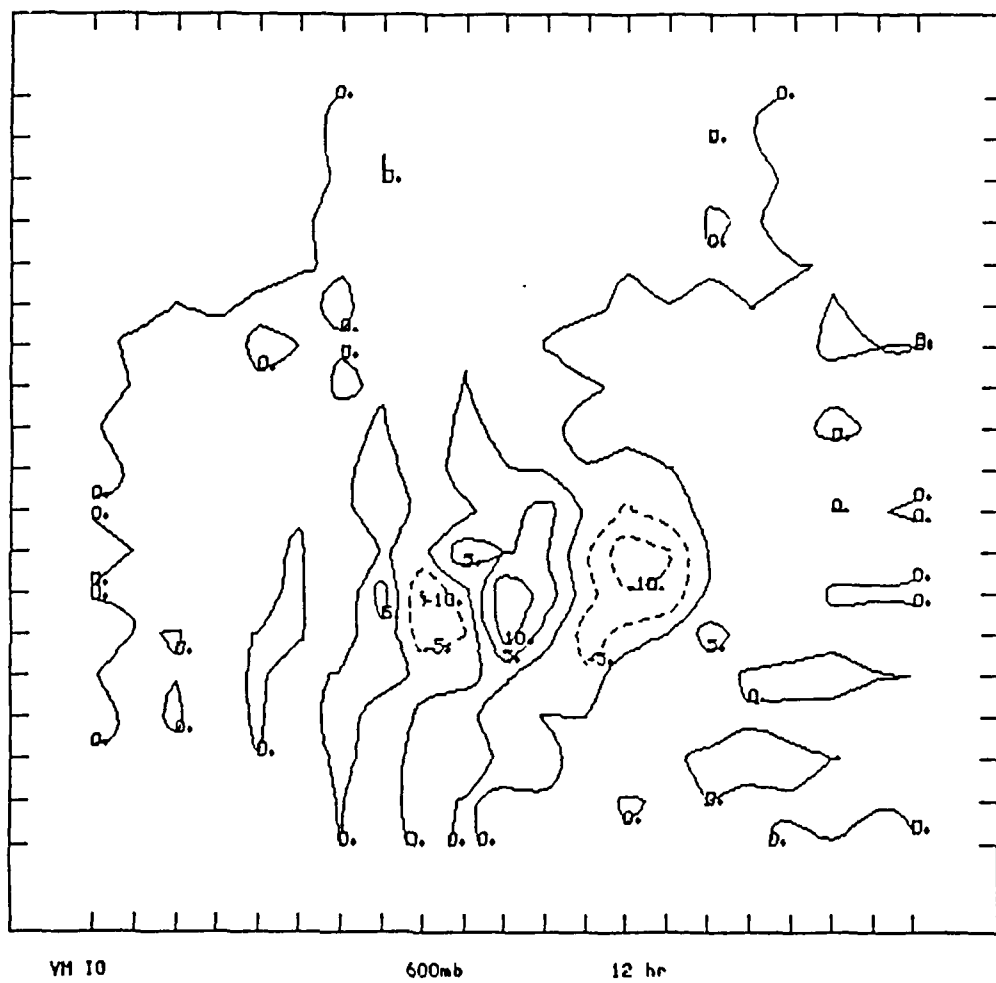


Fig. 57. 12 Hour I-G Vertical Motions EB.

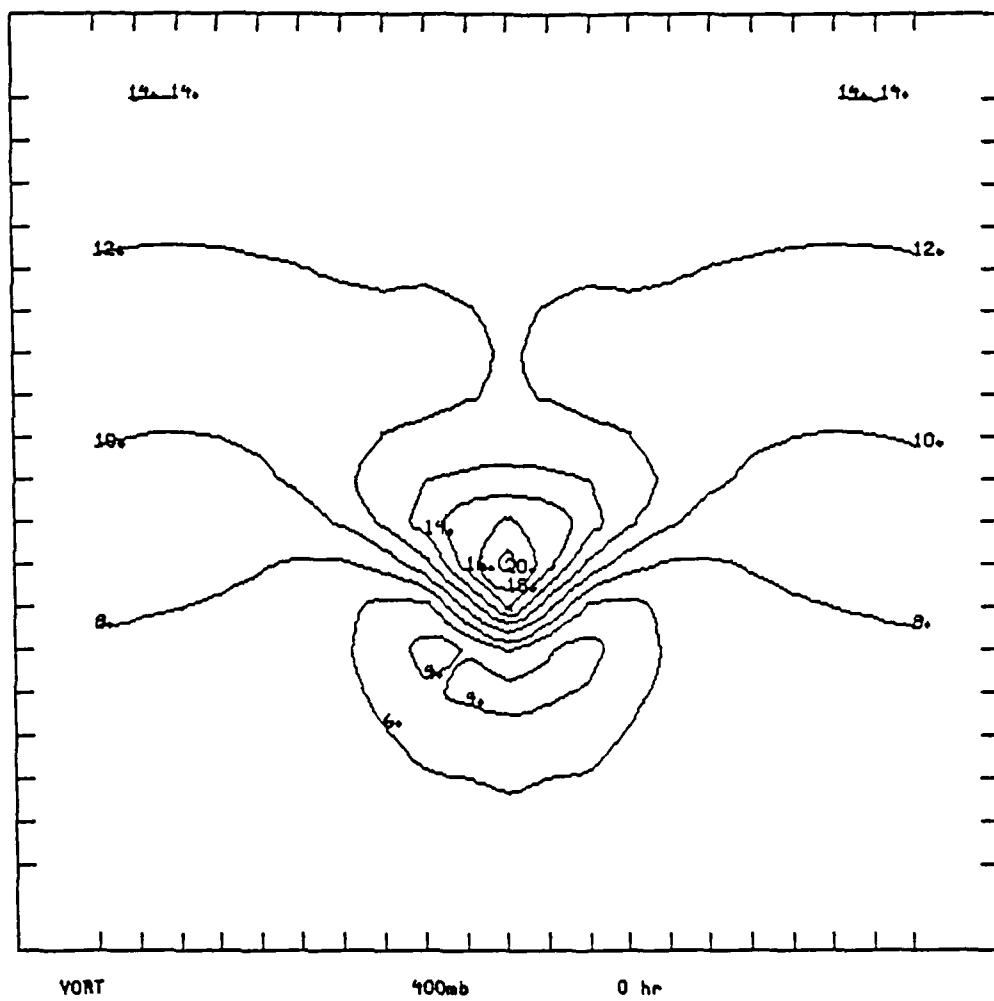


Fig. 58. Initial Hour absolute vorticity.

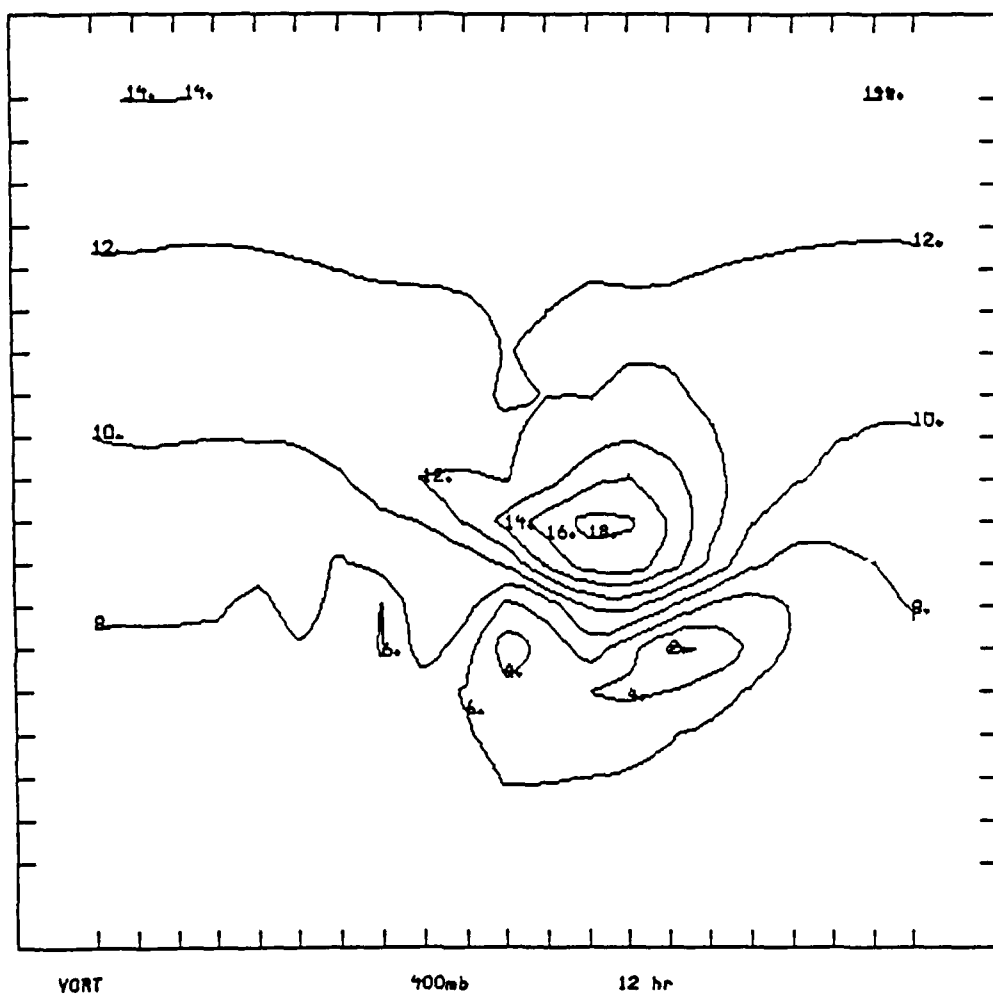


Fig. 59. 12 Hour absolute vorticity values.

in the other two cases A and B (Figs. 60 and 61). A composite diagram of the jet streak axis,  $d\eta/dy$  and  $\eta$  values (Fig. 62) is provided to help evaluate for the presence of barotropic inertial instability. A definitive statement can not be made from the information.

The initial  $\tilde{Ro}$  value is 0.34 which would indicate the same basic ageostrophy as with the corresponding straight line case. The  $Ro$  value began at 1.40 and dropped to about 0.80 after 12 hours (Figs. 63 and 64)  $Ro$  seems to give a much more reliable estimate of the resulting ageostrophy and vertical motions. Also the lowering of  $Ro$  with time suggested that without the presence of hydrodynamic instabilities the jet streaks will adjust with time in the direction of restoring quasi-geostrophic balance.

Although rotational inertial instability is more likely to occur with anticyclonic cases it is not exclusively associated with anticyclonic curvature. The equivalent barotropic cyclonic case with an initial 400mb wind max of 68.9 m/s exhibited negative vorticity values (Fig. 65). The vertical velocity increased dramatically for this case as with the anticyclonic inertially unstable case (Fig. 66). As with the anticyclonic inertially unstable case the Rossby number ( $Ro$ ) increased with time suggesting that the rotational inertial instability was preventing quasi-geostrophic balance from being achieved (Figs. 67 and 68).

#### 4) Beta Plane Cases

Three cases involved the use of a Coriolis parameter that varied linearly with latitude creating a Beta plane. One case each of straight, cyclonic and anticyclonic under equivalent barotropic conditions with an initial jet streak maximum at 400 mb of approximately 36 m/s. The radius of curvature for each case is set constant at  $\pm 2.0 \times 10^6$  meters.

These cases were chosen to avoid rotational inertial instability and isolate changes due to the addition of the Beta plane. One case involving an anticyclonic jet with negative absolute vorticity value is also examined to determine the impact of the

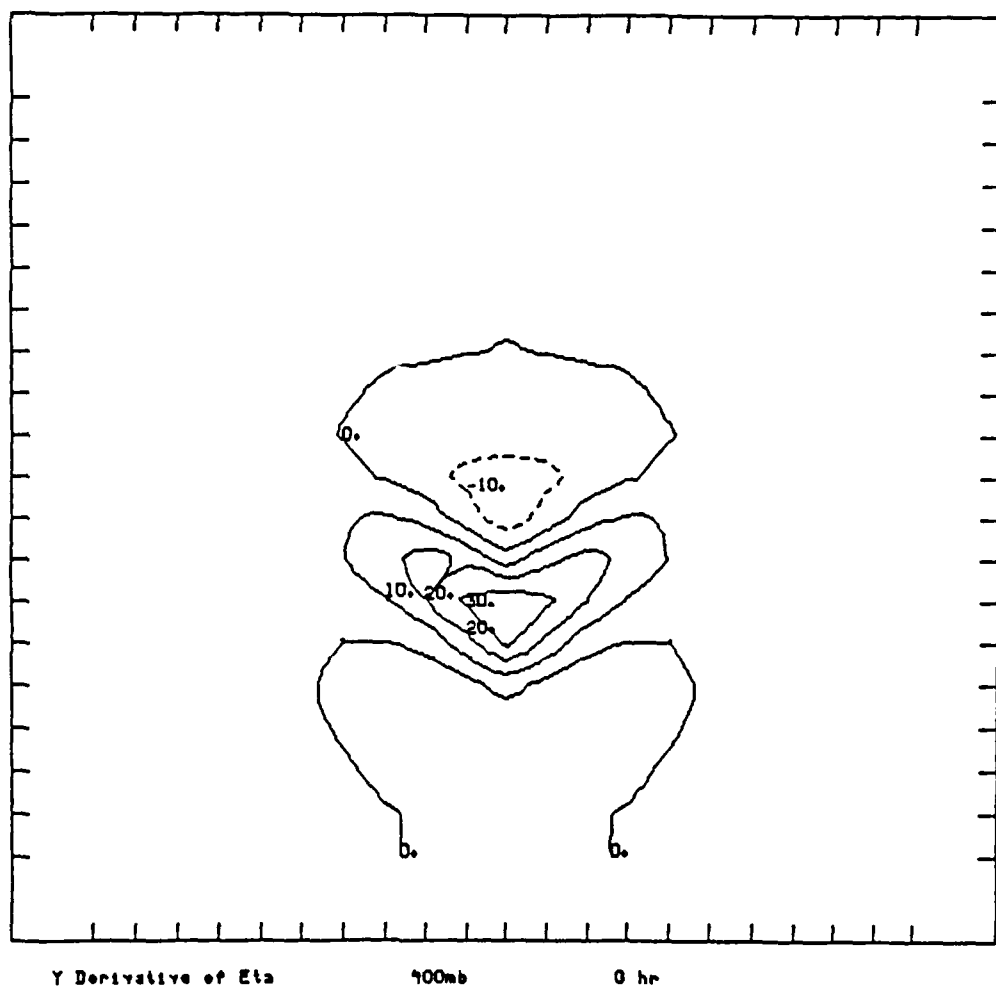


Fig. 60. Initial hour absolute vorticity variation with latitude.

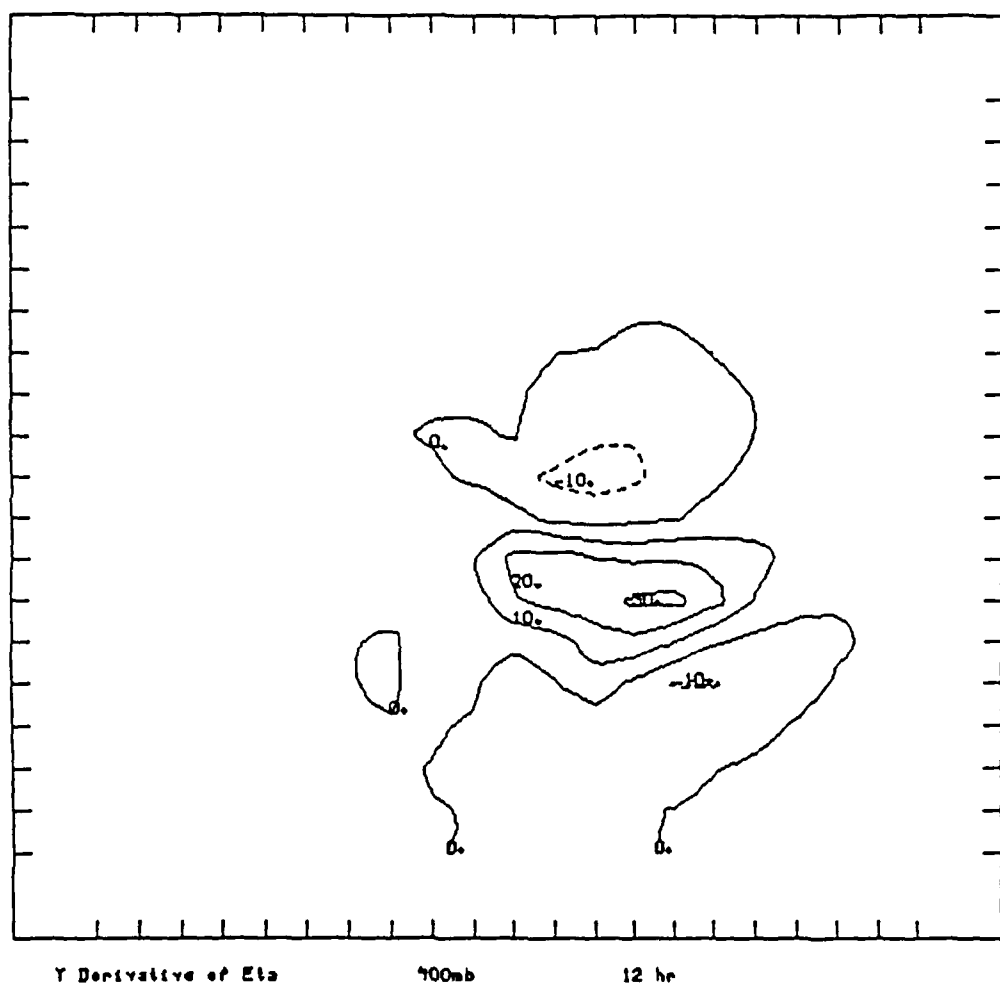


Fig. 61. 12 Hour absolute vorticity variation with latitude.

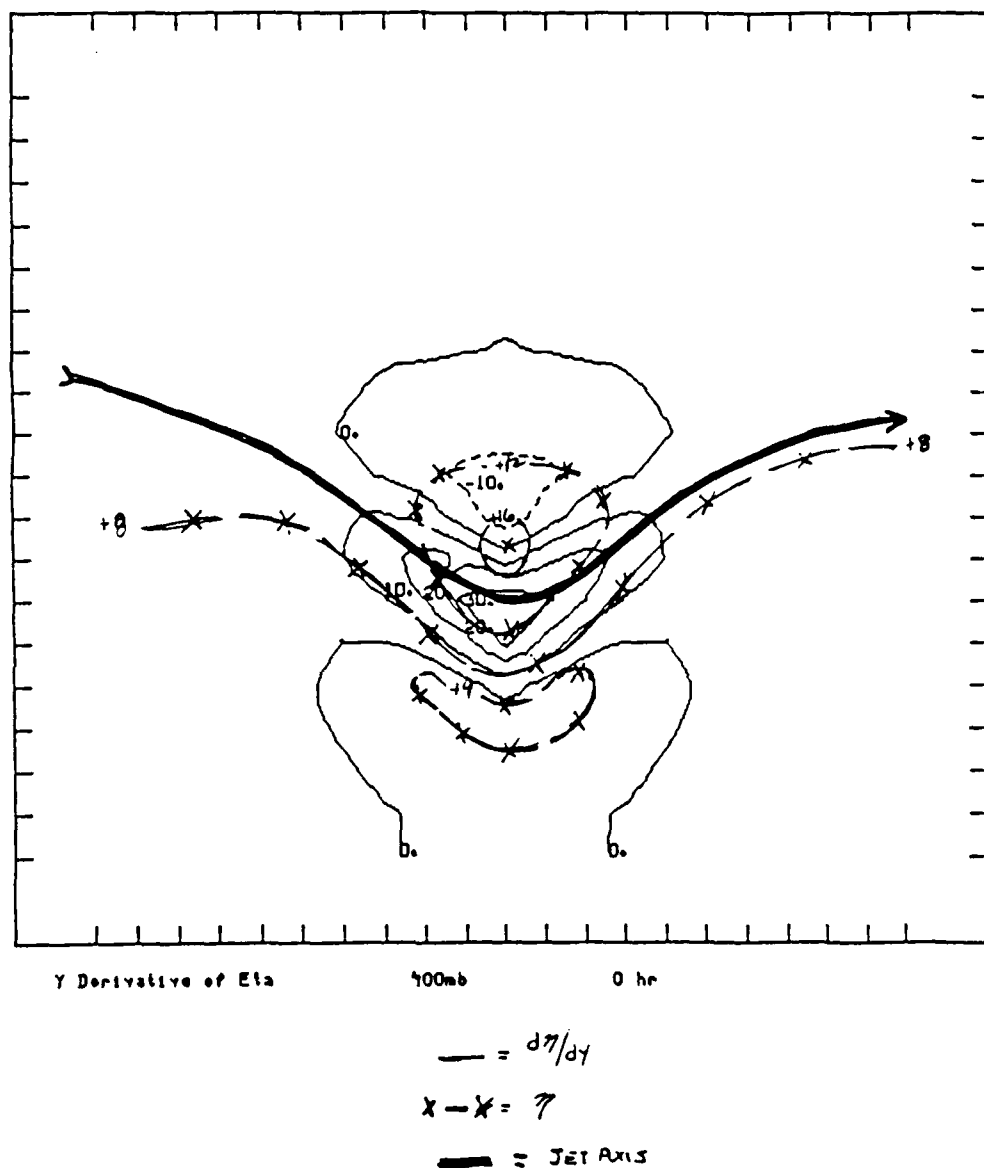


Fig. 62. Overlay of jet axis, vorticity variation with latitude and absolute vorticity for initial hour.

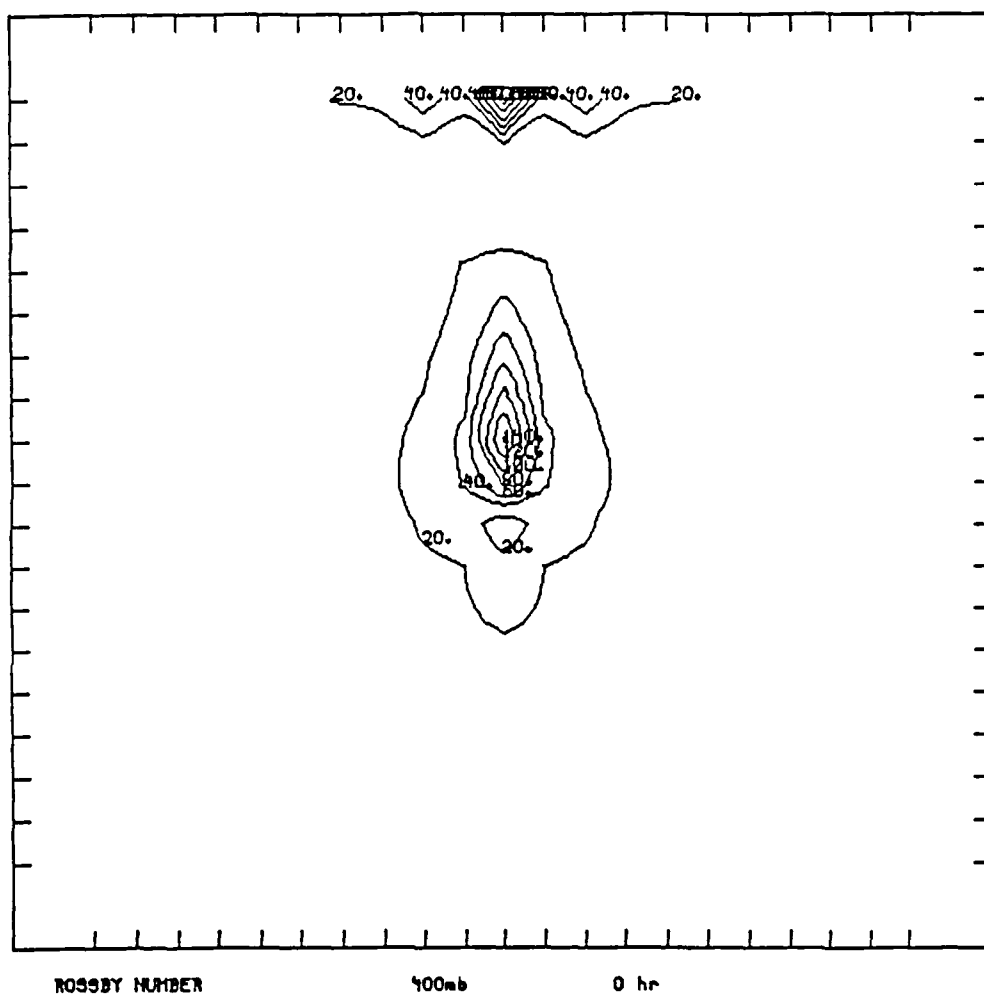


Fig. 63. Initial Hour Rossby Number (Ro).

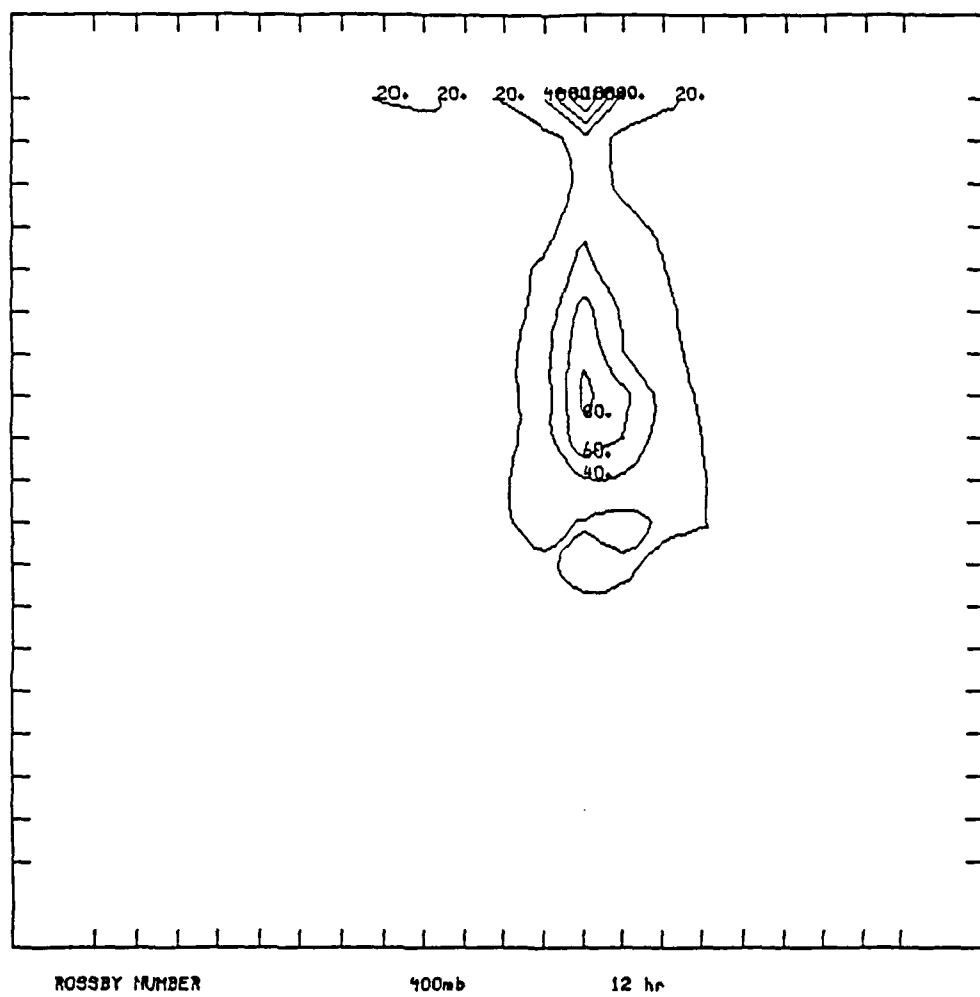


Fig. 64. 12 Hour Rossby Number (Ro).

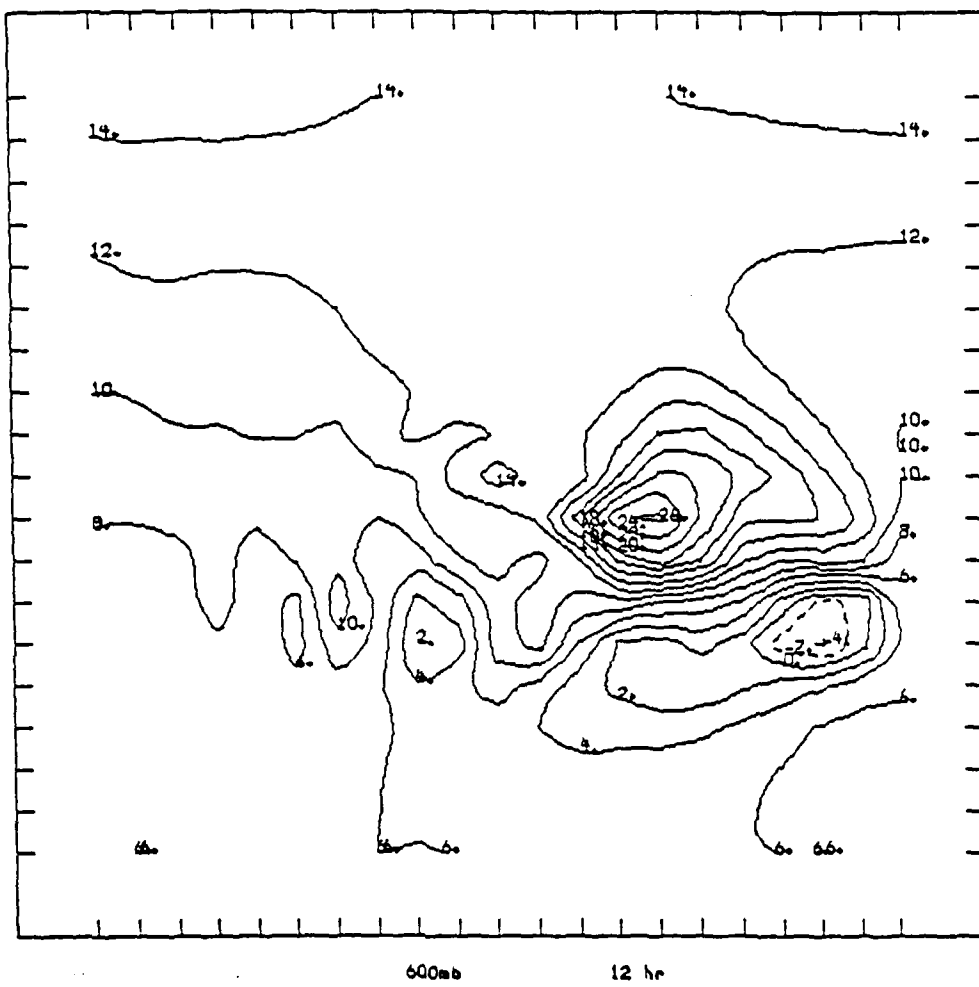


Fig. 65. Inertial unstable absolute vorticity values.

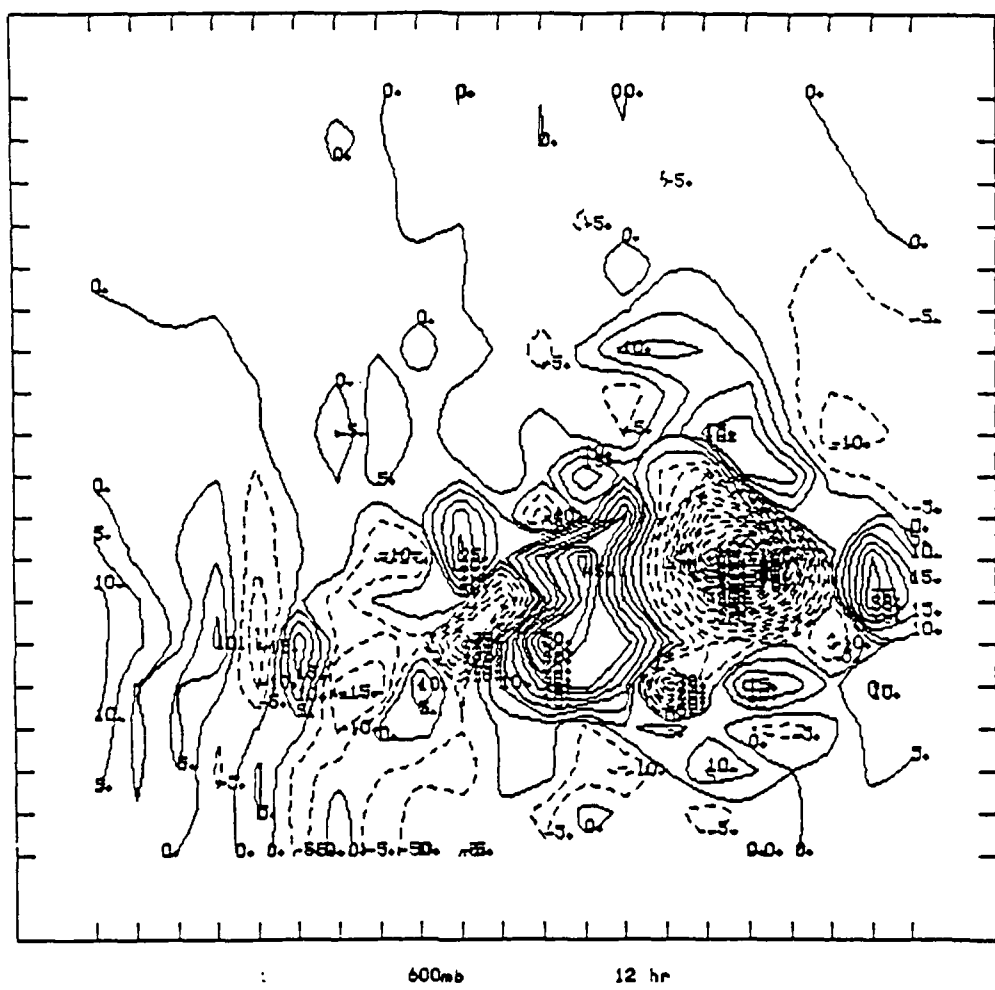


Fig. 66. Inertial unstable PE vertical motion.

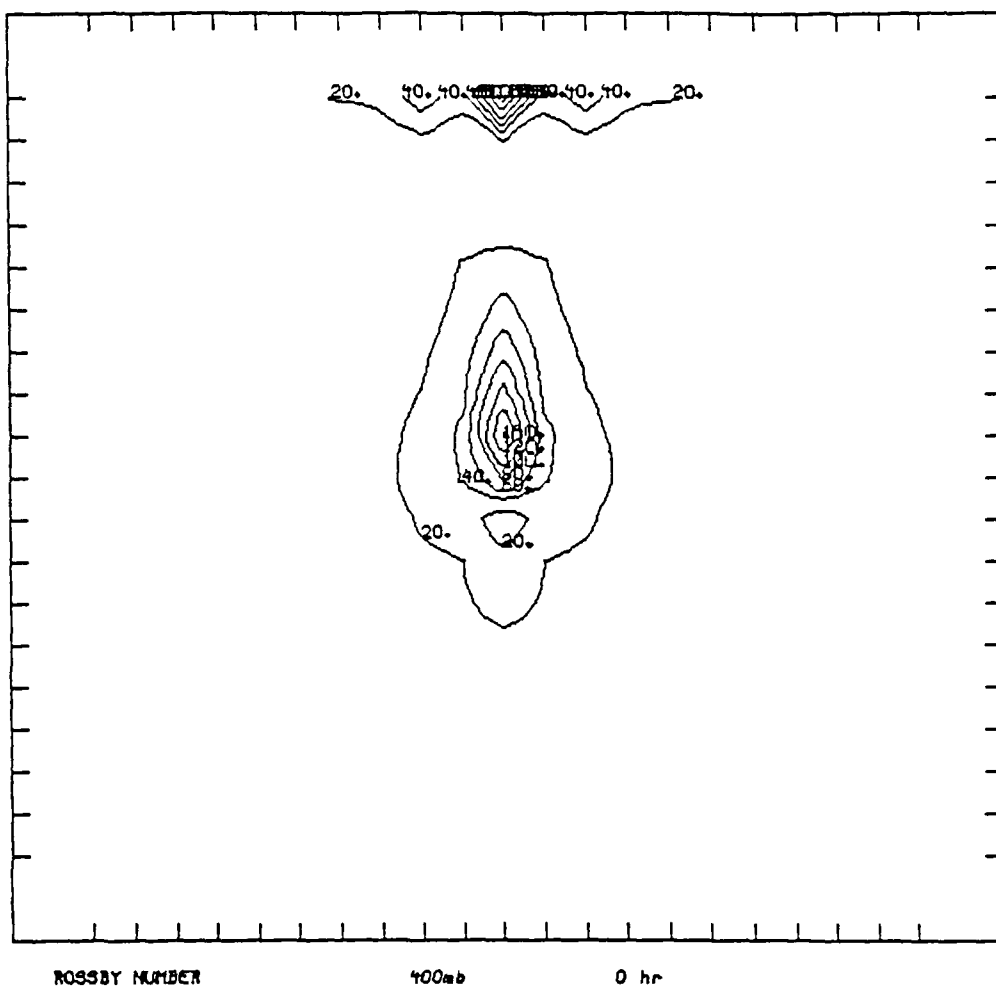


Fig. 67. Initial Hour Cyclonic 400 mb Ro = 1.4.

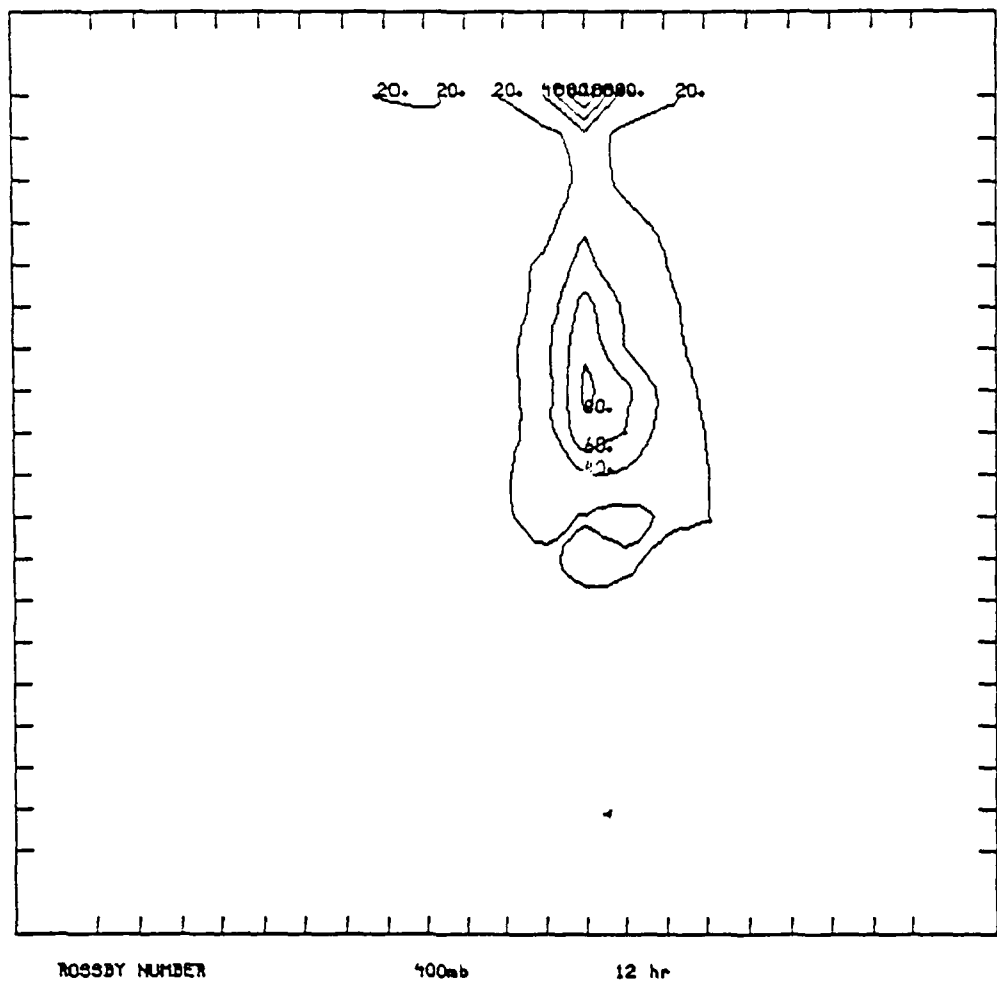


Fig. 68. 12 Hour Cyclonic 400 mb  $Ro = 0.85$ .

Beta plane on the inertial instability. The inclusion of the Beta plane creates a more realistic situation as  $f$  is function of latitude. The center of the grid is taken as 45 degrees so the relationship used is:

$$f = f(45 \text{ deg}) \pm y \frac{df}{dy}$$

The general impact on the model jet simulations was to provide increased stability. This showed up in both the slightly smaller wind speed decreases at 400 mb and more significantly in reducing the I-G vertical motions and increasing the balanced vertical motions. The exact stabilizing effects will be discussed for each case. However the largest effect was on the cyclonic I-G vertical motions which decreased them by 45%.

The impact of the beta plane on the straight-line jet was to increase the balanced vertical motion from the  $f$  plane value of 60 microbars/sec to 80 microbars/sec. Figures 69 and 70 compare the constant  $f$  plane balanced vertical motion values with the balanced vertical motion values for a beta plane.

The curved cases showed similar changes. For the cyclonic case the 12 hour balanced vertical motion for the  $f$  plane of 100 microbars/sec to the beta plane value of 200 microbars/sec for the beta plane case. The anticyclonic case showed a much smaller change from 70 microbars/sec to 100 microbars/sec. In each of the cases the I-G vertical motions decreased. The case of the anticyclonic inertially unstable jet streak clearly shows a decrease in the I-G and PE vertical motions for the beta plane simulation (Figs. 71 and 72).

The Rossby numbers show a general decrease with the addition of the beta plane for each case. This indicates that the addition of the beta plane reduced the ageostrophy as compared to the  $f$  plane cases. Table 9 summarizes the Rossby number and vertical motion values for the beta plane cases. The results strongly suggest that the addition of the beta plane stabilized the jet streak adjustment process decreasing the

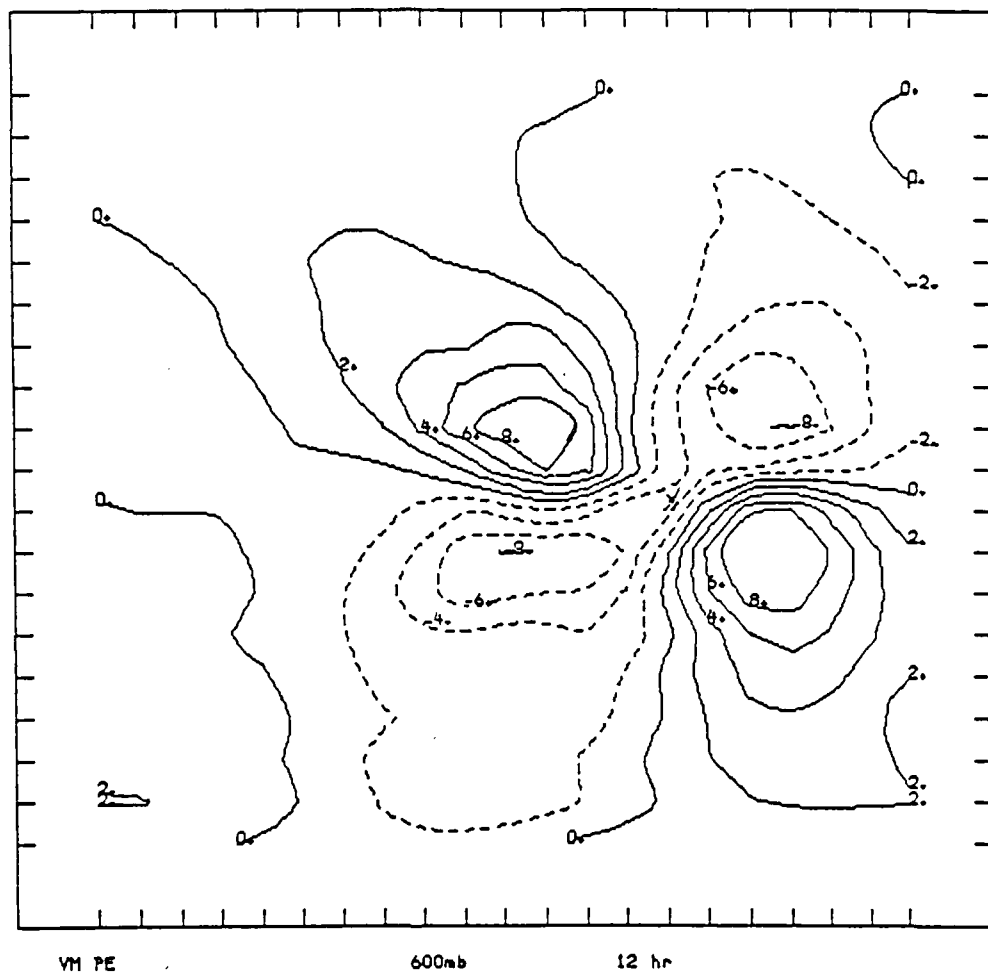


Fig. 69 12 Hour balanced vertical motion for straight-line f plan.

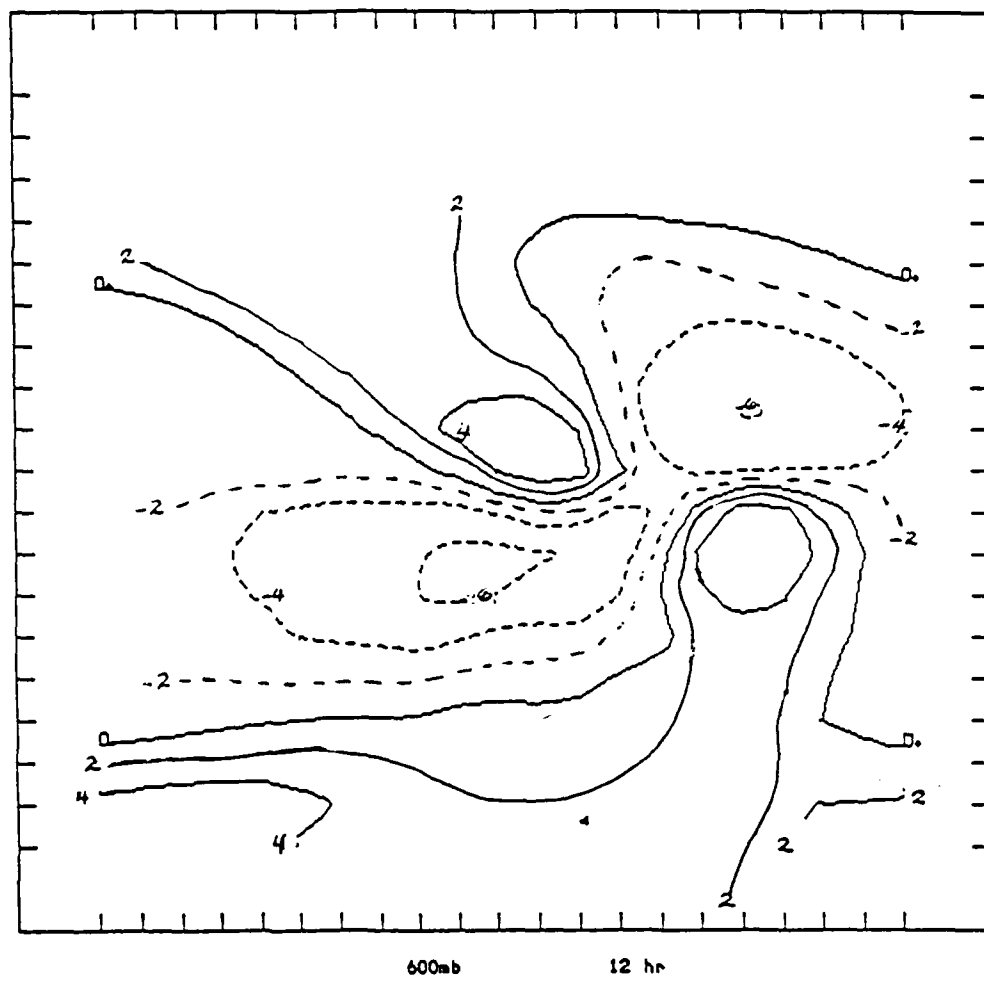


Fig. 70 12 Hour balanced vertical motion for straight-line beta plan.

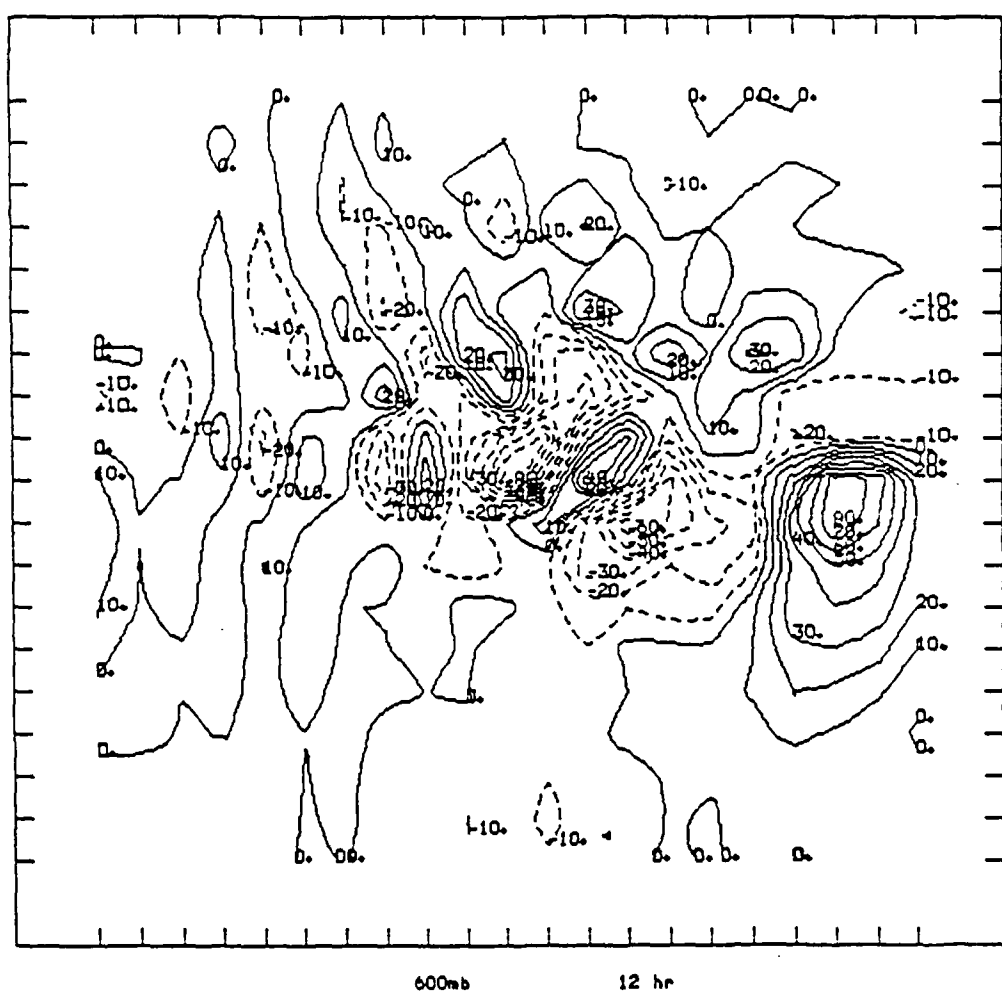


Fig. 71 12 Hour PE vertical motion for inertially unstable anticyclonic jet streak on an  $f$  plane. Note interval is 1/2 Fig. 72.

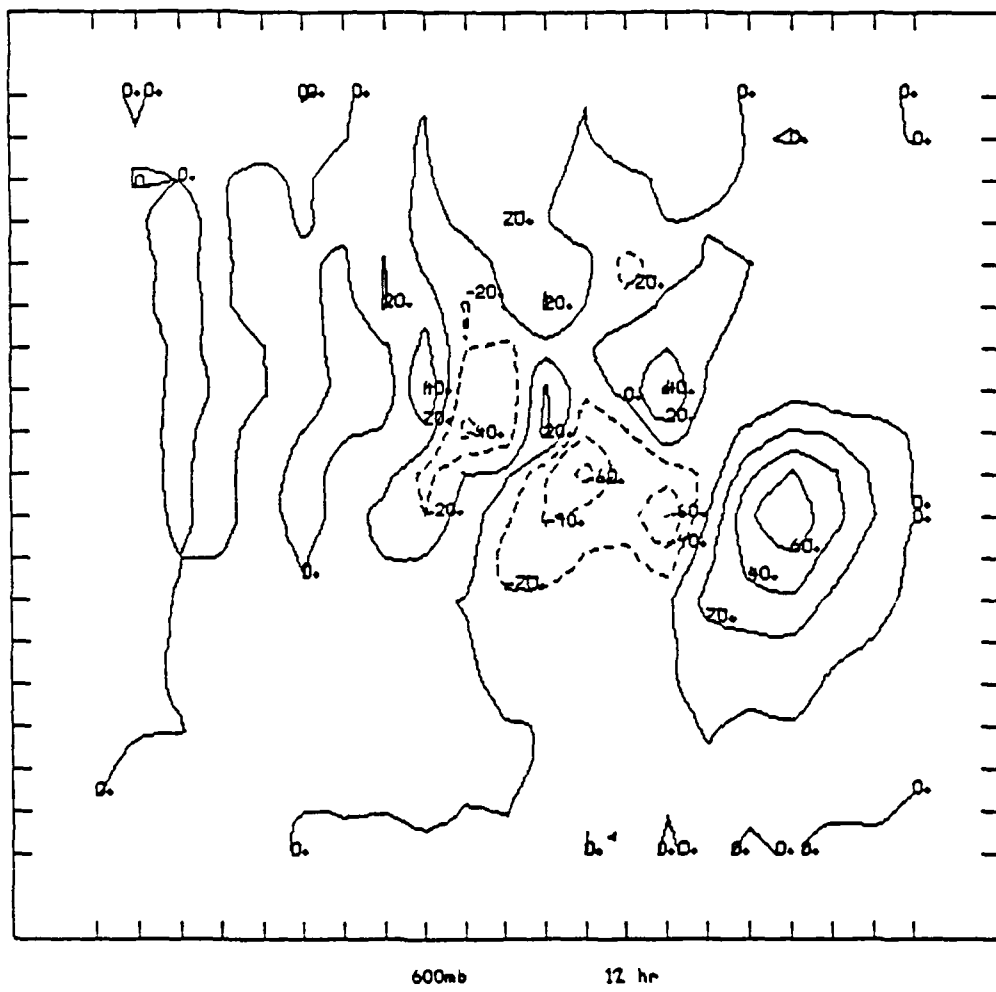


Fig. 72 12 Hour PE vertical motion for an inertially unstable anticyclonic jet streak on a beta plane.

SUMMARY OF BETA PLANE CASES

TABLE 9

TYPE	Ro 0HR	Ro 24HR	PE VM	BL VM	IG VM
ST	0.05	0.05	8	8	3
CY	1.20	1.00	25	20	10
AC	0.50	0.45	12	10	4
AC (UNS)	0.95	1.45	70	55	40

I-G motions while increasing the balance motions.

### 5) Baroclinic Cases

Baroclinicity was achieved by offsetting the upper and lower level jet streaks a chosen number of grid points. Separations of 800, 1400 and 2000 km between the two levels were compared with the equivalent barotropic case (no separation of jet streaks). In order to evaluate the effect of baroclinicity and vertical wind shear the other parameters were set identically for each baroclinic case.

In each of the baroclinic cases the PE vertical motion tended to increase with increasing separation between levels. Table 10 summarizes the Rossby number, vertical wind shear and PE vertical motion changes with increased baroclinicity. The straight line cases showed 350% increase in 24 hour PE vertical motions from the equivalent barotropic to the 200 km separation case. The cyclonic case increased 320% while the anticyclonic case increased 250% when comparing the equivalent and 2000 km separation.

When comparing the initial hour vertical motions with the 24 hour changes there were in general much smaller increases for the initial hour. The straight-line cases increased 150% and the cyclonic cases increased 175% for the initial hour. The anticyclonic case showed the same 250% increase as the 24 hour case.

The results suggest that with increased baroclinicity (increased vertical wind shear) the vertical motions intensify and tend to increase with time. The fact that the 24 hour vertical motions showed larger increases indicates the possibility of baroclinic instability. The results tend to parallel what we see in nature. For example, Mac-Donald and Reiter (1988) determined that the intensity of cyclogenesis was a function of separation of the upper level short wave trough and low level cyclonic baroclinic circulation (frontal wave). The greater the separation the longer the two circulations can reinforce one another.

SUMMARY OF BAROCLINIC CASES				TABLE 10		
CASE	SEP 10 <sup>3</sup> KM	Ro QHR	Ro 24HR	VERT SHEAR	QHR PE PE 10	24 HR PE 10
ST	0	0.20	0.15	4.4	8	10
ST	8	0.25	0.25	4.7	8	15
ST	14	0.35	0.40	4.9	10	30
ST	20	0.40	0.50	5.3	12	35
CY	0	1.30	0.75	4.1	20	30
CY	8	1.50	1.50	5.0	25	70
CY	14	1.60	1.60	5.2	35	90
CY	20	1.30	1.80	5.5	35	95
AC	0	0.80	0.40	4.9	12	18
AC	8	1.40	1.35	5.2	20	35
AC	14	1.00	1.40	5.4	30	40
AC	20	0.80	1.80	5.3	30	40
EJ	0	1.50	1.60	8.7	40	95

The low level easterly jet simulation case was created by placing an upper level westerly straight jet streak over a low level easterly flow jet streak. This is a very typical situation created by the "cold conveyer belt" located north of a warm front and surface low pressure center associated with synoptic scale extra tropical cyclone. Perhaps the results of this case were the most interesting when compared to the westerly upper and low level jet streaks. The initial hour PE vertical motion was nearly identical to the westerly flow case (Fig. 73). The typical four cell pattern was formed with the poleward (cyclonic) quadrants about 15% stronger than the equatorward (anticyclonic) quadrants. As the simulation progressed in time the four cell pattern alters dramatically to a very strong three cell pattern at the 12 hour point. Comparing Figure 74, the 12 hour low level easterly jet PE vertical motions, with Figures 75a, a 12 hour straight-line, and 75 b, a 12 hour cyclonic, the easterly jet case more closely resembles the cyclonic case. In addition to the vertical motion changes both the low level and upper level flow patterns changed from straight line to cyclonic. Because of the increased vertical wind shear for this case, baroclinic instability is possibly responsible for some of the changes observed with time.

The Rossby numbers also increased with increased separation of upper and lower level jet streaks as indicated in Table 10. The fact that both the Rossby number and vertical motions increased with baroclinicity indicates the importance of baroclinicity to ageostrophy.

#### f. Operational Cyclonic Jet Streak Comparison

The vertical motion-jet streak relationship for an operational cyclonic jet streak case of 10 Jan 1990 is compared with the cyclonic model simulation jet streak with a maximum wind speed of 52m/s. The 400 mb isotachs for the operational case was obtained by interpolating between the 500 mb and 300 mb levels. The maximum jet streak speed was estimated to be about 50 m/s at 400 mb. The operational omegas were computed using the kinematic method.

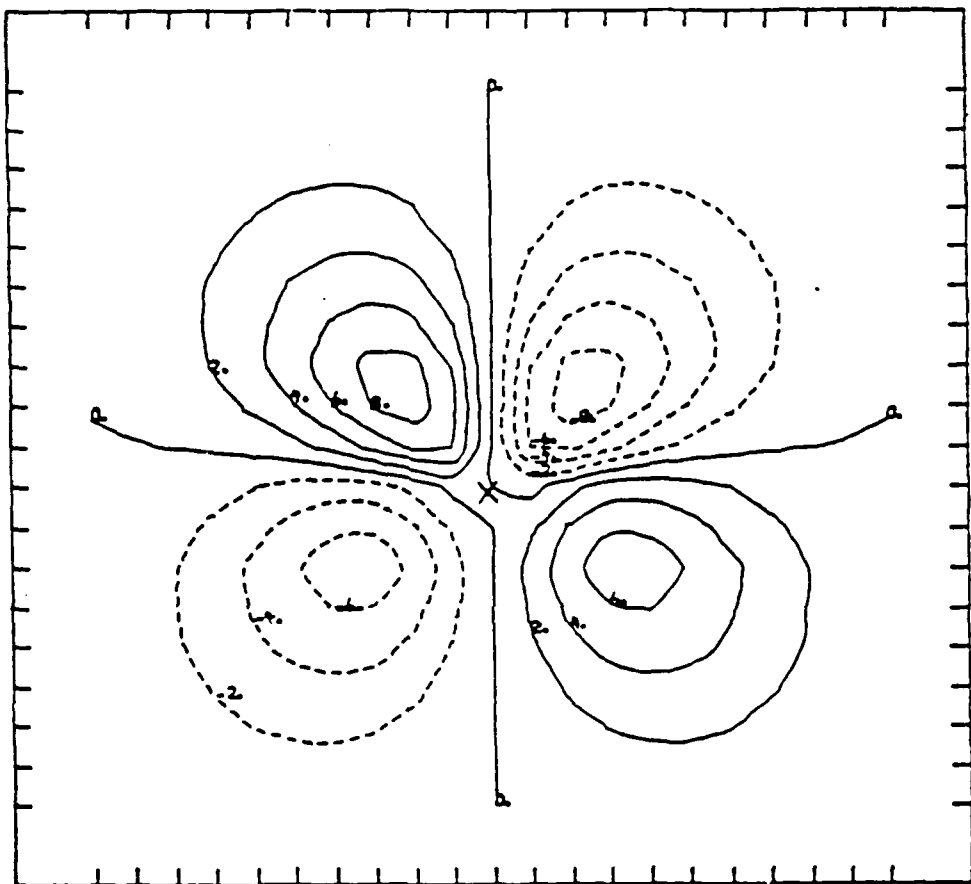


Fig. 73 . Initial hour PE vertical motion easterly low level jet.

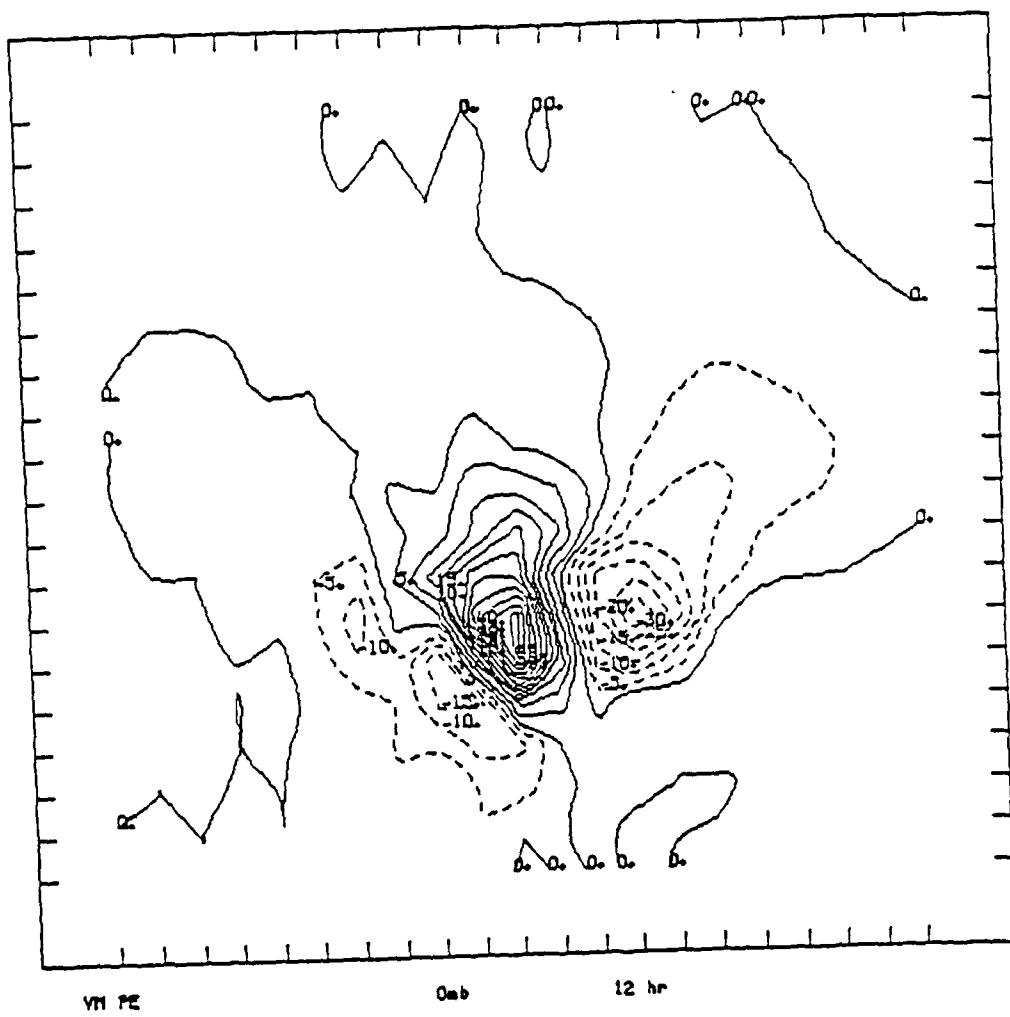
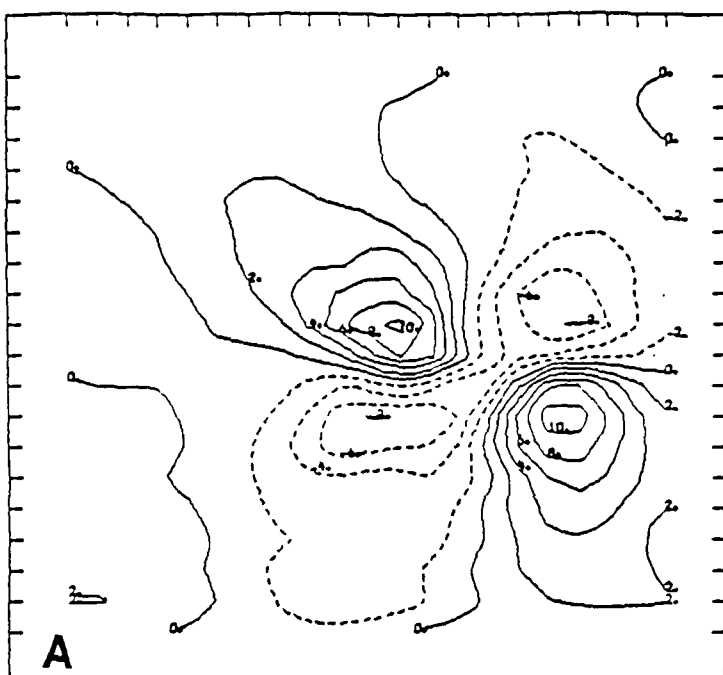
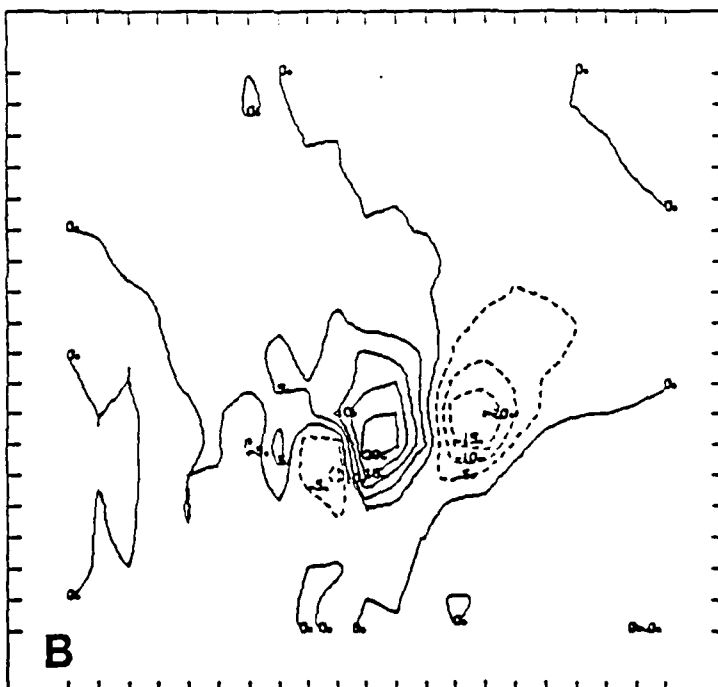


Fig. 74 . 12 Hour PE vertical motion low level easterly jet.



A

12 Hour vertical motion PE Equivalent  
Barotropic.



B

12 Hour PE vertical motion.

Fig. 75 . Comparison of straight-line (A) with cyclonic  
vertical motion(B) .

Figures 76 a and 76 b shows the model's 400 mb isotachs and 600 mb vertical motions while 77 a and b shows the operational 400 mb isotachs and 600 mb vertical motions. The plots are placed on a U.S. background for ease of comparison. Clearly the model patterns resemble the operational patterns. However, because of the sensitivities of the omega value to the accuracy of the winds one must be careful not to over generalize from just one case. Another complicating factor is that in the model case we are dealing with an isolated jet streak while in the real atmosphere one jet streak is very often followed by another. This is the situation in this operational case where a strong jet streak is approaching the northwest portion of the chart.

g. The Role of the Inertial Gravity Wave

Van Tuyl and Young (1982) established the existence of a class of unbalanced I-G wave motion in conjunction with jet streaks. There is growing evidence that I-G Wave motions play a role in many weather events. For example the upward vertical motion associated with an I-G can help break down low level inversions and thereby release convective instability. The release of convective instability can act as a triggering mechanism for convective storms.

Uccellini (1975) demonstrated that a large I-G wave with a period of three hours was likely the mechanism in initiating a severe storm on 18 May 1971. Pecknick and Young (1984) indicated that strong subsynoptic scale I-G wave events occur on the average of once a year in the Midwest.

However, it should not be concluded that I-G waves are only associated with severe weather events. I-G waves are very likely associated with many non-severe events as well. For example, Eom (1975) demonstrated a relationship between mid-level (alto) cloudiness and surface wind speeds with the passage of I-G waves. Evidence from investigations performed by Uccellini (1975) and others has documented the existence of large amplitude subsynoptic scale gravity waves that initiate mesoscale features that range from surface gustiness to severe storm development.

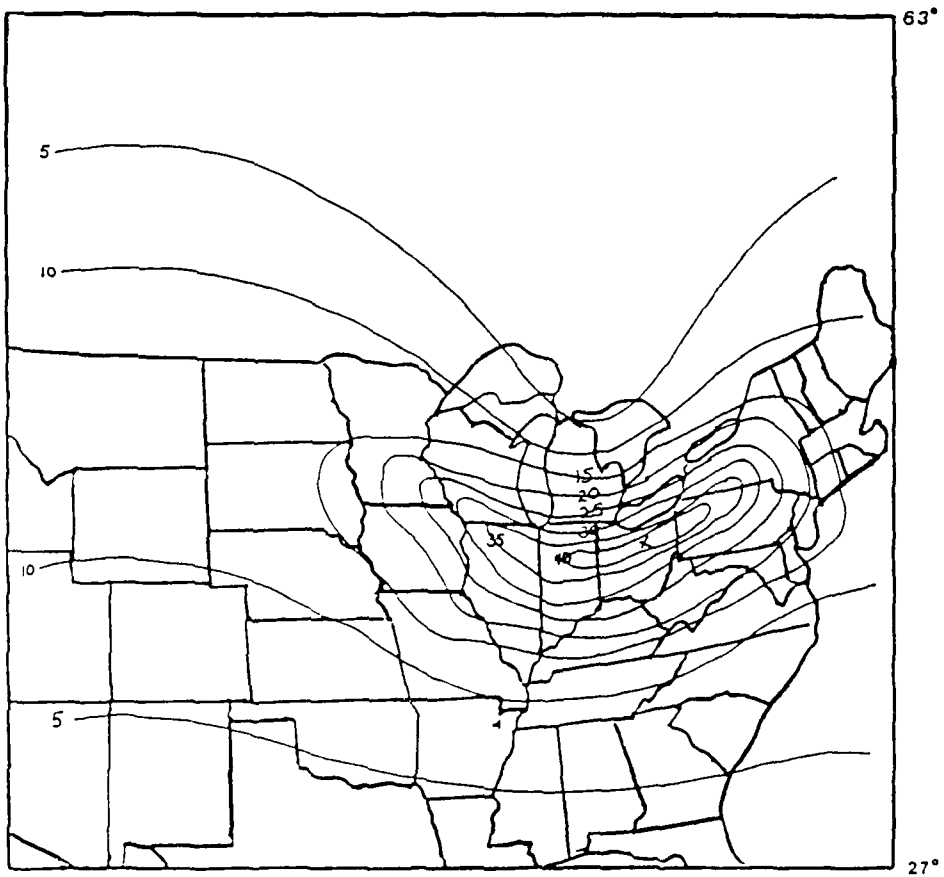


Fig. 76 a. PE model 400 mb 52 m/s cyclonic  
jet streak isotachs.

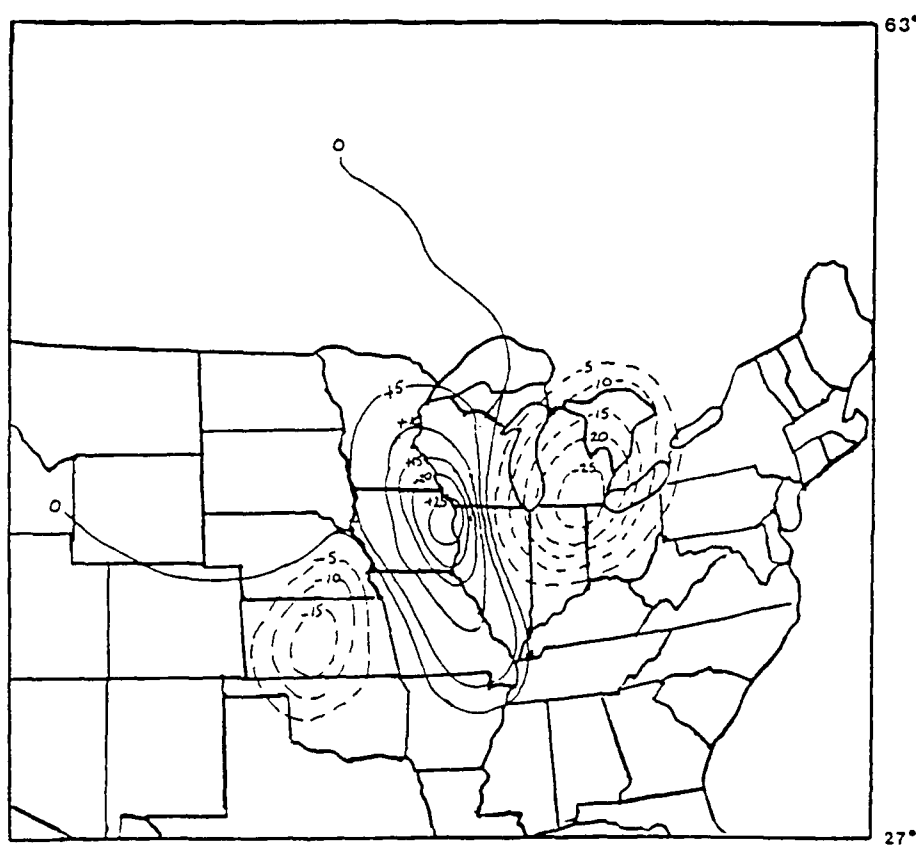


Fig. 76 b. PE model 600 mb vertical motion (PE).

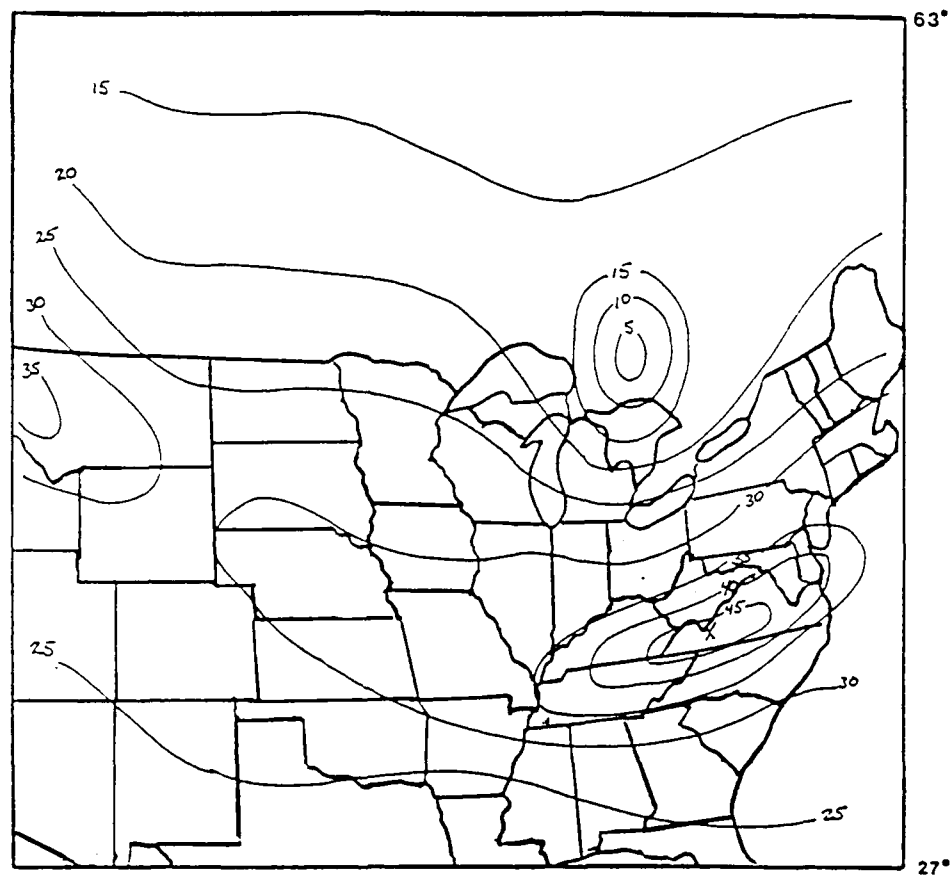


Fig. 77 a. 10 January 1990 400 mb isotachs.

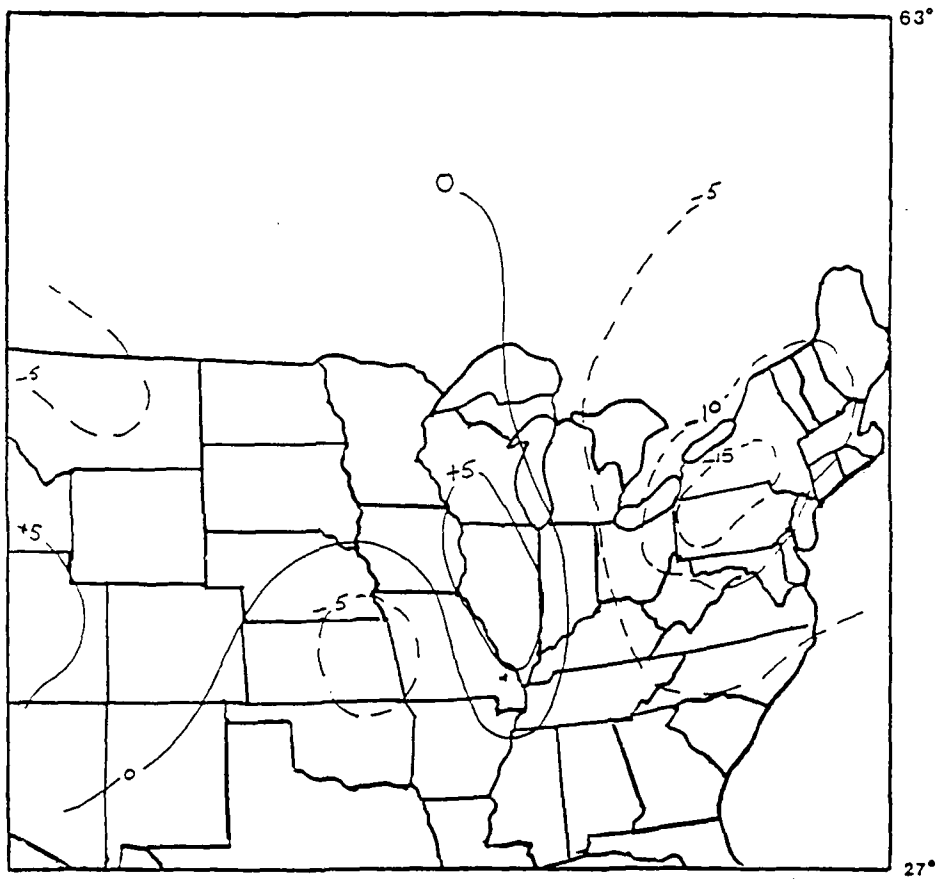


Fig. 77 b. 10 January 1990 mb PE vertical motion 600mb.

Pecknick and Young (1984) deduced the mechanics of strong subsynoptic I-G waves from correlating satellite and surface observations. They concluded that the leading edge of an approaching jet streak generates the I-G waves by concentrating the ageostrophy resulting in unbalanced motion.

Therefore, it is very important to identify the existence of the I-G waves in the model simulations. The I-G wave motions are analyzed to be the difference between the PE and balanced vertical motions. The identified I-G waves are compared with theoretical and observed wave speeds. Using:

$$C = \bar{V} \pm \sqrt{g^* H + (f^2/k^2)} \quad (38)$$
$$g^* = g(\theta_1 - \theta_0)/\theta_1$$

Where  $c$  is wavespeed,  $k$  is the horizontal wave number ( $2\pi/4000$  km),  $H$  is the mean lower layer depth,  $f$  is the Coriolis parameter and  $\theta$  is the potential temperature for the upper (1) and lower (0) layers respectively.

The parameters  $H$ ,  $k\theta_1, \theta_0$  and  $V$  are obtained from the PE model data and are inserted into (38).  $H$  equals 4.2 km,  $f$  equals  $1.0 \times 10^{-4}$ , potential temperature lower layer is 295 K and potential temperature for the upper layer is 325 K. The theoretical I-G wave speed as calculated by (38) ranges between 82.5 to 93.5 m/s. All of the I-G waves identified in the model fell within this range.

The change in I-G vertical motion patterns and magnitude due to increasing wind speed, adding curvature, hydrodynamic instability and baroclinicity are of great interest. For the first 12 hours as the initial adjustment took place, the I-G vertical motion magnitude increased in maximum strength for the straight and cyclonic cases then remained fairly constant. The anticyclonic case strengthened at the six hour point then weakened thereafter over the same time period. The strongest pattern was exhibited in the cyclonic case, indicating that cyclonic curvature is more effective than anticyclonic curvature in increasing the I-G vertical motions. Also of interest, both the straight and cyclonic cases showed a more coherent concentrated pattern at the

twelve hour point as compared to the anticyclonic case (Figs. 78a, b and c).

Increasing wind speed and adding baroclinicity served to enhance the basic I-G patterns with small changes in wind speeds. However, the most dramatic change occurred when rotational inertial instability was present. Also of note was the significant damping of the cyclonic I-G vertical motion in the beta plane case. The changes in the vertical motion pattern of the beta plane case indicates that the north-south variation of  $f$  should not be ignored.

#### h. Potential PE Model Problems

When analyzing model results great caution must be used in trying to apply the results to the actual atmosphere. Several model problem areas may limit its use with the real atmosphere. One problem is the possible effect of strong vertical shears (large thermal wind) on the model's static stability factors. The model controls this problem well by presetting the stability factors inside the PE model program. However, a related problem that could adversely affect results is the model creating unrealistic wind shears for the preset stability factors. This problem does not appear to be significant as the wind shears produced by the model ( $3-8 \text{ sec}^{-1}$ ) fall within the typical vertical wind shear ranges found in the atmosphere between 800 and 400 mb. However, the high speed anticyclonic vertical wind shear of  $10 \text{ sec}^{-1}$  approaches the upper limit of vertical wind shears.

A problem in analyzing the curvature effect on vertical motion arises from the difficulty in estimating the maximum curvature location. Also the manual method used to evaluate curvature is subject to fairly large uncertainty.

Probably the most significant limitation of the PE model is that it consists of only two layers. This serves to greatly exaggerate the actual values of vertical motion calculated at 600 mb as compared to the real atmosphere. The reason for this is the real atmosphere will tend to produce compensating horizontal divergence-convergence throughout a column of air thereby reducing the magnitude of the vertical motions.

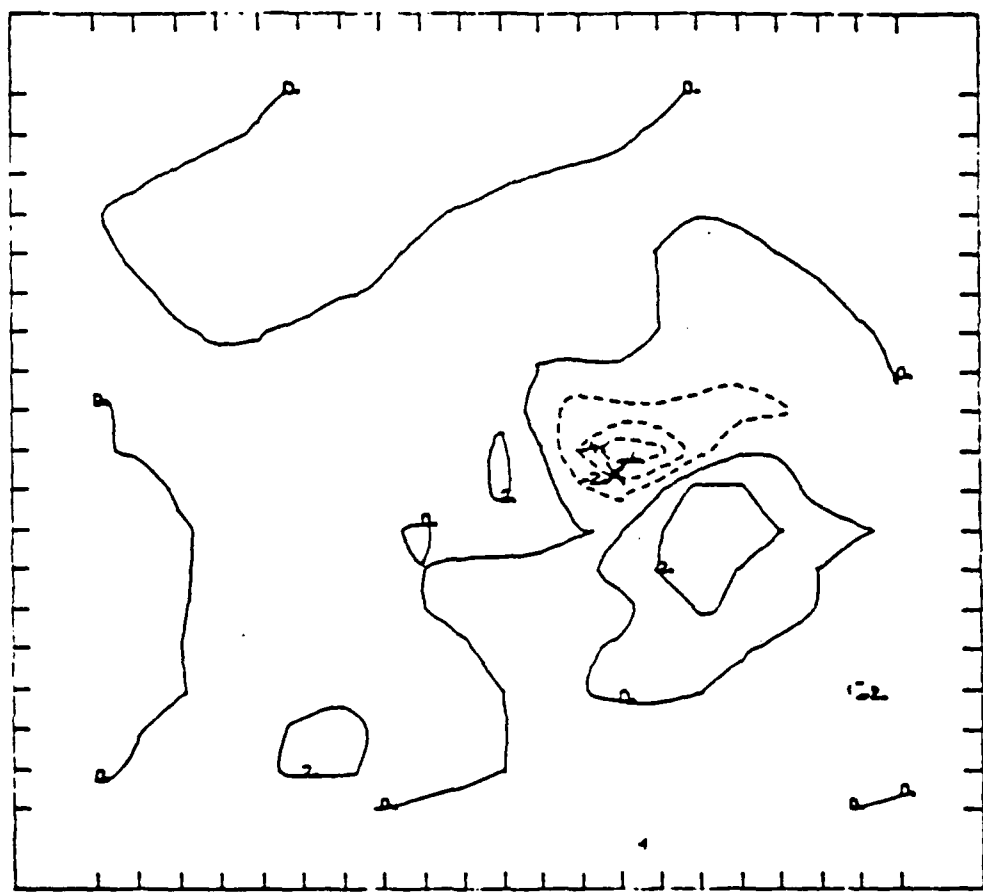


Fig. 78 a. PE model 12 hour I-G vertical motions  
38 m/s straight-line jet streak.

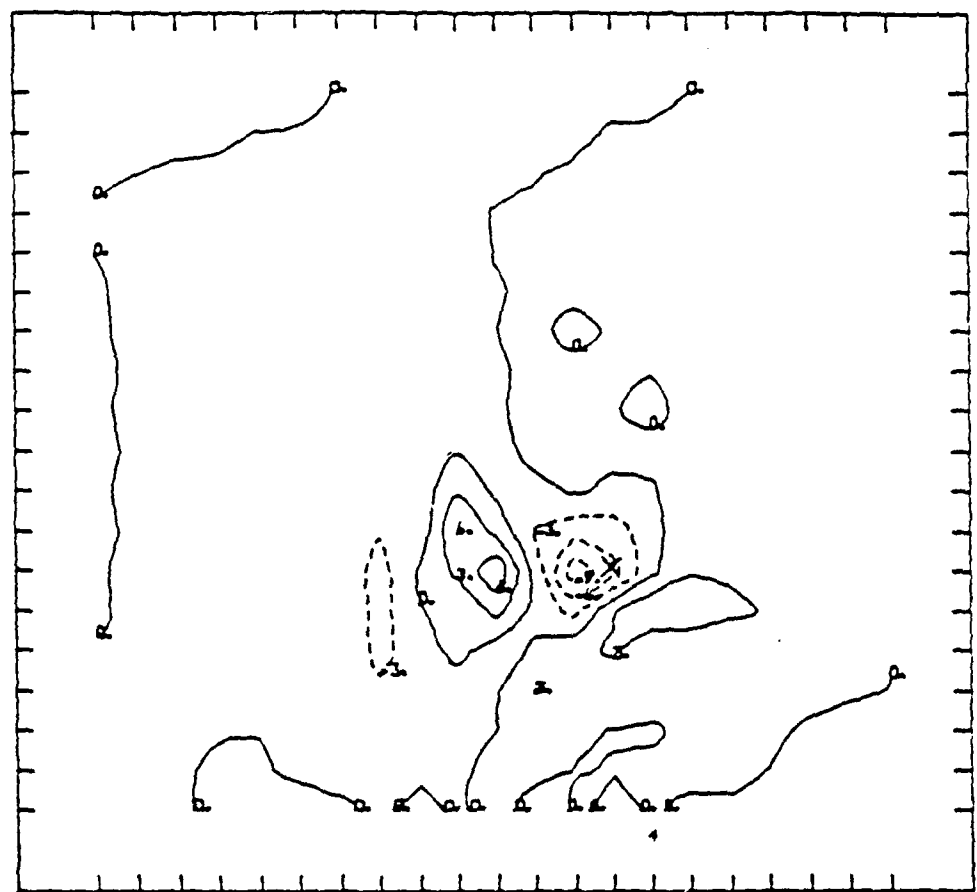


Fig. 78 b. PE model 12 hour I-G vertical motions  
38 m/s cyclonic jet streak.

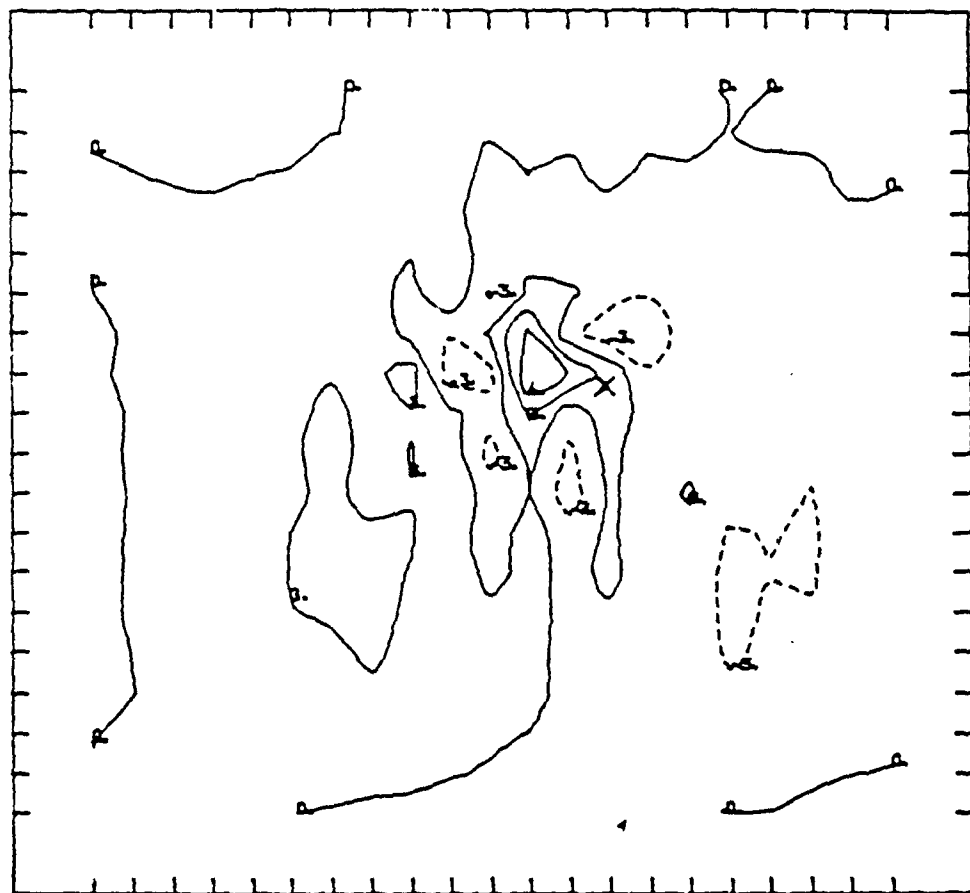


Fig. 78 c. PE model 12 hour I-G vertical motions  
38 m/s anticyclonic jet streak.

The PE model limits the compensating motions to the upper and lower levels of the model. This causes the model to be high on the magnitudes of the vertical motions by a factor of 10. This would greatly limit the use of the model as an operational forecast tool. On the other hand, the vertical motion patterns and relative strengths compared very favorably to the real atmosphere.

Although the comparison of the model output to the operational cyclonic case is very encouraging, there is considerable error in the operational PE omega values due to the random error generated by the method of measuring the winds. Therefore, a general statement as to the direct application of the model results with regard to the real atmosphere is not possible without more comparisons.

#### i. Conceptual Models Consistent with the Results

The results of the PE model simulation may be used to create more detailed conceptual models of transverse circulations associated with the jet streak adjustment process. It is the ageostrophic wind component that causes the transverse circulations to deviate from those predicted by the quasi-geostrophic (Q-G) theory. The ageostrophic winds must be accounted for to improve the conceptual models.

Classic Q-G theory predicts a thermally indirect transverse circulation at the exit (nose) and a thermally direct transverse circulation at the entrance (tail) of the jet streak. The PE model results demonstrate that curvature alters the large scale balanced vertical motion pattern from the classic four cell pattern. Figure 79 describes the changes in the vertical motion and transverse circulation patterns as the jet streak propagates through a short wave trough - ridge system. Figures 80 a-b provide examples of an idealized direct and indirect thermal circulation. Jet streaks located at A, C and E will display essentially the classic four cell pattern of indirect circulation at the nose and direct circulation at the tail of the jet streak. Position B (in the trough) displays one direct circulation and position D (in the ridge) displays one direct thermal circulation.

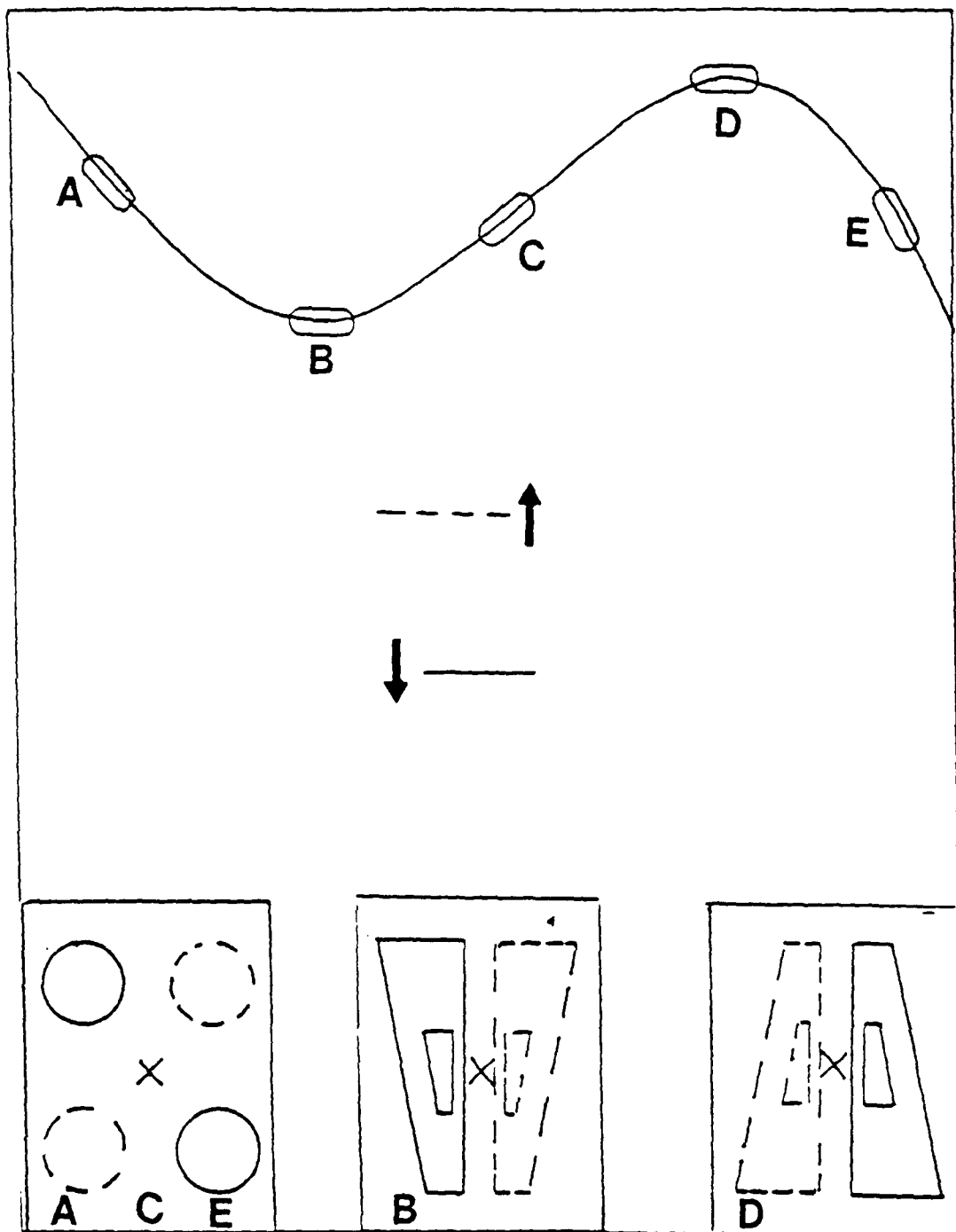
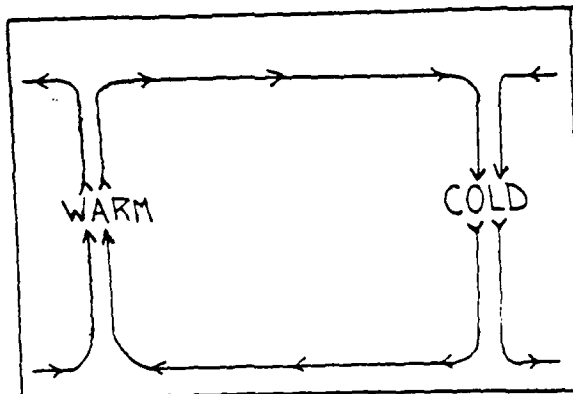
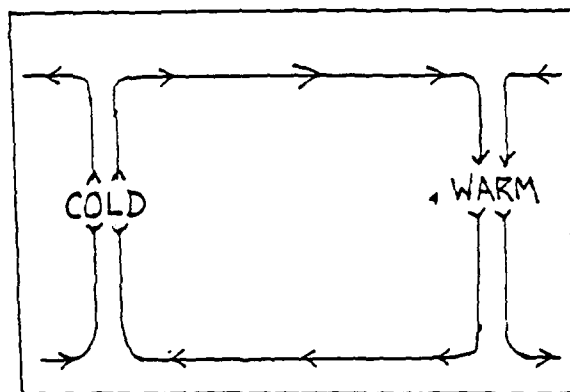


Fig.79. Conceptual model of the large scale balanced kinematic vertical motions as a jet streak propagates through a short wave trough and ridge (after Molinaro, 1988)



A. Direct Thermal Circulation



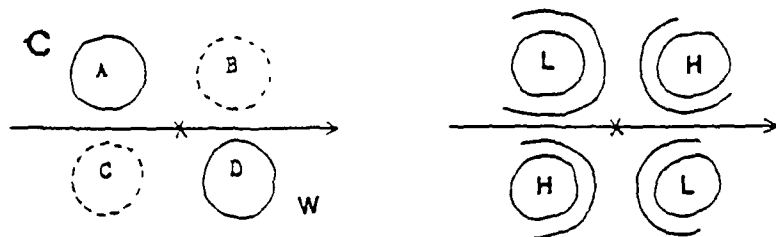
B. Indirect Thermal Circulation

Fig. 80. a) Example of a direct thermal circulation. b) Example of an indirect thermal circulation.

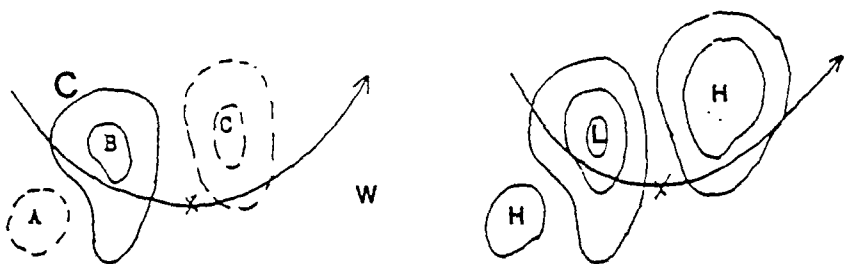
In addition to the large scale balance vertical motion patterns, the I-G waves create significant deviations in the ageostrophic wind patterns predicted by Q-G theory. These deviations result in variations in the vertical motion fields and transverse circulations that must be accounted for in a representative conceptual model. Figure 81 gives a more detailed picture of a conceptual model that includes I-G vertical motions. The typical thermal pattern in the northern hemisphere of colder (C) to the north and west and warmer (W) to the south and east is assumed.

For the straight line case direct circulation result from A to C, while indirect circulation result from D to B. Weaker zonal circulations may develop between A to B and D to C. In the case of the cyclonic streak, a direct circulation set up from A to B and from B to C because of the addition of the I-G dominated vertical motions at A. Finally, a single indirect pattern remains from A to B in the anticyclonic jet streak.

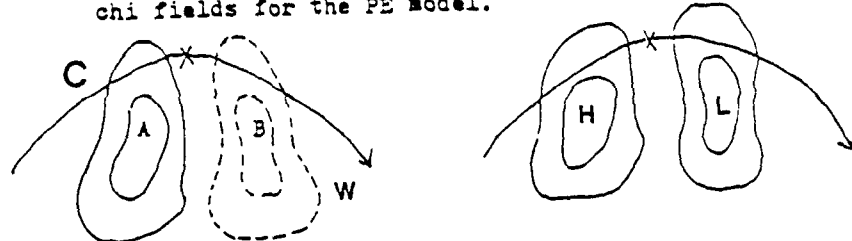
Accurate conceptual models will aid both the operational and theoretical meteorologist by providing a framework with which to work. The more accurate the conceptual model, the more accurate nature can be understood and predicted. The inclusion of I-G waves into such a conceptual model is essential.



A.  
Straight-line jet streak vertical motion  
and chi fields for the PE Model.



B.  
Cyclonic jet streak vertical motion and  
chi fields for the PE model.



C.  
Anticyclonic jet streak vertical motion and  
chi field for the PE model.

Fig. 8T. Conceptual model of idealized kinematic vertical motions and chi fields to include I-G wave motions. Vertical motion is on the left and chi fields are on the right. Dashed lines indicate upward motion, solid lines downward motion for vertical motion.

## 5. Summary and Conclusions

The PE model simulated jet streak cases provided insight into the jet streak adjustment process. Significant information was gained into the imbalance of forces associated with jet streaks by using the more appropriate mesoscale Rossby number ( $Ro$ ). Using the  $Ro$  values versus the large scale  $Ro$  values shows an undelying relationship between Rossby numbers, ageostrophy and vertical motion that is lost when using the large scale Rossby number.

The large scale Rossby number does a reasonable job of indicating the amount of ageostrophy for stable straight-line jet streaks. However, with the addition of curvature this relationship is lost. The reason for this is that curvature increases the amount of ageostrophy. Using  $Ro$  maintains the linear relationship for all the stable jet streaks regardless of curvature. This indicates that  $Ro$  is more dynamically sound in determining ageostrophy. This also indicates that the ageostrophic momentum approximation which  $Ro$  is based on neglects the ageostrophic wind field which is very important especially in the case of cyclonic curature. This means that curvature must be added to the straight-line dynamics when describing the jet streak secondary circulations.

The evaluation of hydrodynamic instabilities seemed to indicate that rotational instability played a significant role in the adjustment process when it was present. On the other hand, barotropic and baroclinic instability seemed to be playing much smaller roles in most cases. However, significant baroclinic instability can not be ruled out with the negative absolute vorticity values. The reason for this is the wind speed required to produce rotational inertial instability also increase the vertical wind shear increasing the possibility of baroclinic instability. The cases most likely to have baroclinic instability were those that had the Rossby number increase with time. One case where baroclinic instability is very likely is the low level easterly jet case where no

negative absolute vorticity values were generated and both the large scale balanced and the I-G vertical motions increased significantly with time.

For the cases involving negative absolute vorticity rotational inertial instability is favored as the dominant cause for the dramatic increase in vertical motion for the following reasons. The first reason is that the generation of negative absolute vorticity values is a necessary and sufficient condition for rotational inertial instability. The second reason is that with the negative absolute vorticity values the I-G waves were increased dramatically as compared to the cases of the likely baroclinic instability where the large scale balanced motions were more affected. The third reason is that the Rossby number - vertical motion linear relationship only broke down significantly with negative absolute vorticity values. The forth reason is that the Rossby number increased with time for these cases. And finally, the vertical motions abruptly increased whenever the negative absolute vorticity values occurred.

The actual cause of the increased vertical motions with the rotational inertial instability would seem to be related to non-linear interactions initiated by the instabilities. The reason for this conclusion is that the vertical motions were increased all over the grid not just in the area of negative absolute vorticity values.

A summary of the conclusions for this investigation follows:

- (1)  $\text{Ro}$  is a much better predictor of ageostrophy and the magnitude of vertical motions than  $\text{Ro}$ .
- (2) Wind speed, curvature, horizontal and vertical wind shear, separation of upper and lower jet streaks and the presence of hydrodynamic instabilities all affect the magnitude of ageostrophy and vertical velocities.
- (3) The higher the maximum wind speed the greater the vertical motion and ageostrophy.
- (4) The smaller the radius of curvature the higher the vertical velocities, with cyclonic curvature being more effective in producing high vertical velocities.
- (5) The stronger the vertical shear the stronger the vertical motions.

(6) The greater the separation of the upper and lower jet streaks, the greater the increase of vertical motion with time.

(7) The presence of hydrodynamic instabilities increased the vertical motion magnitudes. Vertical shear and separation of jet streaks appeared to be directly related to the production of baroclinic instability. However, the largest increases in vertical motions occurred with the presence of rotational inertial instability.

(8) A linear relationship was maintained between  $Ro$  and the magnitude of the vertical motion except for the cases in which  $Ro$  increased with time. This indicated that the jet streak was being forced away from a geostrophic balance by the instability. The most significant deviation from the linear  $Ro$  vertical motion relationship occurred with the inertially unstable cases.

(9) Rotational inertial instability significantly increased the vertical motions through non-linear interactions causing the linear  $Ro$ -vertical motion relationship to break down.

(10) Barotropic inertial instability, although possible, did not seem to be a major factor.

(11) Baroclinic instability is very likely present with the displaced jet streak cases. The low level easterly jet streak case is the most likely to produce baroclinic instability.

There are several additional investigations that could be performed to yield information on the jet streak adjustment process. In each of the investigations significant modification to the PE model used in this paper would be required. The frictional effects should be looked into. This could be done by parameterizing the boundary layer surface friction and the jet streak surface viscous effect. Also, latent heat release could be simulated by adjusting the stability parameters. Another possibility would be to parameterize the effects of changes in the vertical distribution of short wave radiation absorbers. This latter effect is becoming increasingly important with the increase in atmospheric pollutants.

REFERENCES

Barnes, S. L., 1973: Mesoscale Objective Map Analysis Using Weighted Time-Series Observations. NOAA Tech Memo. ERL NSSL-62, 60 pp.

Beebe, R. G. and F. C. Bates, 1955: A Mechanism for Assisting in the Release of Convective Instability. *Mon. Wea. Rev.*, 83, 1-10.

Belt, C. L., and H. E. Fuelberg, 1982: The Effects of Random Error in Rawinsonde Data on Derived Kinematic Quantities. *Mon. Wea. Rev.*, 110, 91-101.

Bluestein, H. B., 1986: Fronts and Jet Streaks: A Theoretical Perspective. *Mesoscale Meteorology and Forecasting*. ed. P. S. Ray., Amer. Meteor. Soc., 173-215.

Bluestein, H. B., and K. W. Thomas, 1984: Diagnosis of a Jet Streak in the Vicinity of a Severe Weather Outbreak in the Texas Panhandle. *Mon. Wea. Rev.*, 112, 2501-2522.

Emanuel, K. A. 1986: Overview and Definitions of Mesoscale Meteorology. *Mesoscale Meteorology and Forecasting*. ed. P. S. Ray., Amer. Meteor. Soc., 1-17.

Eom, J. K., 1975: Analysis of the Internal Gravity Wave Occurrence of 19 April 1970 in the Midwest. *Mon. Wea. Rev.*, 103, 217-226.

Gerhard, M. L., H. E. Fuelberg, S. F. Williams and R. E. Turner, 1979: AVESAME I: 25 mb sounding data. NASA Rep. TM-78256, 364 pp.

Grammeltvelt, A., 1969: A Survey of Finite-Difference Schemes for the Primitive Equations for a Barotropic Fluid. *Mon. Wea. Rev.*, 97, 384-404.

Haltiner, G. J. and F. L. Martin, 1957: Dynamical and Physical Meteorology McGraw-Hill. New York, NY, 470 pp.

Hess, S. L., 1959: *Introduction to Theoretical Meteorology*. Krieger, Malabar, Fl, 304 pp.

Holton, J. R., 1979: *An Introduction to Dynamic Meteorology* (second edition). Academic Press, New York, NY, 391 pp.

Hooke, W. H. 1986: Gravity Waves. *Mesoscale Meteorology and Forecasting*. Amer. Meteor. Soc., 304.

Hoskins, B. J., 1975: The Geostrophic Momentum Approximation and the Semi-Geostrophic Equations. *J. Atmos. Sci.*, 32, 233-242.

Houghton, D. D., W. H. Campbell and N. D. Reynolds, 1981: Isolation of the

Gravity-Inertial Motion Component in a Nonlinear Atmospheric Model. *Mon. Wea. Rev.*, 109, 2118-2130.

Huschke, R. E. (ed), 1959: *Glossary of Meteorology*. Amer. Meteor. Soc. 304.

Keyser, D. and M. A. Shapiro, 1986: A review of the Structure and Dynamics of Upper-Level Frontal Zones. *Mon. Wea. Rev.*, 114, 452-499.

Keyser, D. and L. W. Uccellini, 1987: Regional Models: Emerging Research Tools for Synoptic Meteorologist. *Bull. Amer. Meteor. Soc.*, 68, 306-320.

Koch, S. E., M. Des Jardins, P. J. Kocin, 1983: An Interactive Barnes Objective Map Analysis Scheme for Use with Satellite and Conventional Data. *J. Climate and Appl. Meteor.*, 22, 1487-1503.

Krishnamurti, T. N., 1968: A Diagnostic Balance Model for Studies of Weather Systems of Low and High Latitudes Rossby Number Less Than 1. *Mon. Wea. Rev.*, 96, 197-207.

Kurihara, Y., 1961: Accuracy of Winds-alost Data and Estimation of Error in Numerical Analysis of Atmospheric Motions. *Meteor. Soc. Japan*, 39, 331-345.

Lilly, D. K., 1986: Instabilities. *Mesoscale Meteorology and Forecasting*. ed. P. S. Ray, Amer. Meteor. Soc., 259-271.

MacDonaldald, B. C. and E. R. Reighter, 1988: Explosive Cyclogenesis over the Eastern United States. *Mon. Wea. Rev.*, 116, 1568-1586.

McGinley, J., 1986: Nowcasting Mesoscale Phenomena. *Mesoscale Meteorology and Forecasting*. ed. P. S. Ray., Amer. Meteor. Soc., 657-688.

Miles, J. W. and L. N. Howard, 1981: On the Stability of Heterogeneous Shear Flows and A Note on a paper of John W. Miles. *J. Fluid Mech.*, 10, 496-512.

Molinaro, R. C, 1988: Diagnostic and Kinematic Fieldsn" Associated with Curved and Straight Jet Streaks using a Two-Layer Primitive Equation Model. Doctoral dissertation, Dept. of Meteorology Saint Louis University, 204 pp.

Moore, J. T., 1985: A Case Study of the Effects of Random Errors in Rawinsonde Data on Computations of Ageostrophic Winds. *Mon. Wea. Rev.*, 113, 1633-1643.

O'Brien, J. J., 1970: Alternative Solutions to the Classical Vertical Velocity Problem. *J. Appl. Meteor.*, 9, 197-203.

Orianski, I. ,1975: A Rational Subdivision of Scales for Atmospheric Processes. *BAMS* Vol 56, 527-530.

Pecnick, M. J., and J. A. Young, 1984: Mechanics of a Strong Subsynoptic Gravity

Wave Deduced From Satellite and Surface Observations. *J. Atmos. Sci.*, 41, 1850-1862.

Reiter, E. R., 1963: Jet-Stream Meteorology. The University of Chicago Press, Chicago, IL, 515 pp.

Shapiro, M. A. and P. J. Kennedy, 1981: Research Aircraft Measurements of Jet Stream Geostrophic and Ageostrophic Winds. *J. Atmos. Sci.*, 38, 2642-2652.

Stull, R. B. 1988: *An Introduction to Boundary Layer Meteorology*. Kluher Academic Publishers, Boston, Ma, 454 pp.

Thorpe, S. A., 1971: Experiments on the Instability of Stratified Shear Flows:Miscible Fluids. *J. Fluid Mech.*, 46, 299-319.

Uccellini, L. W., 1975: A Case Study of Apparent Gravity Wave Initiation of Severe Convective Storms. *Mon. Wea. Rev.*, 103, 497-513.

Uccellini, L. W. and D. R. Johnson., 1979: The Coupling of Upper and Lower Tropospheric Jet Streaks and Implications for the Development of Severe Convective Storms. *Mon. Wea. Rev.*, 107, 682-703.

Van Tuyl, A. H. and J. A. Young, 1982: Numerical Simulation of Nonlinear Jet Streak Adjustment. *Mon. Wea. Rev.*, 110, 2038-2054.